THE EFFECT OF COAL COMPOSITION UPON GAS SORPTION AND TRANSMISSIBILITY OF BITUMINOUS COAL

by

CHRISTOPHER RAYMOND CLARKSON

B.A.Sc., The University of British Columbia, 1992

A THESIS SUBMITTED IN PARTIAL FULFILLMENT OF

THE REQUIREMENTS FOR THE DEGREE OF

MASTER OF APPLIED SCIENCE

in

THE FACULTY OF GRADUATE STUDIES

Department of Geological Sciences

We accept this thesis as conforming
to the required standard

THE UNIVERSITY OF BRITISH COLUMBIA

AUGUST 1994

In presenting this thesis in partial fulfilment of the requirements for an advanced degree at the University of British Columbia, I agree that the Library shall make it freely available for reference and study. I further agree that permission for extensive copying of this thesis for scholarly purposes may be granted by the head of my department or by his or her representatives. It is understood that copying or publication of this thesis for financial gain shall not be allowed without my written permission.

(Signature)

Department of Geological Sciences

The University of British Columbia
Vancouver, Canada

Date August 23 / 1994

DE-6 (2/88)

ABSTRACT

The effect of bituminous coal composition, particularly the organic fraction, upon gas sorption and transmissibility is investigated. Micropore capacities of bituminous coals, determined from low pressure carbon dioxide adsorption, show a general increase with total and structured vitrinite content. Conversely, micropore capacities generally decrease with an increase in inertinite and mineral matter content. High pressure methane monolayer capacities show a similar trend. Micropore size distributions indicate an increase in the total number of micropores and a slight decrease in mean pore diameter with vitrinite content.

Mesopore volumes and surface areas, determined through nitrogen sorption, show a general decrease with vitrinite content and increase with inertinite content of bituminous coal. Vitrinite therefore contains more microporosity and less mesoporosity than inertinite. Hysteresis loops of sorption isotherms indicate that mesopores of the coals studied are slit-shaped.

Permeabilities of bituminous coals obtained through the use of a permeameter capable of measuring permeabilities on a bed-by-bed scale show that brighter coal lithotypes are more permeable than dull lithotypes. The order of decreasing permeability with lithotype is: bright > banded > fibrous > banded dull > dull. The increase in permeability with increased brightness of coals is due to the presence of abundant macrofracturing (cleating) in bright coal. For one sample, permeabilties were found to increase with vitrinite content.

TABLE OF CONTENTS

LIST OF FIGURES

LIST OF TABLES

AKNOWLEDGEMENTS

The current thesis was made possible through the help and contributions of several individuals. Firstly, I would like to thank my supervisor, Dr. R. Marc Bustin, for creating an ideal environment in which to do research as well as for his many helpful and insightful discussions. I would also like to thank my supervisory committee, Dr. Roger Beckie, Dr. Rosemary Knight, and Dr. John Ross for their support and helpful discussions. To my friends and colleagues, Dr. Michelle Lamberson and Dr. Maria Mastalerz, I extend a warm thank you for your help, support, and contributions thoughout the course of my study. I also deeply appreciate the support given to me by my family and friends. I would like to thank a very special person, Arlene Batuna, for her patience and support.

Technical support at UBC was provided by Ray Rodway, Bryon Cranston (thesis & hockey!), Marc Baker, Yvonne Douma, and Doug Polson; without you I would not have completed. Further technical support was provided by Core Laboratories of Calgary (John Clow). I would also like to extend deep gratitude to Nancy Myra and the office staff of Geological Sciences at UBC for keeping me "organized".

Financial support was provided by the Natural Sciences and Engineering Research Council, Pan Canadian Ltd., the Geological Survey of Canada, and the Geological Sciences Department of UBC.

CHAPTER 1

INTRODUCTORY STATEMENTS

1.1 INTRODUCTION

Coalbed gas is currently being evaluated as a fuel source to supplement conventional natural gas reserves in several countries. The United States is the only country currently producing coalbed gas commercially.

Canada has an estimated 323 billion metric tons of coal resources (Kuuskraa and Boyer, 1993) with estimates of coalbed gas resources varying from 1.42×10^{13} to 7.37×10^{13} m^3 (500-2600 Tcf) (Schraufnagel, 1993). Much of the coal and hence coalbed gas resources is located within the Western Canadian Sedimentary Basin. The Alberta Geological Survey along with several Canadian gas and petroleum companies such as PetroCanada, Canadian Hunter, BP, Alberta Energy, Norcen, and Pan Canadian are currently in the process of evaluating coalbed gas as a natural gas supplement to current conventional gas reserves.

Successful production of coalbed gas is dependent upon a complex interplay of geologic and economic factors. Among geologic factors affecting the ultimate recovery of coalbed gas are: coal seam thickness, continuity, geometry, and distribution; fracture permeability; rank; coal type; depth of burial; gas saturation; and reservoir pressure and hydrologic conditions to name but a few. Controls of coal composition, particularly the organic fraction, upon the retention of gas has only briefly been investigated. The effects of maceral content of coal upon pore volumes and size distributions requires further investigation in order to completely understand the determinants of gas content and producibility.

This thesis investigates, through the use of the volumetric method of measuring gas sorption isotherms, the effects of maceral and mineral contents upon micropore and mesopore distributions, capacities and associated surface areas. Further, the control of lithotype and maceral composition upon permeabilities, established through the use of a new permeameter

capable of obtaining permeability profiles on a bed (centimeter) scale, will be assessed. This last study investigates the effect of micro- and macrostructure upon coal permeability.

1.2 NATURAL GAS GENERATION FROM COAL

A large quantity of natural gas is produced during the process of coalification, the biochemical and thermal alteration of plant material to peat, lignite, sub-bituminous, bituminous, semi-anthracite, anthracite, and meta-anthracite (Bustin et al., 1985). Natural gas produced from coalification, usually referred to as coalbed gas, is often rich in methane, but may also contain significant amounts of other gases. Other, heavier hydrocarbons may also be produced during coalification. Composition of coalbed gas, in addition to associated products produced during coalification, is dependent upon the original organic matter type and the nature and degree of biochemical and thermogenic alteration. Further, migration of gases external to the system, such as carbon dioxide derived from a magma source (Smith et al, 1985a; Kotarba, 1988, 1990) may affect the ultimate composition of coalbed gas.

Two main types of coalbed gas exist: biogenic and thermogenic. Biogenic gas is primarily composed of methane and carbon dioxide and is formed through bacterial degradation of organic matter (Kim and Douglas, 1972). Two main mechanisms exist for the formation of such gas: carbon dioxide reduction and methyl-type fermentation (Schoell, 1980; Woltemate et al., 1984; Jenden and Kaplan, 1986; Whiticar et al., 1986). Biogenic gas formation may occur at an early and late stage in the burial history of the coal (Rice, 1993).

Thermogenic gas formation initiates at about the high-volatile bituminous stage (> 50°C) and continues throughout the geochemical stage of coalification (Hunt, 1979). Although methane gas is produced during the biochemical stage as a result of bacterial degradation of the original vegetable matter, most of the gas produced is of thermogenic origin. The main gas components of the geochemical stage are methane, carbon dioxide, and water.

The amount of methane produced during coalification is dependent upon coal composition and assessments of gas produced will range depending on the estimation procedure. Estimated values of total methane produced during coalification range from 100 to 300 cm^3/g (Juntgen and

Karweil, 1966; Juntgen and Klein, 1975; Hunt, 1979, Meissner, 1984; Welte et al., 1984; Levine, 1987).

1.3 GAS RETENTION IN COAL

Coal is unique in its ability to act as both a source rock and reservoir to natural gas. The storage capacity of coals varies with rank, pressure and temperature (Meissner, 1984). Much of the gas generated during coalification is lost to: a) surrounding sediments, possibly forming a conventional gas reservoir; b) the atmosphere; and c) groundwater flow through the coal seam. Some of the generated gas may be retained in the coal seam, depending upon the character of the coal reservoir.

Coalbed gas is retained in coal seams in the following ways: a) adsorption upon the internal surfaces (i.e. in microporosity) or absorption within the molecular structure of the coal; b) as free gas, or gas in excess of which can be adsorbed or absorbed, within cleats and fractures of the coal; and c) as a solute within groundwater present within the coal seam (Rightmire, 1984; Murray et al., 1991; Ertekin et al., 1991; Rice, 1993). By far the most important mechanism for methane retention is that of gas adsorption upon the internal surfaces of the coal, particularly with high rank coals. Hence the controls upon the micropore structure, and the pore structure in general, of coals is hence of interest in determining the ultimate natural gas content of such material.

The micropore system (pore diameters < 2 nm), which makes up the bulk of coal porosity at higher ranks, acts as a molecular sieve or as a clathrate cage (Van Krevelin, 1981).

Gas retention within microporosity, and indeed its physical significance are a matter of debate. According to some workers (i.e. Dryden, 1963; Fuller, 1981; and Given, 1984) microporosity in coal may not be a fixed property of coal and is dependent upon the particular sorbate/coal system. Further, Levine (1993) states that sorption may be modeled as either adsorption (chemi- or physisorption) within the micropore network or as dissolution of sorbate within the molecular structure of the coal; sorption within coal is likely a combination of a variety

of different processes. The equations and sorption theories adhered to in this thesis are dependent upon physical adsorption taking place within coal porosity.

In addition to microporosity, the pore structure of coal may be further broken down into the following size classification as defined by the International Union of Pure and Applied Chemistry (IUPAC): mesoporosity, or pores with a diameter between 2 and 50 nm; and macroporosity, or pores with a diameter greater than 50 nm. The physical mechanism of gas adsorption appears to be dependent upon pore size. The dependence of these pore filling mechanisms upon pore size will be discussed in Chapter 2.

1.4 STRUCTURE OF THE THESIS

One chapter is dedicated to the discussion of gas sorption theory and terminology and three chapters are prepared as independent papers addressing the issues discussed above. Chapter 3 investigates the effects of coal (maceral) composition upon the micropore capacity and size distributions and the implications for coalbed methane potential.

Chapter 4 investigates the effects of coal (maceral) composition upon mesopore volumes, size distributions and associated surface areas.

Chapter 5 studies the variation of permeability with lithotype (megascopic) and maceral (microscopic) composition of coal.

1.5 REFERENCES

Bustin, R.M., Cameron, A.R., Grieve, D.A., and Kalkreuth, W.D., 1985. Coal Petrology: Its Principles, Methods and Applications, Geological Association of Canada, Short Course Notes, Volume 3, Second Edition, 230 pp.

Dryden, I.G.C., 1963. Chemical constitution and reaction of coal. In: H.H. Lowry (Editor) , Chemistry of Coal Utilization Supplementary Volume. New York, John & Sons, pp. 232-295.

Ertekin, T., Sung, W., and Bilgesu, H.I., 1991. Structural properties of coal that control coalbed methane production. In: D.C. Peters (Editor), Geology in Coal Resource Utilization. pp 105-124.

Fuller, E.L., Jr., 1981. Pfysical and chemical structure of coals: sorption studies. In: M.L. Gorbaty, and K. Ouchy (Editors), Coal Structure: Advances in Chemistry Series 192, Washington, D.C., American Chemical Society, p. 293-309.

Given, P.H., P.H., 1984. An essay on the organic geochemistry of coal. In: M.L. Gorbaty et al. (Editors), Coal Science, v. 3. New York Academic Press, p. 63-252, 339-341.

Gregg, S.J., and Sing, K.S.W., 1982. Adsorption, Surface Area and Porosity, Second Edition. Academic Press, New York. 303 pp.

Hunt, J.M., 1979. Petroleum geochemistry and Geology: San Francisco, W.H. Freeman and Co. 617p.

Jenden, P.D., and Kaplan, I.R., 1986. Comparison of microbial gases of the Middle America Trench and Scripps Submarine Canyon: implications for the origin of natural gas. Applied Geochemistry, 1: 631-646.

Juntgen, H., and Karweil, J., 1966. Gasbildung and Gasspeicherung in Steinkohlenflozen, Part I and II. Erdol Kohle, Erdgas, Petrochem, 19: 251-258, 339-344.

Juntgen, H., and Klein, J., 1975. Entstehung von Erdgas gus kohligen Sedementen. Erdol, Kohle, Erdgas, Petrochem, Erganzungsband, 1: 52-69.

Kim, A.G., and Douglas, L.J., 1972. Hydrocarbon gases produced in a simulated environment. U.S. Bureau of Mines Report of Investigations 7690: 15p.

Kotarba, M., 1990. Isotopic geochemistry and habitat of the natural gases from the Upper Carboniferous Zacler coal-bearing formation in Nowa Ruda coal district (Lower Silesia, Poland). In: B. Durand and F. Behar (Editors). Advances in Organic Geochemistry, 1989. Oxford Pergamon Press, 1, pp.549-560.

Kotarba, M., 1988. Geochemical criteria for the origin of natural gases accumulated in the Upper Carboniferous coalseam-bearing fromations in Walbrzych Coal Basin (in Polish with English summary. Stanislaw Staszio Academy of Mining and Metallurgy Scientific Bulletin 1199: 119p.

Kuuskra, V.A., and Boyer, C.M., II, 1993. Economic and parametric analysis of coalbed methane. In: B.E. Law and D.D. Rice (Editors), Hydrocarbons from Coal, AAPG Studies in Geology # 38, pp. 373-394.

Levine, J.R., 1993. Coalification: the evolution of coal as a source rock and reservoir rock for oil and gas. In: B.E. Law and D.D. Rice (Editors), Hydrocarbons from Coal, AAPG Studies in Geology # 38, pp. 39-77.

Levine, J.R., 1987. Influence of coal composition on the generation and retention of coalbed natural gas. Proceedings of the 1987 Coalbed Methane Symposium, pp. 15-17.

Meissner, F.F., 1984. Cretaceous and lower Tertiary coals as sources for gas accumulations in the Rocky Mountain area. Source rocks of the Rocky Mountain Region, 1984 Guidebook, Rocky Mountain Association of Geologists, pp. 401-431.

Murray, D.K., 1991. Coalbed methane: natural gas resources from coal seams. In D.C. Peters (Editor), Geology in Coal Resource Utilization, pp. 97-103.

Rice, D.R., 1993. Composition and origins of coalbed gas. In: B.E. Law and D.D. Rice (Editors), Hydrocarbons from Coal, AAPG Studies in Geology # 38, pp. 159-184.

Rightmire, C.T., 1984. Coalbed methane resource. In: C.T. Rightmire, G.E. Eddy, and J.N. Kirr (Editors), Coalbed methane resources of the United States. American Association of Petroleum Geologists, Studies in Geology, 17: 1-13.

Schraufnagel, R.A., 1993. Coalbed methane production. In: B.E. Law and D.D. Rice (Editors), Hydrocarbons from Coal, AAPG Studies in Geology # 38, pp 341-359.

Smith, J.W., Gould, K.W., Hart, G., Rigby, D., 1985a. Isotopic studies of Australian natural and coal seam gas. Bulletin of Australasian Institute of Mining and Metallurgy, 290: 43-51.

Van Krevelen, D.W., 1981. Coal (reprinted from 1961 edition). Amsterdam, Elsevier. 514, pp.

Welte, D.H., Schaefer, R.G., Stoessinger, W., and Radke, M., 1984. Gas generation and migration in the Deep Basin of western Canada. American Association of Petroleum Geologists Memoir 38: 35-47.

Whiticar, M.J., Faber, E., and Schoell, M., 1986. Biogenic methane formation in marine and freshwater environments, CO_2 reduction vs. acetate fermentation - isotopic evidence. Geochemica et Cosmochimica Acta, 50: 693-709.

Woltemate, I., Whiticar, M.J., Schoell, M., 1984. Carbon and hydrogen isotopic composition of bacterial methane in a shallow freshwater lake. Limnology and Oceanography, 29: 985-992.

CHAPTER 2

GAS SORPTION THEORY

2.1 INTRODUCTION

This chapter outlines the basic principles of gas adsorption relevant to the determination of the internal surface area and pore size distributions of coal. Definitions of terms and descriptions of concepts used in gas adsorption theory are given. In addition, the theories and equations utilized in the current study to determine surface areas and pore size distributions based on gas adsorption are outlined; these include BET (Brunauer, Emmett, and Teller) Theory and associated equations, Dubinin Theory of Volume Filling for Micropores and associated equations, and BJH (Barrett, Joyner, and Halenda) Theory and associated equations. Finally, the choice of an adsorbate for coals is discussed.

2.1.1 Definitions

The following list of terms and corresponding definitions is not meant to be exhaustive, but merely an introduction to the terminology applied in gas adsorption theory. These terms are ones in general use in adsorption literature, and are not limited to a specific gas adsorption theory. Terms specific to each theory will be defined in a later section.

1) Specific Surface Area:

Specific surface area of a solid is defined as the surface area (internal and/or external) per unit mass of solid. The units used in the current study are m^2/g.

2) External vs. Internal Surface Area:

External surface area of a solid containing surface irregularities is defined as that surface area including " all the prominences and all those cracks which are wider than they are deep " (Gregg and Sing, 1982, p. 23). The internal surface area of such a solid is thus defined as the surface area which comprises " the walls of all cracks, pores and cavities which are deeper than they are wide " (Gregg and Sing, 1982, p. 24). The distinction between these two forms of surface area is arbitrary and forms the basis for the cut-off between inter- and intra-particle porosity. Figure 2-1 illustrates the difference between external and internal surface area using the example of the coal maceral, semifusinite; the external surface area includes the outer surface of the maceral fragment, whereas the internal surface area comprises the inner walls of the pores. For many porous materials, including coal, the internal surface area far exceeds the external surface area of the material due to the area contribution of the pore walls and throats and microfractures in the sample.

3) Porosity:

Porosity of a solid refers to the ratio of the total pore volume of the solid to the solid's total volume. Porosity may be inter- or intra-particle porosity.

4) Adsorption, Absorption, Sorption:

These terms have often been used interchangeably in the literature and for the purposes of this thesis are defined in an unambiguous fashion as follows:

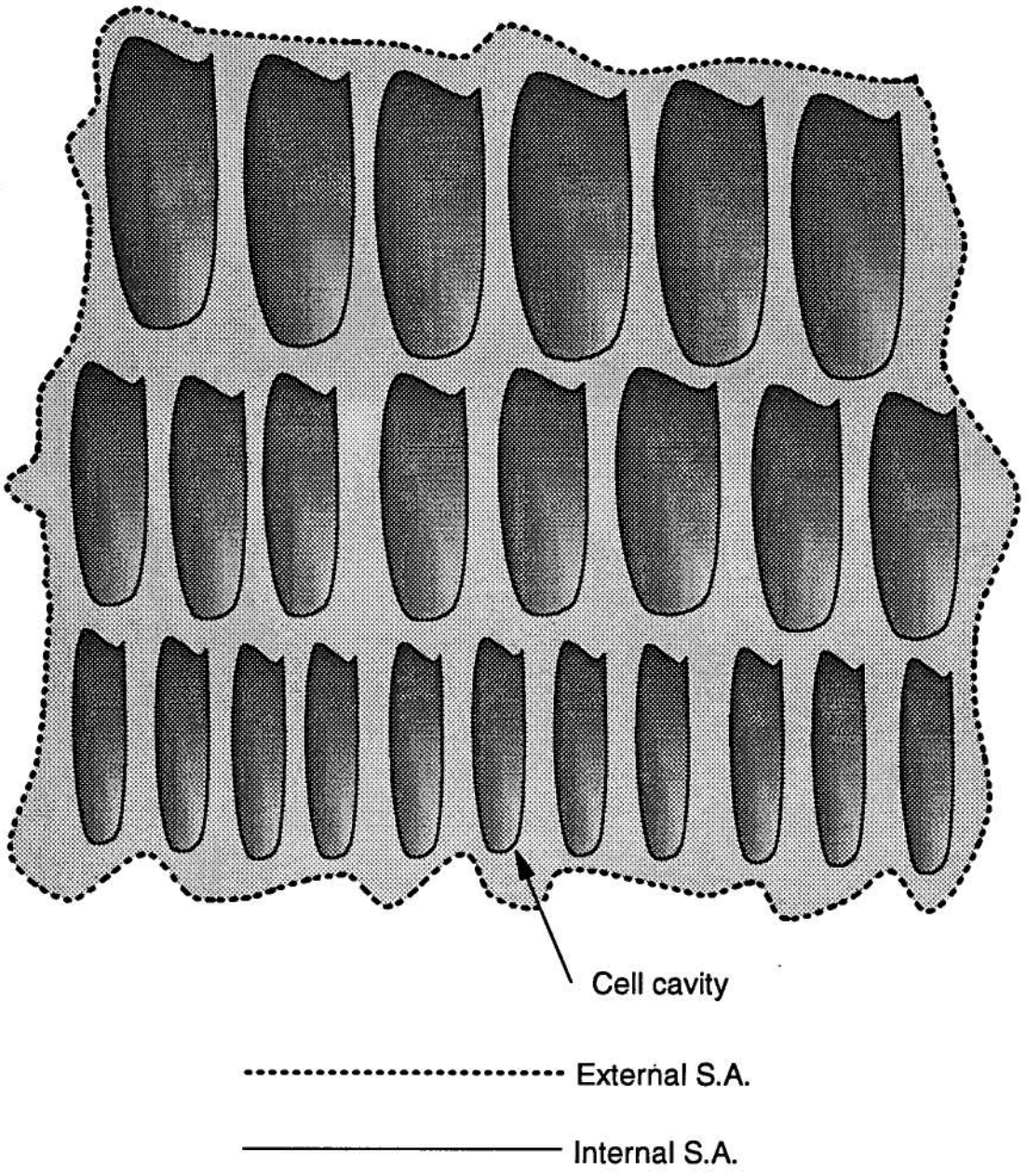

Figure 2-1. Diagram illustrating the difference between internal and external surface area. Illustration is a hypothetical semifusinite maceral fragment.

Adsorption: Gregg and Sing (1982, p. 2) define (physical) adsorption as "the enrichment or depletion of one or more components in an interfacial layer". The distinction between physical and chemical adsorption will be discussed in a later section. Adsorption is used in the current study as in Gregg and Sing (1982) to embrace the physical uptake of gas by either pore volume filling causing enhanced adsorption in microporosity or monolayer formation, both of which involve surface adsorption, or by capillary condensation.

Absorption: This physical process refers to the actual incorporation or assimilation of gas molecules into the solid's molecular structure.

Sorption: Sorption, as defined by Gregg and Sing (1982), is a general term which includes surface adsorption, absorption, and capillary condensation. Desorption is the opposite process.

5) Adsorptive, Adsorbate, Adsorbent

Adsorptive: This is a general term referring to any gas or vapour which is capable of being adsorbed (Gregg and Sing, 1982).

Adsorbate: This term is more specific and refers to the material that is physically or chemically adsorbed to the surface of the solid, such as a gas molecule occupying an adsorbed monolayer. The adsorbate may have properties which differ from that of the adsorptive gas or bulk liquid.

Adsorbent: This is the material upon whose surface adsorption takes place (e.g. coal).

6) Adsorption Isotherm:

Adsorption isotherms are central to the discussion of adsorption theory, and as used in this study, refer to plots of the amount (volume at stp, mass, number of moles) of vapour adsorbed (adsorbate) onto a solid (adsorbent) at a constant temperature, versus the relative pressure. Relative pressure is defined as the ratio of the equilibrium vapour pressure (P) to the saturation vapour pressure (P_0) of the adsorbate gas and is used instead of equilibrium pressure if the gas is below its critical temperature. Brunauer, Deming, Deming and Teller (Brunauer et al., 1940) classified isotherms in terms of their functional form. Isotherm types are dependent upon the particular adsorbate-adsorbent system as well as the pore structure of the adsorbent.

7) Sorption hysteresis

Sorption hysteresis refers to the non-coincidence of the adsorption and desorption branches of the isotherm curve.

2.1.2 Concepts

1) Forces of Adsorption

A gas or vapour will be adsorbed to the surface of a solid through various mechanisms depending upon the type of adsorption forces that govern the interaction between the adsorbate and the adsorbent. Dispersion and electrostatic forces are the most common forces governing adsorption (Gregg and Sing, 1982).

Dispersion forces between atoms refer to those forces that arise from asymmetry of the electron cloud of an atom over a short term (Fyfe, 1964; Gregg and Sing, 1982; Lowell and Shields, 1984). An atom that is non-polar over a larger interval of time can be either polar or dipolar over a short period of time (Fyfe, 1964). If two atoms that exhibit dipolar behavior over a short term are brought into proximity, the dipole moments may couple in phase and lead to a small binding force. For example, helium has a spherically symmetric cloud consisting of two *s*

electrons in its electron shell. This spherical shape is the statistical average shape of the electron cloud described by a Schrödinger wave function (ψ) (Fyfe, 1964). Over a very short period of time, the average spherical symmetry of the electron cloud is not observed, but a transient dipole moment is imparted to the helium atom (Lowell and Shields, 1984). The helium atom may induce a dipole moment in a neighbouring atom, leading to a net attraction.

Dispersion forces are attractive in nature, but some repulsion is experienced due to the inter-penetration of the electron clouds of two atoms and the proximity of their nuclei. These forces are very small in magnitude relative to a typical covalent bond. The bonds created by dispersion forces are thus weak and easy to break.

Electrostatic (coulombic) forces may also be important in determining adsorbate-adsorbent interactions. Examples of such interactions are: polar solids with gas molecules that possess an induced dipole moment; polar solids with gas molecules which possess a permanent dipole moment; and polar solids with gas molecules possessing a quadrupolar moment (e.g. CO_2) (Gregg and Sing, 1982; Lowell and Shields, 1984). Electrostatic forces are therefore highly dependent upon the nature of the adsorbate and adsorbent.

2) Physical and Chemical Adsorption

From the discussion above, it is apparent that a variety of adsorbate-adsorbent interactions are possible based on the nature of the forces involved. Two basic types of adsorption are defined depending upon which of the two main groups of forces (dispersive or electrostatic) are dominant. Physical (or non-specific) adsorption occurs where dispersion and short term repulsive forces predominate; chemical (or specific) adsorption occurs where electrostatic forces predominate (Gregg and Sing, 1982; Lowell and Shields, 1984). Combinations of the two types of adsorption occur, and Gregg and Sing (1982) give the range of possibilities based on the nature of the adsorbate and adsorbent. A continuum between chemical and physical adsorption probably exists.

The two types of adsorption differ in several ways (Lowell and Shields, 1984):

a) physical adsorption, due to the weak nature of dispersion forces, is reversible.

b) physical adsorption is associated with a small heat of adsorption, whereas chemical adsorption involves a larger heat of adsorption.

c) chemical adsorption unlike physical adsorption involves true chemical bonding and has an associated activation energy.

d) the adsorbate is normally restricted to a single adsorbed layer in chemical adsorption, whereas in physical adsorption the adsorbate is less rigidly held to the surface and may form a number of layers (multilayer adsorption).

e) chemisorbed vapours are adsorbed to specific sites on the adsorbent surface, whereas physisorbed adsorbates have a greater translational freedom.

f) equilibrium is achieved more rapidly with physical adsorption than with chemical adsorption, except perhaps in the case of micropores where activated diffusion processes may occur.

Physical adsorption is thus desirable for surface area measurement due to the non-localized nature of adsorbate and hence greater surface coverage, as well as the lower equilibrium times and reversibility of the process.

3) Heat of Adsorption

The potential energy of an adsorbate interacting with an adsorbent reaches a minimum at some point close to the adsorbent surface (Gregg and Sing, 1982). This potential "well" represents the equilibrium or adsorbed position of the adsorbate.

The process of adsorption is necessarily an exothermic one due to the loss of translational freedom of the adsorbate. The kinetic energy lost is converted to heat and the enthalpy change (Δ H) is necessarily negative. Heat of adsorption is related to this process with the exact thermodynamic derivation given in Gregg and Sing (1982). Heats of adsorption can be determined experimentally and are important in separating physical and chemical adsorption, distinguishing pore structures in which adsorption is enhanced (such as in micropores), and in monitoring completion of monolayer formation, etc.

4) Classification of Adsorption Isotherms

Five basic types of adsorption isotherms were described by Brunauer, Deming, Deming, and Teller (Brunauer et al., 1940) and are shown in Figure 2-2. Most adsorbate-adsorbent systems yield isotherms that fall into this basic classification. Type I, II, III, IV, and V isotherms are described below.

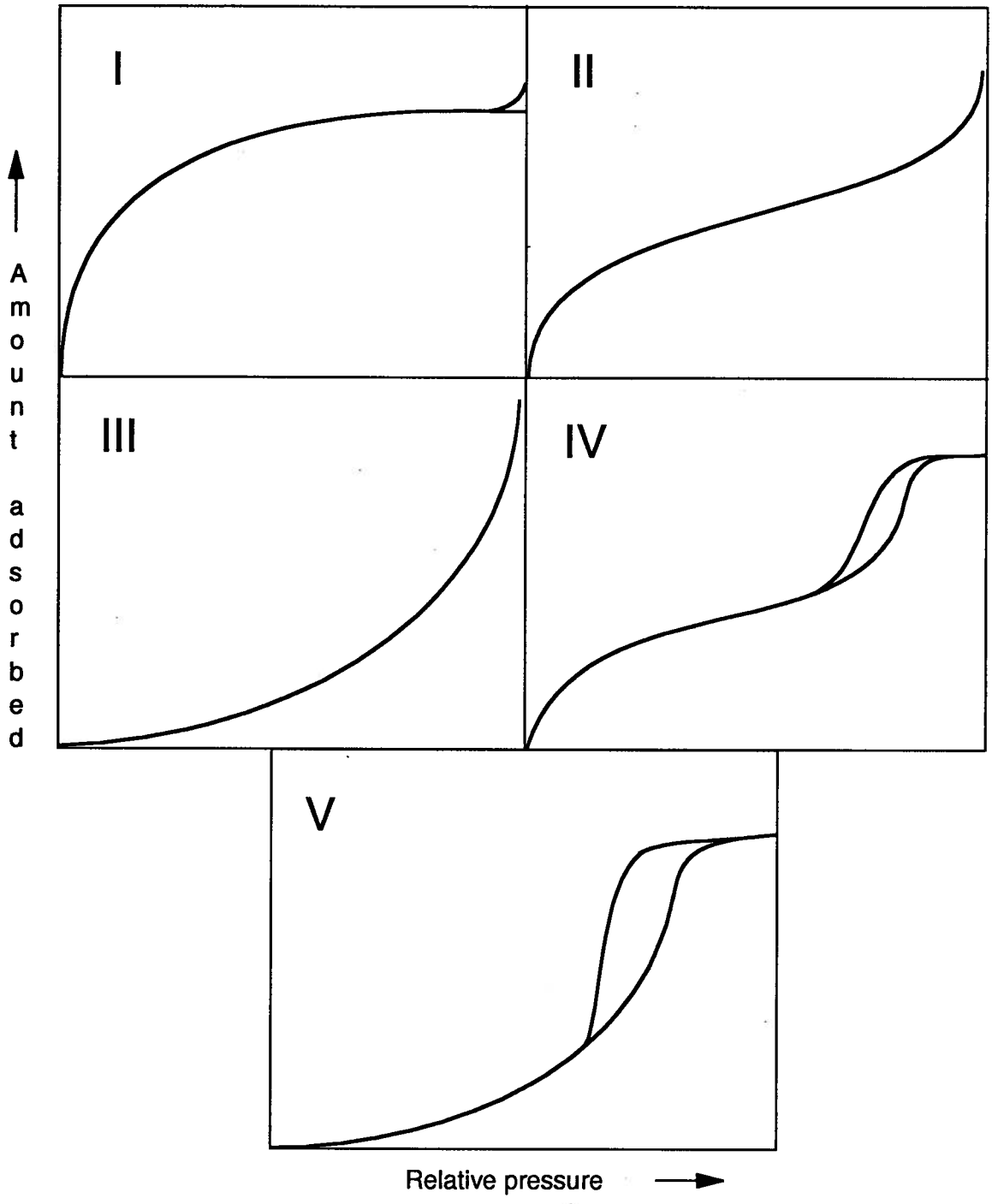

Figure 2-2. Isotherms of the Brunauer, Demming, Demming and Teller classification. Modified from Gregg and Sing (1982).

Type I isotherms, also referred to as Langmuir isotherms (Langmuir, 1916), are produced by adsorption onto microporous solids or by adsorbate-adsorbent systems in which adsorption is restricted to a few monolayers. In physisorbed systems, the adsorbent must contain a very fine pore structure with a small external surface to approximate the Type I isotherm shape (Figure 2-2). In such systems, enhanced uptake occurs at low relative pressures due to the overlapping of adsorption potentials between pore walls of pores with diameters only slightly wider than the adsorbate gas molecule (Lowell and Shields, 1984). This effect is illustrated by the initial steep slope of the Type I isotherm. Adsorption fall off once the micropore system has been filled and little additional adsorption occurs until the system reaches its saturation point ($P/P_O=1$). Hysteresis is normally absent from this type of isotherm (Orr, 1977). Type I isotherms are also produced by chemisorbed systems where adsorption is necessarily restricted to a single monolayer (Lowell and Shields, 1984). The "plateau" section of the isotherm is then interpreted to represent the completion of a single monolayer (Orr, 1977).

Type II isotherms, also referred to as sigmoid or S-shaped isotherms (Brunauer et al., 1940), are produced by adsorption onto non-porous or macroporous solids. Adsorption is believed to occur through the formation of layers of adsorbed gas which are only one adsorbate molecule thick (a monolayer). The first point of inflection of the Type II isotherm is believed to be approximately coincident with the BET monolayer capacity (volume of adsorbate gas occupying a layer of molecular thickness) (Orr, 1977; Gregg and Sing, 1982; Lowell and Shields, 1984). At higher relative pressures, multilayers are formed on the nonporous surface until saturation is achieved (Lowell and Shields, 1984). The Type II isotherm is described by classical BET Theory.

Type III isotherms display an increase in adsorption with the total amount adsorbed due to a greater interaction of the adsorbate with the adsorbed layer than with the adsorbent. In such a system the heat of adsorption is greater than the heat of liquefaction of the adsorbate (Lowell and Shields, 1984).

Type IV isotherms are produced by adsorption onto mesoporous solids, i.e. solids with pores in the 1.5 - 100 nm range. The initial portion of the isotherm is similar to the Type II isotherm, but enhanced adsorption occurs at higher relative pressures due to the onset of capillary condensation (discussed later). Type IV isotherms are also distinguished by the presence of a distinct hysteresis loop at higher relative pressures, which indicates non-coincidence of the adsorption and desorption branches of the isotherm. Hysteresis is thought to occur subsequent to the completion of the first adsorbed monolayer ($P/P_0 \sim 0.3$). As will be seen, the shape of the hysteresis loop is characteristic of the pore shape of the adsorbent.

Type V isotherms result from weak adsorbate-adsorbent interactions and are rare.

5) Pore Size Classification

A pore size classification was defined at The International Union of Pure and Applied Chemistry (IUPAC) meeting in Washington, D.C. on July 23, 1971 (Orr, 1977). The meeting established the definition of micropores, mesopores (or transitional pores), and macropores as follows:

Micropores: pores with diameters of less than 2 nm.
Mesopores: pores with diameters between 2 and 50 nm.
Macropores: pores with diameters greater than 50 nm.

The pore size classification is arbitrary, but has a convenient application for many materials in the chemical industry. This classification is the one adhered to in the current study.

Dubinin (1982) proposed a size classification for pores that is based on the linear sizes of carbonaceous adsorbents. This classification is as follows:

Micropores: pore (radii) less than 0.6 - 0.7 nm in size.

Supermicropores: pores between 0.6 - 0.7 nm and 1.5 - 1.6 nm.

Mesopores: pores between 1.5 - 1.6 nm and 100 - 200 nm.

Macropores: pores greater than 100 - 200 nm in size.

The Dubinin classification is such that the pore sizes correspond to the interpreted mechanism of pore filling for a carbonaceous adsorbent. For example, the micropore classification is utilized for pores in which Dubinin's Theory of Volume Filling for micropores applies (see later), and the mesopore range is coincident with multilayer formation and capillary condensation (Dubinin, 1982). Supermicropores are ones in which "cooperative" effects occur (Gregg and Sing, 1982), and macropores are pores in which the capillary condensation mechanism cannot feasibly apply. Marsh (1987) warns, however, that "Close distinctions between the classes of porosity cannot be rigorous since they are based on adsorption behaviour, adsorbate with adsorbent, rather than a physical measurement".

2.2 THEORIES OF ADSORPTION

The following section includes a description of the basic concepts underlying the theories of adsorption used in the current thesis. The main formulas used in each theory are given as well as the range of applicability (in terms of relative pressure) and limitations of the theories.

2.2.1 BET Theory

The Brunauer, Emmett, and Teller (BET) Theory has enjoyed widespread use in the field of surface area measurement since its introduction in 1938. The theory is a modification of Langmuir's kinetic model of adsorption (Gregg and Sing, 1982). The BET equation was developed to describe a Type II isotherm.

The BET equation

The BET Theory assumes that the surface of an adsorbent is simply an "array of adsorption sites" (Gregg and Sing, 1982, p 42), where the most energetic sites are occupied first as the pressure increases (Lowell and Shields, 1984). Physical adsorption is achieved through the formation of incomplete monolayers (Figure 2-3) stacked outward from the surface; the greater the number of monolayers formed, the greater the area of adsorbent surface covered. A dynamic equilibrium is thought to occur whereby the rate of evaporation from the first formed monolayer is equal to the rate of condensation upon the adsorbent surface (Brunauer et al., 1938). The equation representing the state of equilibrium with the adsorbent surface for the first adsorbed layer is (Brunauer et al., 1938; Gregg and Sing, 1982; Lowell and Shields, 1984):

$$N_m\theta_1\nu_1[e^{-E_1/RT}] = A_1\kappa P\theta_0$$

where N_m is the number of adsorbate molecules occupying a completed monolayer, θ_1 is the fraction of surface sites occupied by the adsorbate, ν_1 represents the frequency of oscillation of the adsorbate molecule perpendicular to the adsorbent surface, E_1 is an average adsorption energy for the first layer, A_1 is the condensation coefficient, κ is a constant derived from the kinetic theory of gases (Gregg and Sing, 1982; Lowell and Shields, 1984), P is the equilibrium adsorptive gas pressure, R is the Universal Gas Constant, and T is temperature.

In the second and successive layers, the adsorption energy is assumed to be equal to the heat of liquefaction of the adsorbate, E_L, and the constants ν and A remain constant (Lowell and Shields, 1984). The rate of condensation onto the first layer is assumed to be equal to the rate of evaporation from the second layer (Brunauer et al., 1938) and the rate of condensation on the nth layer is assumed to be equal to the rate of evaporation from the n+1 layer. Also, the number of adsorbate layers at saturation is assumed to be infinite. After algebraic manipulation (Gregg and Sing, 1982; Lowell and Shields, 1984), the following relation, the BET equation, is arrived at:

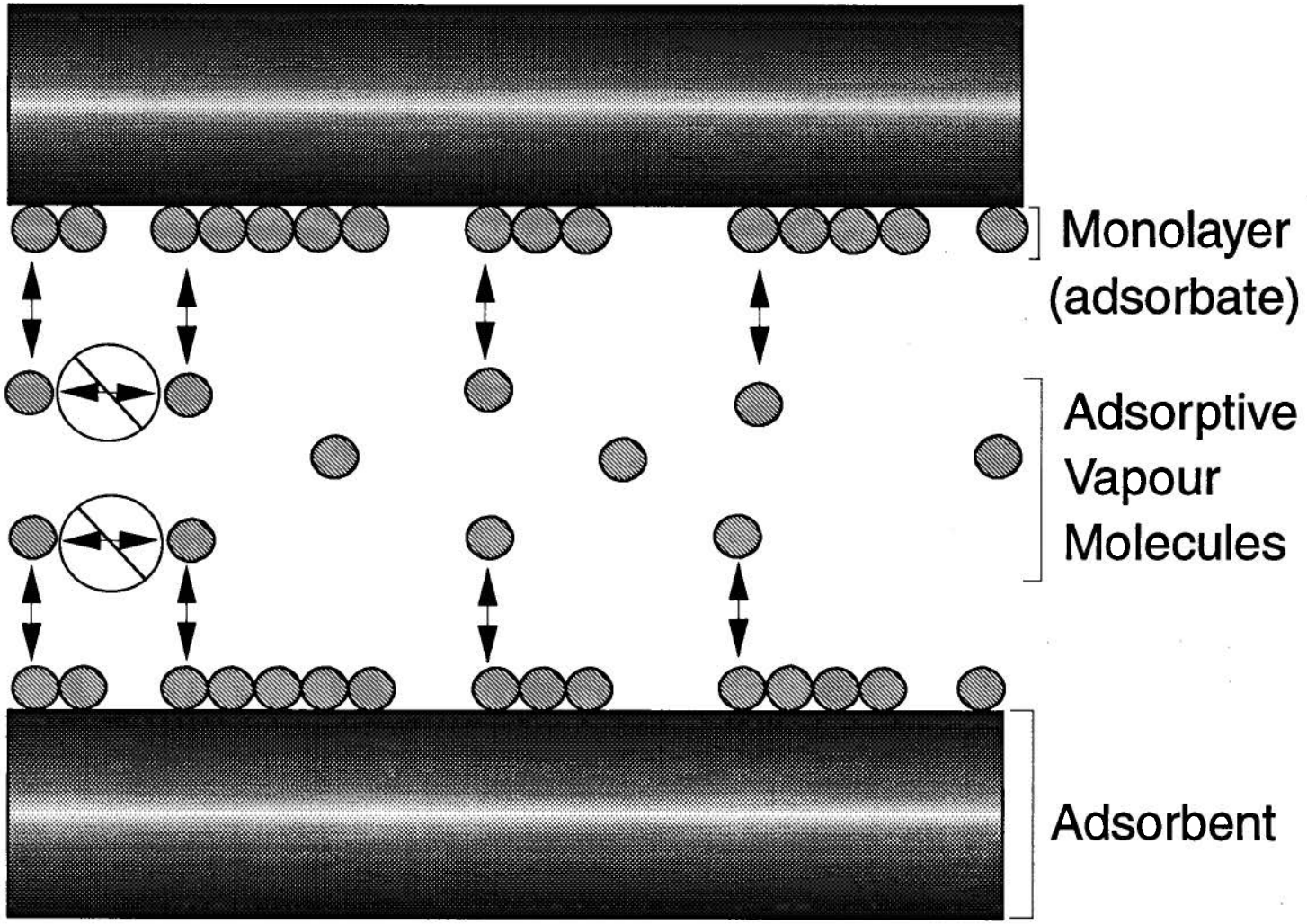

Figure 2-3. Simulation of monolayer formation in a capillary. Arrows indicate direction of interaction of adsorptive molecules. Interaction is assumed to occur in the vertical direction only; arrows with cross through indicate no interaction.

$$(1) \qquad \frac{P}{[V(P_0 - P)]} = \frac{1}{V_m C} + \frac{C - 1}{V_m C}\,[P/P_0]$$

where P_0 is the saturation pressure of the adsorbate, V is the volume adsorbed at equilibrium, and V_m is the volume of adsorbate occupying a monolayer (monolayer volume, or capacity). A version of equation (1) in which a finite number of adsorbed layers is assumed, has been developed (Brunauer et al., 1938; Gregg and Sing, 1982; Lowell and Shields, 1984). An approximation of C is taken to be:

$$(2) \qquad C = \exp\{[E_1 - E_L] / RT\}$$

where the terms are defined as above. The difference between E_1 and E_L is equal to the net heat of adsorption (Gregg and Sing, 1982).

A plot of the left side of equation (1) versus relative pressure should yield a straight line. The values of C and V_m can be obtained from the slope (slope = $[C-1]/V_mC$) and from the intercept (intercept = $1/V_mC$). The monolayer capacity may then be converted to surface area if the adsorbate cross-sectional area is known (Lowell and Shields, 1984).

In summary, the major assumptions made in the derivation of the BET equation are: 1) the energy of adsorption is equal to the heat of liquefaction of the adsorbate for every layer but the first; 2) the conditions of dynamic equilibrium are the same for the second and higher layers; and 3) at saturation, the number of multilayers is infinite, i.e., the adsorbate condenses to a bulk liquid (Gregg and Sing, 1982).

Significance of the BET C value

The BET 'C' value is a parameter that may be used to predict the shape of the isotherm and thus the nature of the adsorbate-adsorbent system. For example, for values of C greater than two, the isotherm described by the BET equation (plot of V/V_m vs. relative pressure), conforms to the shape of a Type II isotherm (Gregg and Sing, 1982). For large values of C, the knee of the isotherm becomes sharper (Figure 2.1, Gregg and Sing, 1982, p.46). If the value of C is less than about 20, it is thought that estimation of the monolayer capacity from either the BET equation or the Point B method may be in error (Gregg and Sing, 1982). This is understandable, since the point of inflection of the Type II (and IV) isotherm is thought to be approximately coincident with the completion of the first monolayer; if the point of inflection of the isotherm is not well developed, the monolayer may not be complete at that point.

An estimation of the relative affinity of an adsorbate for adsorption onto an adsorbent may also be obtained from the C value. The BET C value, as discussed above, is estimated by the relation: $C = \exp \{[E_1 - E_L] / RT\}$. The C value will increase as the net heat of adsorption increases, or in other words, as the affinity of the adsorbate for adsorption upon the adsorbent surface increases. For example, for a Type I and II composite isotherm obtained from a microporous material described in Gregg and Sing (Figure 4.11, 1982), the initial part of the isotherm was steep due to enhanced adsorption. This is reflected in large values of C calculated from the BET equation for the initial portion of the isotherm.

Range of Applicability of the BET Equation

The BET equation is useful for a variety of different isotherms, but application of the equation is generally limited to the relative pressures at which monolayer formation is believed to occur. The range of relative pressures that correspond to nearly complete monolayers for C values between 3 and 1000 is $0.05 \leq P/P_0 \leq 0.35$ (Lowell and Shields, 1984). This range is applicable to most experimental isotherms, and generally good agreement between experimentally

derived isotherms and the calculated BET isotherms has been achieved. Various examples of departure of the BET linear plot (left side of equation (1) vs. relative pressure) from linearity below relative pressures between 0.2 and 0.3 do exist, however (Gregg and Sing, 1982). The BET equation also fails to reproduce experimental isotherm data in the multilayer region (relative pressures $> \sim 0.3$).

Criticisms of BET Theory

The main assumptions of the BET equation were given earlier. Although these assumptions simplify the BET treatment, they are the main source of criticism of the theory.

Lateral interactions between adsorbate molecules are ignored in favour of the adsorbate-adsorbent interactions in BET Theory. Although adsorbate-adsorbent interactions may be negligible far from the adsorbent surface, this is not so within the adsorbate monolayer.

BET Theory assumes that surface adsorption sites are energetically identical. Due to the heterogeneous nature of many solid surfaces (e.g. coal), however, this is likely an erroneous assumption.

The assumption that the heat (or energy) of adsorption in all layers but the first is equal to the heat of liquefaction of the adsorbate may also be in error. As pointed out by Lowell and Shields (1984), polarizing forces are likely to enhance adsorption potentials within at least the first few monolayers and not just the first layer.

Finally, the BET Theory seems to be applicable mainly to a range of relative pressures and adsorbate-adsorbent systems in which monolayer formation occurs. For example, at low relative pressures in an adsorbate-adsorbent system in which the adsorbent is microporous, it is likely that monolayers do not form due to the enhanced potential between pore walls of pores of molecular dimensions.

2.2.2 Type I Isotherm - Dubinin Theory of Volume Filling for Micropores

The initially steep portion of the Type I isotherm, at low relative pressures, is due to enhanced adsorption within a pore with pore walls that are only a few adsorbate molecule diameters apart. Dubinin (1966) envisioned this process as being due to the overlapping of adsorption potentials between the pore walls. Dubinin (1966) also concluded that this process cannot be adequately described by monolayer formation as described by the Langmuir and BET theories. These conclusions were reached from the adsorption of vapours upon carbonaceous adsorbents, in particular activated carbon, at various stages of burn-out. The differential heats of adsorption were found to be considerably higher for the porous activated carbon than for the non-porous carbon black (Figure 3, Dubinin, 1966). The mechanism of volume filling was thus invoked for pores of diameters less than about 2 nm.

Gregg and Sing (Sing, 1982) referred to the process of volume filling as the primary process of adsorption for slit-shaped micropores that are approximately .3 - .7 nm in width as determined from nitrogen at 77 K. They also stated that the degree of enhancement of the interaction potential and thus enthalpy of adsorption is "dependent upon the nature of the adsorbate-adsorbent interaction and the polarizeability of the adsorbate" (Gregg and Sing, p.242). Gregg and Sing went onto define a secondary process for slightly wider slit-shaped pores (.7 - 1.8 nm, obtained as before) in which cooperative effects enhance adsorption to a lesser degree than the primary process. At still larger pore diameters, the process of capillary condensation is believed to occur. The degree of enhancement of adsorption at low relative pressures is thus not strictly a function of pore diameter, but of the ratio of pore diameter to the adsorbate molecule diameter.

Dubinin (1975) states that the process of adsorption in micropores is thermodynamically analogous to the process of solution. The adsorbate-adsorbent system may be treated as a uniphase system in which no interface exists between the adsorbate molecule and the adsorbent surface. The concept of micropore surface area is thus thought to be meaningless. The main control upon gas adsorption in such pores is therefore pore volume, not micropore surface area.

Dubinin (1975) also stated that the main difference between the 'theory of volume filling' for micropores and multilayer adsorption in mesopores, in reference to binary mixtures of vapours, specifically, is that for microporous solids, the selectivity of one adsorbate over the other occurs throughout the entire micropore space whereas in mesoporous materials, the selectivity with respect to the adsorbate is mainly restricted to the first adsorbed monolayer. The adsorption forcefield in micropores may be viewed as continuous throughout the system.

Dubinin and various co-workers went on to formulate equations that described adsorption in the low to medium pressure region of the isotherm starting from Polanyi's potential theory of adsorption, described in the next section.

Polanyi's Potential Theory of Adsorption

The Polanyi Theory of Adsorption is described in Dubinin (1975) and Lowell and Shields (1984) and is only briefly touched on here.

Polanyi envisioned the surface of an adsorbent (Figure 2-4) as having an adsorption potential gradient that extended from the surface to a distance at which the equipotential line for the adsorbate in question is equal to zero (Lowell and Shields, 1984). The adsorbate molecule is thus assumed to occupy a space, referred to as the adsorption volume, between the surface and the zero equipotential line.

A critical parameter is A, defined initially as the adsorption potential (Lowell and Shields, 1984), but later referred to as the differential molar work of adsorption by Dubinin (1966). A is given by the expression:

$$A = RT\ln(P_0/P)$$

An important postulate is that the volume adsorbed at equilibrium relative pressure is dependent upon A. Plots of the adsorption volume vs. A are called "characteristic curves".

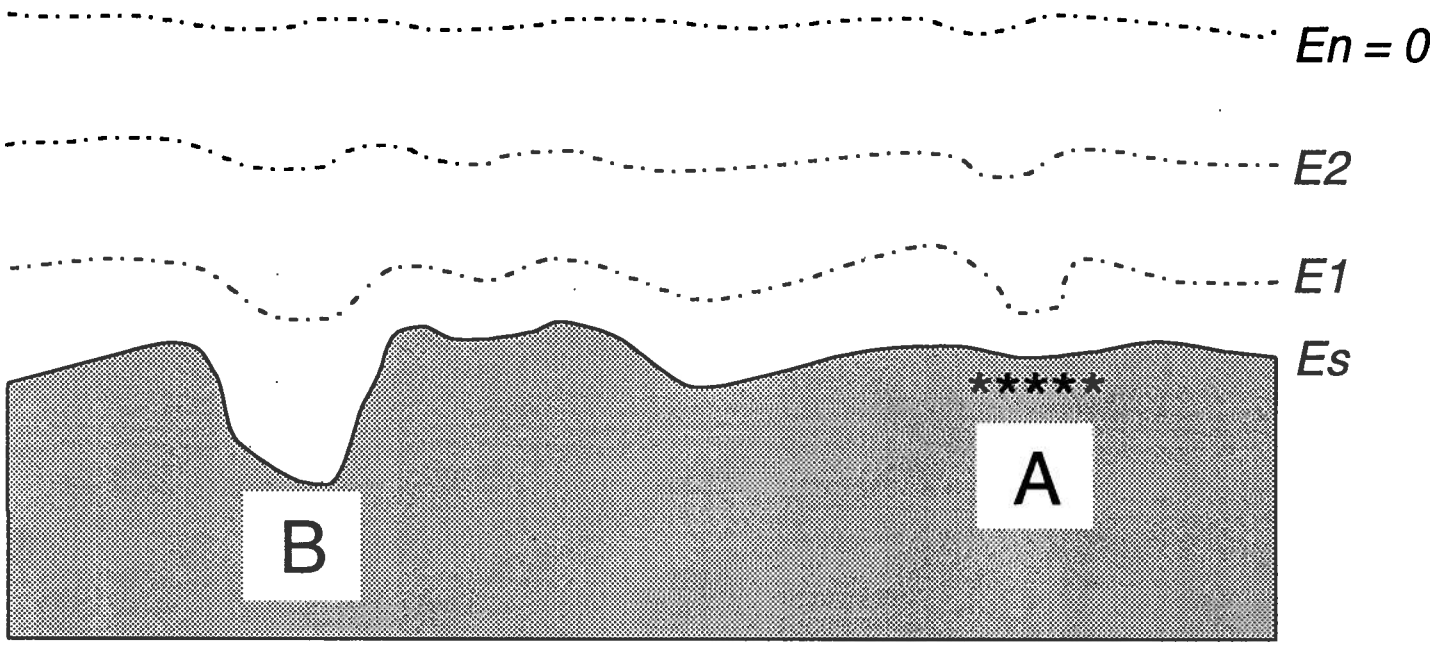

Figure 2-4. Diagram depicting Polanyi's equipotential planes. Points A and B represent a surface impurity and irregularity, respectively. *Es* and *En* are equipotential lines. Modified from Lowell and Shields (1984).

Dubinin-Radushkevich Equation

Several postulates are important to the development of the Dubinin-Radushkevich equation (Dubinin, 1965,1966; Gregg and Sing, 1982).

The first postulate is that the micropore volume is filled through volume filling of the pores, not by conventional multilayer adsorption as described by BET Theory. The parameter θ represents the degree of filling of the micropores and is equal to the ratio of the volume filled by adsorbate at equilibrium pressures to the limiting micropore volume (W/W_0).

Secondly, characteristic curves, or plots of θ vs A, are invariant with temperature ($\{dA/dT\}_W = 0$). Thus, it is assumed that the forces governing adsorption are van der Waals forces, because these are temperature invariant (Marsh, 1987). This postulate is supported by the plotting of characteristic curves for various adsorbate-adsorbent systems at different temperatures. The curves for each adsorbent-adsorbate pair at different temperatures coincide (Figures 5 - 7, Dubinin, 1966).

An important parameter, defined by Dubinin, is β, the relative differential molar work of adsorption or affinity coefficient of the characteristic curve. This parameter is an outcome of a third postulate given by Dubinin, where $\{A/A_0\} = \beta$. According to Dubinin (1965,1966), " at equal filled volumes of the adsorption space, W, the ratio of the differential molar work of adsorption A of a given vapour to the differential molar work of adsorption A_0 of the vapour chosen as the standard is a constant value" (Dubinin, 1966, p.60). The standard adsorbate is often chosen to be benzene, with $\beta = 1$.

A fourth proposition used in the derivation of the Dubinin-Radushkevich equation is that the distribution of pore sizes (or more correctly, the distribution of differential molar works of adsorption (A)) is Gaussian (Dubinin, 1965, 1966; Gregg and Sing, 1982; Lowed and Shields, 1984; Marsh, 1987). The equation thus assumes that the microporous carbonaceous adsorbent is homogeneous (Dublin, 1982) and that the pore size distribution is narrow and does not include

supermicroporosity (Marsh, 1987). Equations to describe wider pore size distributions have been developed (Dubinin, 1982; Rozwadowski and Wojsz, 1984).

Using all of the above propositions, the following equation was formulated:

$$W/W_0 = \theta = \exp[- k(A/\beta)^2]$$

Substituting the equation for A, this becomes (Dubinin, 1966; Gregg and Sing, 1982):

(3) $$W/W_0 = \theta = \exp[- k/\beta^2(RT\ln P_0/P)^2]$$

or

$$W/W_0 = \theta = \exp[-\mathbf{B}(T/\beta)^2\log^2(P_0/P)]$$

where: $\mathbf{B} = 2.303R^2/k$; k is a structural parameter related to pore size (energy) distribution of the adsorbent.

Equation (3) may also be written in the following form for plotting purposes:

$$\log W = \log W_0 - \mathbf{B}(T/\beta)^2[\log^2(P_0/P)]$$

According to Gregg and Sing (1982), W is equal to n/ρ^*, where ρ^* is the adsorbate density. If the temperature of measurement is well below the critical temperature of the adsorbate, ρ^* may be taken as the density of the liquid adsorptive. The limiting volume of the adsorption space may be obtained from equation (3). A monolayer capacity (volume) and monolayer equivalent surface area may also be calculated. The value of W is also referred to as the micropore volume which is obtained from the micropore capacity, the amount of vapour adsorbed into the micropores. The calculated micropore volume may be in error if the effect of the proximity of micropore walls upon the degree of packing of the adsorbate is not taken into account (Sing, 1989). The validity of a micropore surface area has also been questioned by some authors (Marsh, 1987) due to its

dependence upon method of measurement. Micropore surface area must then be referred to as the *equivalent* surface area.

A plot of logW versus $\log^2(P^0/P)$ should yield a straight line if the theory of volume filling of micropores is obeyed. The intercept will give W_0, the limiting volume of the adsorption space, and the slope will yield the ratio $\mathbf{B}/\beta^2$. The gradient of the Dubinin plot is thought to be related to the average pore size and width of the Gaussian distribution (Marsh, 1987); the width of the distribution is given by the parameter k (Gregg and Sing, 1982). Dubinin (1966) found that a linear fit was applicable for a range of adsorbate-adsorbent systems, and that for a particular adsorbate system, the value of W_0 should remain constant for a variety of adsorbates. As Dubinin explains (1966), this fact is not an outcome of the Gurvich rule, since the original rule was formulated for non-microporous adsorbents whose pores filled through capillary condensation.

Marsh (1987) illustrates several examples of non-linearity of the transformed Dubinin plot, and discusses the effect upon obtained pore size distributions. Figure 2-5 shows these deviations and gives explanations for them.

Dubinin-Astakhov Equation

In an attempt to rectify the problem of non-linearity of the transformed Dubinin plot for adsorbents with a broad pore size distribution, Dubinin and Astakhov (Dubinin and Astakhov, 1971; Dubinin, 1975) introduced the Dubinin Astakhov equation, a generalized version of the Dubinin-Radushkevich equation:

(4) $$W/W_0 = \theta = \exp\left[-(RT/E)^n \ln^n(P_0/P)\right]$$

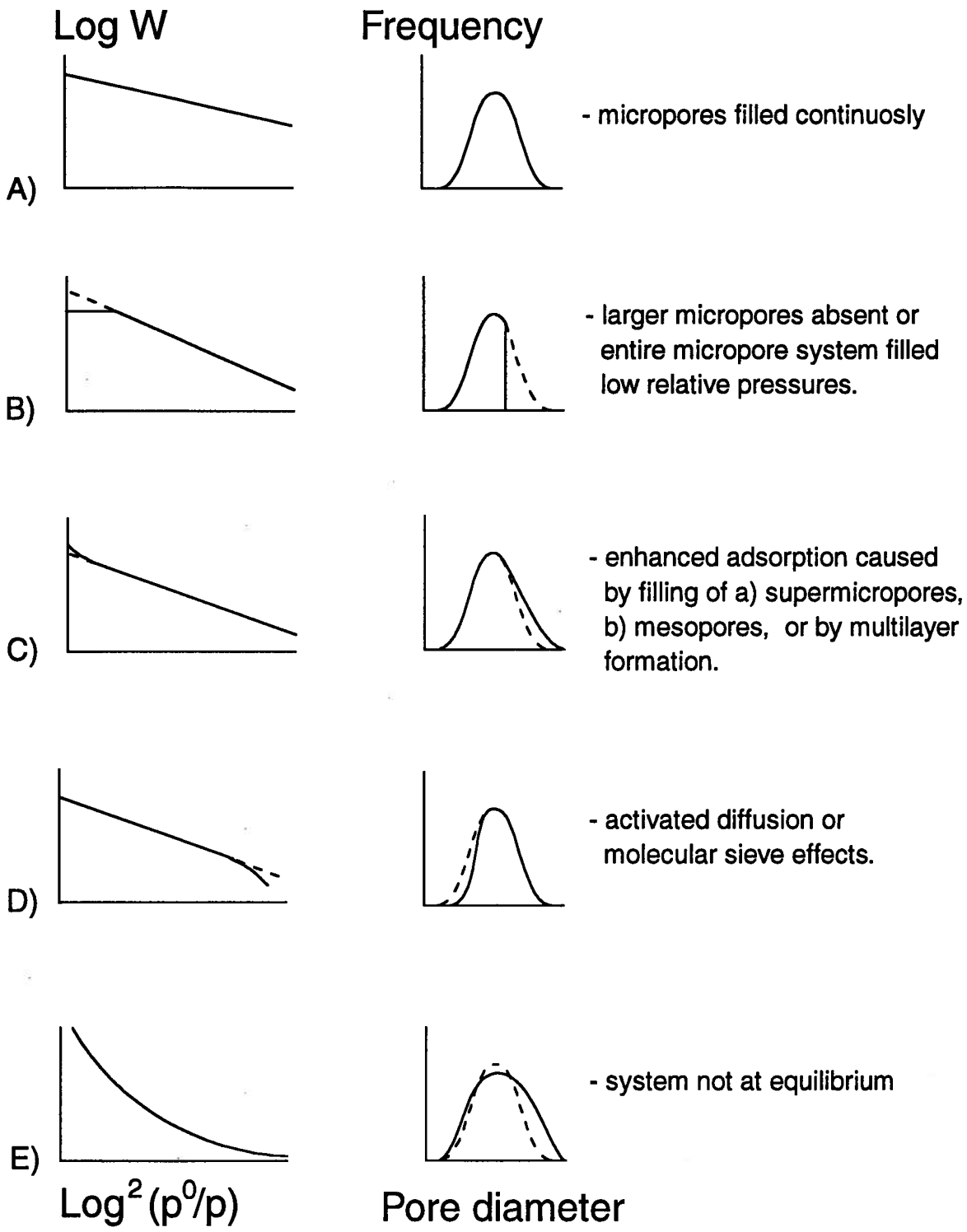

Figure 2-5. Diagram illustrating variations in Dubinin-Radushkevich plots and corresponding pore size distributions. Explanations are obtained from Marsh (1987). Modified from Marsh (1987).

where E is the characteristic free energy of adsorption and is equal to the differential molar work of adsorption for $\theta = .368$ (Gregg and Sing, 1982). This value is thought to be an inverse function of the average micropore size (Stoeckli et al., 1989) and has been related to the half-width of slit-shaped micropores using the radius of gyration obtained from small-angle scattering x-ray techniques (Dubinin, 1982).

The pore size distribution, or more correctly, the energy distribution, in the case of the Dubinin-Astakhov equation is assumed to be Weibull (Dubinin, 1975; Greg and Sing, 1982), not Gaussian. The value of n in the Dubinin-Astakhov equation is optimized between the values of 1 and 4 to obtain a best fit to the linear regression obtained for the transformed Dubinin plot (plot of logW vs $\log^n(P_0/P)$). For the case of $n = 2$, the Dubinin-Astakhov equation assumes the form of the Dubinin-Radushkevich equation. The value of n can thus give an indication of the nature of the pore size distribution. Stoeckli et al. (1989) state that as n varies from 3 to 1.5, the heterogeneity of the micropore size distribution increases; $n = 3$ for truly homogeneous molecular sieve activated carbons, which is contrary to the assumption made by Dubinin (1966) that $n = 2$ for a homogeneous micropore system.

Range of Application of the Dubinin Equations

The Dubinin-Radushkevich equation is generally thought to be valid over the relative pressure range of about $10^{-5} < P/P_0 < 0.1$ (Rozwadowski and Wojsz, 1984). This range is convenient if one uses carbon dioxide as an adsorptive, since the carbon dioxide has a saturation pressure at 298 K of ~ 48,200 mmHg. The high saturation pressure allows measurements to be taken below one atmosphere (760 mmHg). Most other methods of isotherm interpretation are not valid at relative pressures below 0.02.

The Dubinin-Astakhov equation has been shown (Dubinin, 1975) to have a lower boundary of application at pore fillings (θ) of about 0.15 - 0.2. The second Dubinin postulate ($\{dA/dt\}_W = 0$) is not obeyed for lower values of filling.

Criticisms of Dubinin Theory

Sing (1989) states that " at present, there is no reliable procedure available for the computation of the micropore size distribution from a single isotherm". This statement stems from the fact that there is no strict mathematical description of the adsorption process in micropores that takes into account the variability of all adsorbate-adsorbent systems.

The Dubinin equations attempt to determine a micropore size distribution based on the distribution of adsorption potentials which is assumed to obey a standard distribution type (Gaussian, Rayleigh, or Weibull). As Marsh (1987) states " the fact that so many adsorption isotherms can be linearized in Dubinin-Radushkevich coordinates (whereas random curves resembling isotherms cannot be linearized) is telling us that some property of microporosity is being exhibited". This is contrary to some criticisms (Sutherland, 1967) that accuse the Dubinin equations of linearizing random curves (Freeman et al., 1970). The Dubinin-Radushkevich transformed isotherm plot is not linear for many adsorbate-adsorbent systems, which is in direct contradiction to the accusations made by Sutherland (1967). The fact that the Dubinin plots are not linear for many systems leads to the following criticism, however.

Deviation of the Dubinin-Radushkevich plot from linearity in some systems may result from several reasons. Some degree of heterogeneity in the micropore system may cause the deviation, in which case the Dubinin-Astakhov equation may provide a better model for the system. Other modifications of the Dubinin-Radushkevich equation have also been developed to account for micropore heterogeneity (Dubinin, 1966; Dubinin and Stoeckli, 1980). Deviation from linearity in the Dubinin-Radushkevich plot can also be caused by chemical adsorption which may occur in addition to physical adsorption. Since chemisorption is temperature dependent, the amount of adsorbate uptake is also dependent upon temperature (Marsh, 1987). The gradient of Dubinin-Radushkevich (D-R) plots appears to be dependent upon temperature in that the gradient decreases with increasing temperature for polar adsorbates. Thus, if chemisorption is occurring, it can be predicted through the use of the D-R plots, and therefore the results may be examined

critically. One additional cause of D-R plot deviation at low relative pressures is activated diffusion or molecular sieve effects (Figure 2-5).

Although the semi-empirical Dubinin equations are not able to model all adsorbate-adsorbent systems accurately, their value comes in their ability to predict the nature of the micropore size distributions and adsorbate-adsorbent interactions.

2.2.3 Type IV Isotherm - BJH Theory

The Type IV isotherm is unique in that at relative pressures of ~0.42 and above (for nitrogen as an adsorbate at 77 K), a hysteresis loop is encountered (Gregg and Sing, 1982). Mesoporous solids typically yield a Type IV isotherm. Significant enhancement of adsorption may occur at relative pressures above and below the point of closure of the hysteresis loop for a mesoporous solid as compared to the equivalent non-porous solid. This is thought to be due to the occurrence of capillary condensation within the mesopores. The concept of capillary condensation and the Kelvin equation are key to the BJH (Barrett, Joyner, Halenda) Theory as well as many other theories describing the Type IV isotherm. Before BJH Theory is discussed, however, the Kelvin and Halsey equations are examined.

The Kelvin Equation

The basic form of the Kelvin equation used in examination of the Type IV isotherm is (Gregg and Sing, 1982):

$$\ln P/P_0 = (-2\gamma V_L)/(RTr_m)$$

where P/P_0 is the relative pressure, γ is the surface tension of the liquid adsorptive, V_L is the molar volume of the liquid adsorptive, and r_m is the mean radius of curvature of the meniscus between the liquid adsorptive and its vapour at equilibrium.

The Kelvin equation, when applied to cylindrical pores, takes the form:

$$\ln P/P_0 = \frac{(-2\gamma VL)}{(r_k RT)} \cos\theta$$

where r_k (Figure 2-6) is the Kelvin pore radius (or core radius), and θ is the angle of contact between the capillary condensate and an adsorbed film on the pore wall, which is often assumed to be equal to zero (Sato, 1981; Gregg and Sing, 1982; Lowell and Shields, 1984). The assumption that the contact angle is equal to zero has been questioned (Gregg and Sing, 1982) but is widely used.

The Kelvin equation was derived on thermodynamic grounds, and accounts for the mechanical and physicochemical equilibrium established between a liquid and its vapour across a meniscus at a particular relative pressure. The equation states that at equilibrium pressures less than the saturation pressure, the vapour may be in equilibrium with the condensed liquid adsorbate, depending on the radius of curvature of the (concave) meniscus. At saturation vapour pressure, the radius is infinite, and the equation describes the equilibrium between the vapour and the bulk liquid across a planar surface. The Kelvin equation therefore gives the radius of the core of a pore in which capillary condensation occurs at a given P/P_0.

Pore size distributions are obtained by relating the curvature of the liquid/vapour interface to the radius of the pore. Assuming that the pore shape is cylindrical, and that the angle of contact between the capillary condensate and the adsorbed film is zero, the Kelvin radius is taken as being equal to the radius of the pore core (Figure 2-6). The Kelvin radius is thus not equal to the radius of the pore itself, but of the pore core since an adsorbed film already exists on the pore walls at the given relative pressure. The pore radius is then given by:

$$r_p = r_k + t$$

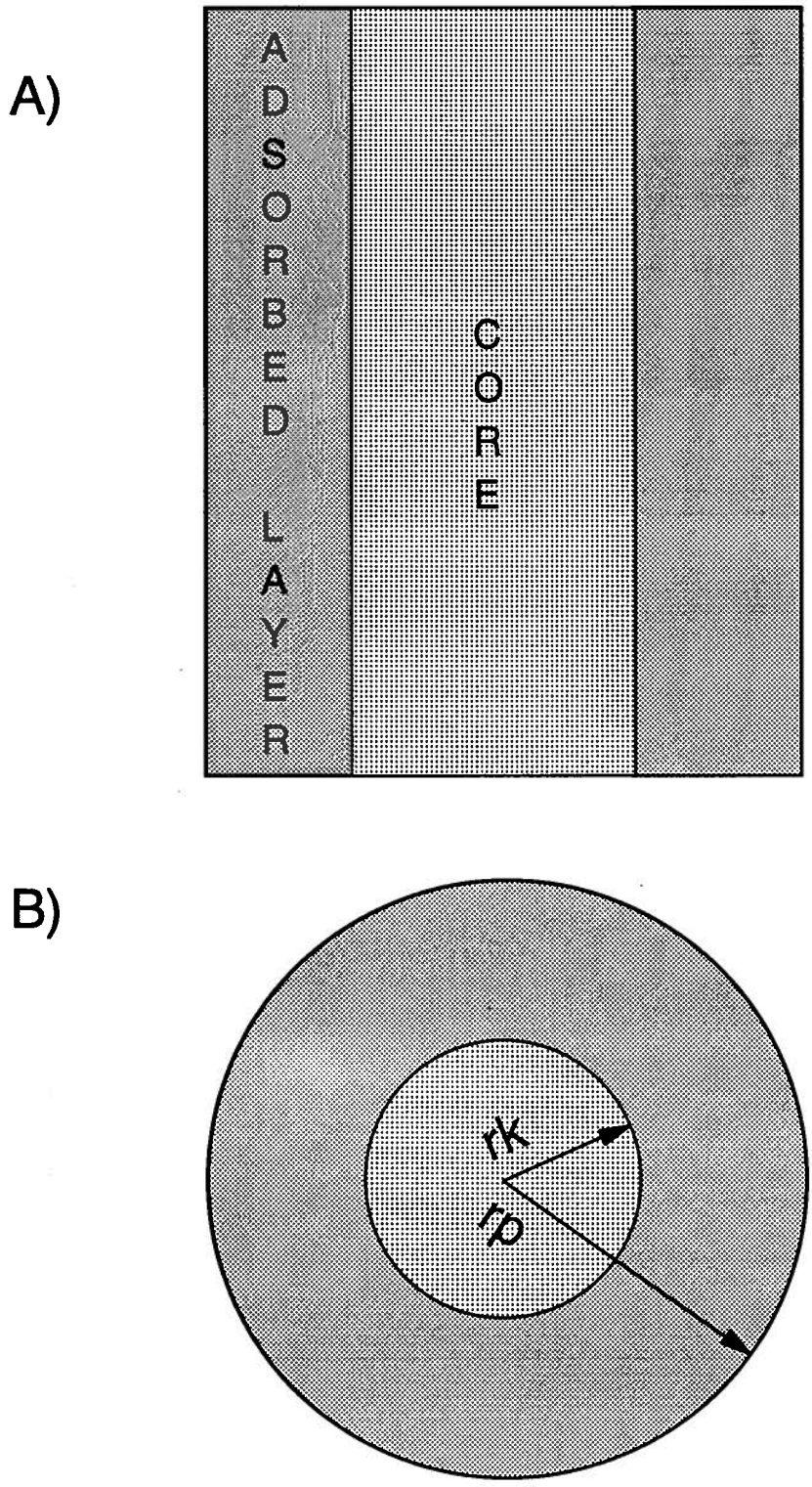

Figure 2-6. Diagram A) shows the location of the adsorbed film and pore core in a cylindrical capillary; B) illustrates the difference between the Kelvin (rk) and pore (rp) radii.

where r_p is the radius of the pore, r_k is the Kelvin radius, and t is the thickness of the adsorbed film. The thickness of the adsorbed film may be calculated by various methods, but only the Halsey equation will be discussed here.

The Halsey Equation

The Halsey equation is based on the assumption that the thickness of an adsorbed layer on a planar surface is the same as that on the the internal surface of a pore (Sato, 1981; Lowell and Shields, 1984). The thickness of the absorbed film is given by the following expression:

$$t = W_a/W_m \times \tau$$

where t is the thickness of the adsorbed film, W_a is the amount adsorbed at the given relative pressure, W_m is the amount adsorbed in a layer of adsorbate molecular thickness (BET monolayer capacity), and τ is the thickness of the monolayer. The thickness of the monolayer may be obtained from:

$$\tau = V_L/S$$

where V_L is the adsorbate molar liquid volume, and S is the surface area occupied by spreading a mole of liquid adsorbate over a planar surface to a thickness of one adsorbate molecule. For nitrogen, the monolayer thickness is ~ .354 nm. A plot of W_a/W_m versus the relative pressure yields a Type II isotherm which may be described by the Halsey equation in the form of (Lowell and Shields, 1984):

$$t = .354 \times [5/\ln(P_0/P)]^{1/3}$$

BJH Theory

The BJH Theory (Barrett et al., 1951) is based upon the Wheeler equation which may be expressed as:

$$V_0 - V = \pi \int (r - t)^2 L(r)\, dr$$

where the integration is carried from r_{Pn}, the radius of largest pore filled at a given pressure, to infinity; V_0 is the volume of adsorbate adsorbed at saturation vapour pressure; V is the volume adsorbed at the equilibrium pressure; L(r) is the length of pores with radii lying between r and r + dr; t is the multilayer thickness at equilibrium pressure.

BJH Theory does not make the assumption that the pore size distribution has a definite shape (Gaussian or Maxwell) or that the adsorbed layer does not change thickness, as assumed in earlier theories. The theory does, however, make two fundamental assumptions: the pores are cylindrical in shape, and the two mechanisms of capillary condensation and multilayer formation lead to pore filling.

The step by step description of how BJH calculates pore size distributions, volumes and surface areas are discussed by Barrett et al. (1951) and Gregg and Sing (1982).

Range of Applicability of BJH Theory

The range of applicability of the BJH method for predicting pore size distributions is intimately related to the range of applicability of the Kelvin equation. Gregg and Sing (1982) discuss the various different controls upon the range of the Kelvin equation including the curvature and the tensile strength effects. Gregg and Sing also state that although a theoretical limit for the upper range of the Kelvin equation does not exist (if $\theta < 90°$), a practical limit does occur. In using nitrogen as an adsorbate at T = 77 K, uncertainty in temperature measurements at relative pressures close to unity may lead to large errors in the calculation of r_m. Barrett et al.

(1951) impose a practical upper limit of about 30 nm for pore radius measurements. The lower limit imposed for the Kelvin equation stems from the uncertainties involving adsorbate molar volumes and surface tensions in very fine pores and is usually set at about 1 - 1.5 nm (Lowell and Shields, 1984). Kadlec (1989) has proposed a more generalized version of the Kelvin equation.

Type IV Isotherm Hysteresis

As mentioned earlier, the desorption and adsorption branches at relative pressures > 0.3 are not coincident for the Type IV isotherm, and therefore the process of adsorption-desorption is not reversible. Pore shape is interpreted as being the cause of hysteresis in mesopores as evaporation and condensation occur in different portions of the pore at the same relative pressure (Gregg and Sing, 1982). The fact that two relative pressures occur for the same degree of uptake is cause for concern in trying to obtain pore size distributions through the use of the Kelvin equation. The desorption branch of the isotherm is often chosen for pore size distribution analysis on thermodynamic grounds (Lowell and Shields, 1984). There are exceptions to this rule, however (see Gregg and Sing, 1982).

Five types of hysteresis loops are given by de Boer (1958) based on various different pore shapes. Three of the common hysteresis loops are given in Figure 2-7. Type A hysterisis is generally associated with agglomerates with narrow pore size distributions (Sing et al., 1985); Type B hysteresis is caused by slit shaped pores; and Type E hysteresis is caused by "bottleneck" pores. Gregg and Sing (1982) analyze the various different pore shape models and resulting hystersis by utilizing the Kelvin equation.

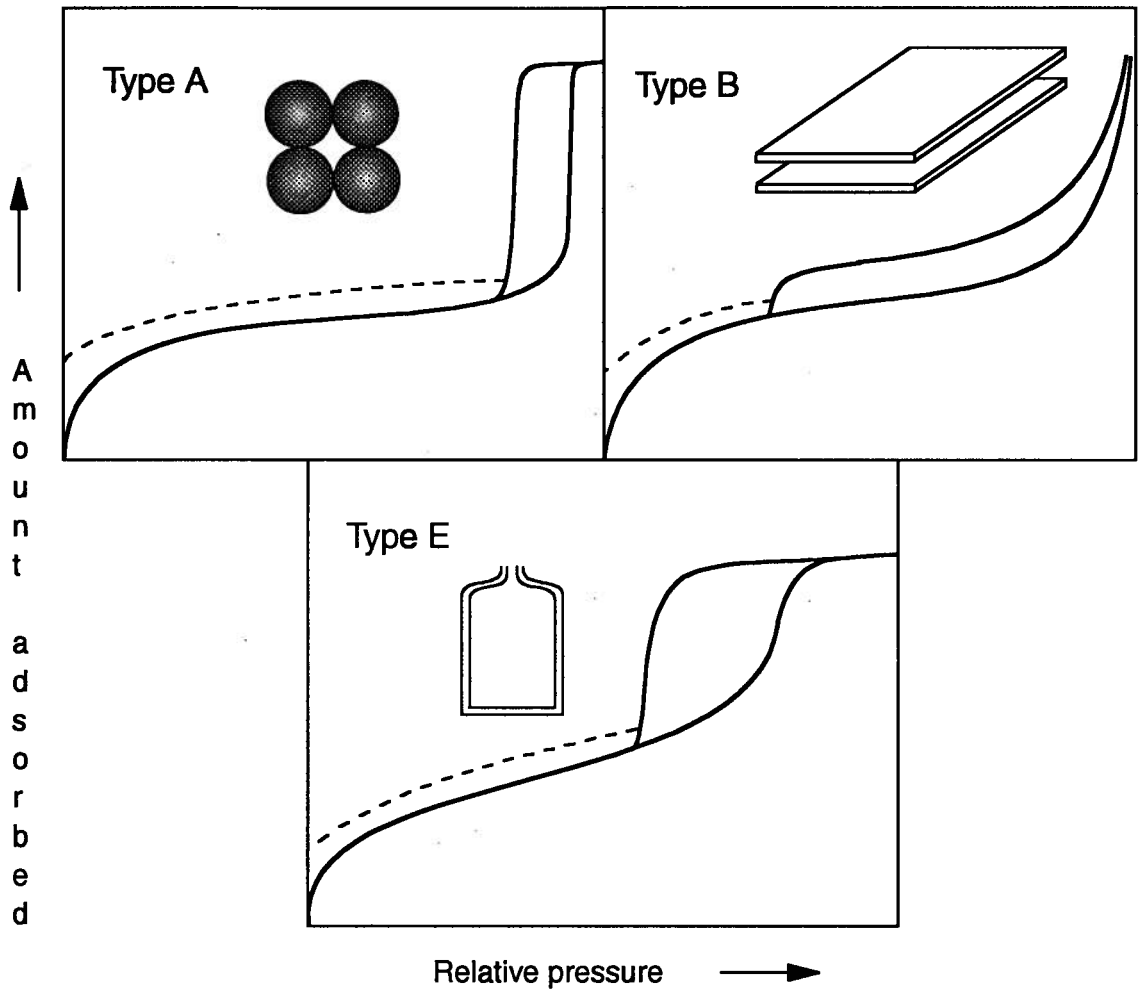

Figure 2-7. Revised de Boer hysteresis loop classification showing the three most common forms. Also shown are the corresponding pore shapes. Possible low pressure hysteresis is indicated with dotted lines. Modified from Gregg and Sing (1982).

2.3 CHOICE OF ADSORBATE

As can be inferred from the discussion of the forces governing adsorption, the choice of adsorbate in a particular adsorbate-adsorbent system is critical in determining the type of interaction during adsorption. Indeed, if the interaction between the adsorbent-adsorbate pair is not governed strictly by dispersion forces (i.e. van der Waals forces), such as would be the case if the adsorbate possessed a permanent dipole moment and the adsorbent were polar, then the above equations (BET, Dubinin etc.), which are based on physical adsorption, are not valid. The following discussion will address this issue as well as others in choosing the proper adsorptive for the meso-microporosity of coals.

Nitrogen gas at analysis temperatures of 77 K is a popular choice for determining BET surface areas and pore size distributions of mesoporous solids. The properties of nitrogen gas that make it an effective adsorbate are: 1) small enough BET C value to preclude localized adsorption, but not too small to be excessively mobile at the adsorbent surface (Lowell and Shields, 1984); 2) the saturation pressure of the gas is sufficiently large that a wide range of relative pressures may be obtained accurately (Gregg and Sing, 1982); 3) nitrogen gas is inert; 4) the cross-sectional area of the molecule is well established from liquid density calculations (0.162 nm^2) and is relatively small; and 4), the analysis bath temperature of 77 K is easily achieved with liquid nitrogen.

Some problems are encountered with the use of nitrogen as an adsorbate for microporous solids such as coals. Nitrogen has been shown to exhibit a positive temperature dependence with respect to uptake (Mahajan, 1991). This is thought to be due to activated diffusion effects in which a significant activation energy for diffusion must be overcome by the nitrogen molecule before entry into fine pores is allowed. The activation energy for diffusion of nitrogen has been shown to be significantly larger than that for carbon dioxide, despite the small difference in their average diameters (0.365 nm for nitrogen, 0.33 nm for carbon dioxide; Mahajan, 1991). Rao (1991) gives the example that the energy barrier for carbon dioxide for entry into a pore 0.542 nm

in diameter is zero, whereas for nitrogen the energy barrier is 24.3 kJ/mol. Thus, microporous materials such as coal display molecular sieving characteristics towards the nitrogen molecule.

Due to the problem of activated entry of nitrogen into micropores, the carbon dioxide molecule was suggested as an adsorbate to be used for microporous materials (Walker and Kini, 1965; Mahajan, 1991). At the temperatures commonly used in the measurement of surface area with carbon dioxide as an adsorbate gas (273 - 298 K), the carbon dioxide molecule does not appear to display activated diffusion effects, and therefore is adsorbed more readily than the nitrogen molecule at 77 K (Marsh, 1987). Mahajan (1991, p. 736) states: "adsorption of CO_2 at 25°C should invariably measure essentially the total surface area of coals" and that at the same temperature "essentially the entire pore volume of all the coals studied would be filled with CO_2".

Use of carbon dioxide as an adsorbate for microporous adsorbents has been criticized for several reasons, however. Firstly, the carbon dioxide molecule is known to possess a quadrupolar moment, and may interact with the hydroxyl- and oxygen- containing functional groups at the coal surface to form chemical bonds. Not all authors are in agreement with this view, however (Mahajan, 1991). Secondly, the carbon dioxide molecule is thought to induce swelling behaviour in coal due to imbibition, and therefore lead to artificially high surface areas. Mahajan (1991, p. 740) states, however, that: "CO_2 gives higher surface areas compared to other adsorbates because, through imbibition, it is available to both open and closed porosity, and at CO_2 pressure < 760 mmHg and short 'equilibrium' times the contribution of swelling to total surface area is small". The reporting of carbon dioxide and surface areas are suspect, however, because the cross-sectional area of the molecule is not well established in micropores.

In summary, for the current study, nitrogen is used as an adsorbate gas for the determination of mesopore size distribution and surface area analyses, due to its universal acceptance for this purpose, and carbon dioxide is used for micropore size distributions and monolayer capacities due to lack of activated diffusion characteristics. In the results of Chapter 3, the potential problems associated with using carbon dioxide as an adsorbate are considered.

2.4 CONCLUSIONS

It is obvious from the above discussion that the process of adsorption of vapour onto the internal porosity of adsorbents, particularly microporous adsorbents, is a complex process. There is no universal mathematical treatment that adequately describes all aspects of the adsorption process for all adsorbate-adsorbent systems under all conditions, nor for microporous systems, is it possible to observe the process. The current theories of adsorption for meso- and microporosity make many assumptions, often tacit, about the process of adsorption, and their critical application is recommended. The IUPAC has published a guide to reporting adsorption data that attempts to minimize the ambiguity that is often found in the literature (Sing et al., 1985). Indeed, pore size distributions and surface area results obtained are a function of the theories of adsorption and experimental procedure used in their calculation.

2.5 REFERENCES

Barrett, E.P., Joyner, L.G., and Halenda, P.P., 1951. The determination of pore volume and area distributions in porous substances. I. Computations from nitrogen isotherms. The Journal of the American Chemical Society, 73: 373-380.

Brunauer, S., Deming, L.S., Deming, W.S., and Teller, E., 1940. On a theory of van der Waals adsorption of gases. The Journal of the American Chemical Society, 62: 1723-1732.

Brunauer, S., and Emmett, P.H., 1937. The use of low temperature van der Waals adsorption isotherms in determining surface areas of various adsorbents. The Journal of the American Chemical Society, 59: 2682-2689.

Brunauer, S., Emmett, P.H., and Teller, E., 1938. Adsorption of gases in multimolecular layers. The Journal of the American Chemical Society, 60: 309-319.

de Boer, J.H., 1958. In: D.H. Everett and F.S. Stone (Editors), The Structure and Properties of Porous Materials. Butterworth, England, p. 68.

Dubinin, M.M., 1965. Theory of the bulk saturation of microporous activated charcoals during adsorption of gases and vapours. Russion Journal of Physical Chemistry, 39: 697-704.

Dubinin, M.M., 1966. Porous structure and adsorption properties of active carbons. In: P.L. Walker, Jr. (Editor), Chemistry and Physics of Carbon, Volume 2. Edward Arnold, Ltd., New York. pp. 51-120.

Dubinin, M.M., 1975. Physical adsorption of gases and vapors in micropores. In: D.A.Cadenhead, J.F. Danielli, and M.D. Rosenberg (Editors), Progress in surface and membrane science, Volume 9. Academic press, New York. pp. 1-70.

Dubinin, M.M., 1982. Microporous structures of carbonaceous adsorbents. Carbon, 20: 195-200.

Dubinin, M.M., and Astakhov, V.A., 1971. Description of adsorption equilibria of vapors on zeolites over wide ranges of temperature and pressure. Advances in Chemistry Series, No. 102: p102.

Dubinin, M.M., and Stoeckli, H.F., 1980. Homogeneous and heterogeneous micropore structures in carbonaceous adsorbents. Journal of Colloid and Interface Science, 75: pp. 34-42.

Emmett, P.H. and Brunauer, S., 1937. The use of low temperature van derWaals adsorption isotherms in determining the surface area of iron synthetic ammonia catalysts. The Journal of the American Chemical Society, 59: 1553-1564.

Freeman, E.M., Siemieniewska, T., Marsh, H., and Rand, B., 1970. A critique and experimental observations of the applicability to microporosity of the Dubinin equation of adsorption. Carbon, 8: 7-17.

Fyfe, W.S., 1964. Geochemistry of solids. Mcgraw-Hill Book Company, New York, 199 pp.

Gregg, S.J., and Sing, K.S.W., 1982. Adsorption, Surface Area and Porosity, Second Edition. Academic Press, New York. 303 pp.

Jaroniec, M., Madey, R., Choma, J., McEnaney, B., and Mays, T.J., 1989. Comparison of adsorption methods for characterizing the microporosity of activated carbons. Carbon, 27: 77-83.

Kadlec, O., 1989. On the theory of capillary condensation and mercury intrusion in determining carbon porosity. Carbon, 27: 141-155.

Langmuir, I., 1916. The constitution and fundamental properties of solids and liquids. The Journal of the American Chemical Society, 38: 2221-2295.

Lowell, S., and Shields, J.E., 1984. Powder Surface Area and Porosity, Second Edition. Chapman and Hall, London, 234 pp.

Mahajan, O.P., 1991. CO_2 surface area of coals: the 25 year paradox. Carbon, 29: 735-742.

Mahajan, O.P., and Walker, P.L., Jr. 1978. Porosity of coal and coal products. In: C. Karr, Jr (Editor), Analytical Methods for Coal and Coal Products, Volume I. Academic Press, New York. pp. 125-162.

Marsh, H., 1987. Adsorption methods to study microporosity in coals and carbon - a critique. Carbon, 25: 49-58.

McEnaney, B., 1987. Estimation of the dimensions of micropores in active carbons using the Dubinin-Radushkevich equation. Carbon, 25: 69-75.

Orr, C., 1977. Pore size and volume measurement. In: I.M. Kolthoff, P.J. Elving, and F.H. Stross (Editors), Treatise on Analytical Chemistry Part III, Volume 4. John Wiley and Sons, New York. pp. 359-402.

Orr, C., 1977. Surface area measurement. In: I.M. Kolthoff, P. J. Elving, and F.H. Stross (Editors), Treatise on Analytical Chemistry Part III, Volume 4, John Wiley and Sons, New York. pp. 321-358.

Rao, M.B., 1991. Diffusion through carbon micropores - 4 years later. Carbon, 29: 813-815.

Rodriguez-Reinoso, F., Garrido, J., Martin-Martinez, Molina-Sabio, M., and Torregrosa, R., 1989. The combined use of different approaches in the characterization of microporous carbons. Carbon, 27: 23-32.

Rozwadowski, M., and Wojsz, R., 1984. An attempt at determination of the structural heterogeneity of microporous adsorbents. Carbon, 22: 363-367.

Sato, T., 1981. Methane recovery from coal beds: surface and physical properties of western United States coals; M. Sci thesis, The University of New Mexico, 78 pp., unpublished.

Sing, K.S.W., D.H. Everett, Haul, R.A.W., Moscou, L., Pierotti, R.A., Rouquerol, J., and Siemienewska, T., 1985. Reporting physisorption data for gas/solid systems with special reference to the determination of surface area and porosity. Pure and Applied Chemistry, 57: 603-619.

Sing, K.S.W., 1989. The use of physisorption for the characterization of microporous carbons. Carbon, 27: 5-11.

Sutherland, J.W., 1967. In: R.L. Bond (Editor), Porous Carbon Solids. Academic Press, New York. p. 1.

Stoeckli, H.F., Kraehenbuehl, Ballerini, L., and De Bernardini, S., 1989. Recent developments in the Dubinin equation. Carbon, 27: 125-128.

Wojsz, R., and Rozwadowski, M., 1989. The micropore structure analysis of active carbons. Carbon, 27: 135-139.

CHAPTER 3

VARIATION IN MICROPORE CAPACITY AND SIZE DISTRIBUTION WITH COMPOSITION IN HIGH AND MEDIUM-VOLATILE BITUMINOUS COAL OF THE WESTERN CANADIAN SEDIMENTARY BASIN: IMPLICATIONS FOR COALBED METHANE POTENTIAL.

3.1 ABSTRACT

The effect of lithotype, maceral composition and mineral content upon the micropore capacity and size distribution is investigated for a medium-volatile bituminous coal from the mid-Cretaceous Gates Formation of northeast British Columbia and a high-volatile bituminous coal from the Cretaceous of Alberta. Vitrinite content ranges from 18 to 95 % (volume %, mineral matter-free) for the Gates coal and 36 to 85 % for the Alberta coal. Ash yields vary from 4.4 to 33.7 (weight %) for the Gates coal and 1.2 to 10.6 % for the Alberta coal. Dubinin-Radushkevich carbon dioxide micropore capacities, measured at 298 K, range from 21.7 to 39.8 cm^3/g (mineral matter-free) for the Gates coals and 34.1 to 49.7 cm^3/g for the Alberta coal. Low -pressure Dubinin micropore capacities, Langmuir and BET monolayer volumes, measured at 298 and 273 K, generally increase with total and structured vitrinite content and, conversely, decrease with inertinite and mineral matter content. A similar trend is found for high-pressure Langmuir methane monolayer capacities determined for the Gates coals; the methane monolayer capacities are smaller but correlatable with the carbon dioxide micropore capacities. The increase in micropore capacity with vitrinite content is due to an increase in the number of micropores, as demonstrated by Dubinin-Astakhov micropore size distributions. For the Gates suite, a sample with both a high total vitrinite content and semifusinite content yielded the largest micropore capacity which may be due to the creation of micropore capacity through burning (charring) during semifusinite formation. Micropore heterogeneity and mean pore size increase with an increase in inertinite and mineral matter content. Coal composition thus appears to be an

important control upon the micropore capacity, size distribution, and hence, the gas content of bituminous coals.

3.2 INTRODUCTION

Large quantities of natural gas, often mainly methane, are produced during the biochemical and geochemical or thermogenic stage of coalification. Much of this gas is lost to surrounding sediments, groundwater or to the atmosphere but significant quanitities may be retained, depending upon the character of the coal reservoir.

Gas may be retained in the coalbed reservoir in several forms: 1) as free gas (gas in excess of that which can be sorbed, in the cleats, fractures and porosity of the coal) 2) as a solute in groundwater occupying the coal reservoir; and 3) as sorbed gas upon the internal surfaces (e.g. in micropores) or within the molecular structure of the coal (Rightmire, 1984; Murray et al., 1991; Ertekin, 1991; Rice, 1993). The third mechanism, sorbed gas, is the primary mechanism for methane gas retention in coal (Rightmire, 1984).

The amount of gas that may be sorbed appears to be dependant upon pore size (Gan et al., 1972). In meso- (pore diameters between 2 and 50 nm) and macroporous (pore diameters > 50 nm) materials, the pores are thought to be filled with adsorbate by multilayer adsorption upon the internal pore surface (Chapter 2). Total internal surface area therefore appears to be the primary controlling factor upon gas sorption in such materials.

Greater gas sorption has been shown to occur in microporous substances (pore diameters < 2 nm) such as activated carbons, zeolites (Dubinin, 1966), and coals (Gan et al., 1972) than in mesoporous and macroporous solids of similar composition. Micropores are believed to be filled by volume filling (Dubinin, 1975; Jaroniec and Choma, 1989) as opposed to layer by layer adsorption on the internal surface of the pores, therefore micropore volume, not surface area, appears to be the main control on gas sorption for microporous materials. The proportion that microporosity contributes to the total pore volume is thus an important parameter in evaluating the gas sorption characteristics of a solid.

The portion of total pore volume occupied by the various pore size fractions (micro-, meso-, macroporosity) was determined for coals of varying rank by Gan et al. (1972). For vitrinite-rich coals with carbon contents between 76 and 84 %, micropores and mesopores make up the bulk of the porosity but, for coals of similar maceral composition but with carbon contents less than 75 %, the porosity is mainly macroporosity. It should be noted that Gan et al. defined micropores as pores with diameters between 0.4 and 1.2 nm, transitional (meso-) pores as pores with diameters between 1.2 and 30 nm, and macropores as pores with diameters between 30 and 2,960 nm. This pore size classification differs from the current IUPAC classification (Chapter 2) which is used in this thesis.

Carbon dioxide surface areas of the coals studied by Gan et al. (1972) were found to vary in the following way with rank: coals of medium-volatile bituminous to anthracite (> 85 % C) rank yielded surface areas between 196 - 426 m^2/g, high volatile bituminous coals (75 - 85 % C) yielded surface areas between 96 - 228 m^2/g and low rank coals (< 75 % C) had surface areas between 225 and 359 m^2/g.

Another important factor affecting pore size distributions and surface areas in coal is composition. Considerable scatter exists in the surface area values given by Gan et al. (1972) for coals of similar rank which may be due to the variability in coal composition (Lamberson and Bustin, 1993). Harris and Yust (1976;1979) studied high volatile bituminous coal using a transmission electron microscope to determine the pore size and porosity distributions associated with the three major maceral groups (vitrinite, inertinite, and liptinite). Vitrinite was found to be mainly micro- and mesoporous; inertinite, the most porous maceral group, was found to be mainly mesoporous; and liptinite, the least porous maceral group, was found to be mainly macroporous. Detailed studies of how coal composition affects gas adsorption characteristics have occurred only recently (Clarkson et al., 1993; Lamberson and Bustin, 1993).

Coal composition may also have an impact upon the producibility of the coalbed methane resource.Ertekin et al. (1991) have shown that a typical coalbed methane production well has two characteristic production rate peaks. The first peak occurs as entrained water is flushed from the fracture system, leading to an increase in the permeability of the reservoir to gas. The second

peak occurs as gas is desorbed and diffuses through the micropore network and ultimately into the fracture system. Ertekin et al. (1991) demonstrated that the magnitude and time of occurrence of the first and second production peaks are affected by several reservoir properties including coal seam thickness, porosity, permeability, and sorption characteristics. Studies involving the determination of gas adsorption characteristics of coals of varying composition should therefore provide valuable production information.

3.2.1 Research Objectives

Factors affecting the natural gas content of and producibility from coal such as thickness and continuity of the coal seam, rank, pressure, fracture permeability, amount of mineral matter, and hydrologic conditions have been investigated in some detail (Kim, 1977; Meissner, 1984; Fassett, J.E., 1987; Dawson and Clow, 1992; and Ayers and Kaiser, 1992). The pore structure and resulting pore volume and associated effective internal surface area of a coal is an important control upon methane gas adsorption and hence retention within coalbeds. The effect of rank upon the pore structure and internal surface area of coals as well as methane gas retention has been investigated thoroughly (Gan et al., 1972; Meissner, 1984) but little attention until now has been focused upon the effect of coal composition, particularly the organic fraction, on the pore structure and gas adsorption characteristics of coal.

Coal composition (organic and inorganic) has an important control upon gas sorption characteristics, and, hence, total gas content. It is the objective of the current study to evaluate the effect of coal composition upon the gas sorption characteristics of coal suites from two regions of the WCSB. In this study, the micropore capacity (monolayer capacity), surface area, and micropore size distribution of coals of varying maceral and mineral composition are investigated.

3.3 BACKGROUND

3.3.1 Dubinin Theory of Volume Filling for Micropores

Micropores are thought to fill by the mechanism of volume filling (Dubinin, 1966, 1975; Jaroniec and Choma, 1989; Stoeckli, 1990) as opposed to multilayer formation and capillary condensation which occurs in the larger mesopores. The adsorption capacity in micropores is large due to the availability of the total (accessible) micropore volume as adsorption space (Jaroniec and Choma, 1989). Enhanced adsorption in microporous materials occurs over meso- and macroporous materials of similar composition due to the overlapping potentials between pore walls of pores commensurate in size with the adsorbate molecule.

Two basic equations are derived from Dubinin's theory of volume filling of micropores (TVFM) (Dubinin 1965; 66; 75; 82; 83, 85; 89). The first is the Dubinin-Radushkevich (D-R) equation (Gregg and Sing, 1982; McEnaney, 1987) which may be written for plotting purposes as:

1) $$\log W = \log W_0 - \mathbf{B}(T/\beta)^2 \log^2(P_0/P)$$

where W is the volume filled by adsorbate at equilibrium pressure; W_0 is the limiting micropore volume; **B** is a structural parameter related to the pore size (energy) distribution of the adsorbent; R is the Universal Gas Constant, T is the temperature in K, β is the relative differential molar work of adsorption or affinity coefficient of the adsorbate relative to benzene or nitrogen (standard adsorbate); P is the equilibrium adsorbate vapour pressure; and P_0 is the adsorbate vapour saturation pressure. A critical parameter from which the D-R equation was derived is the differential molar work of adsorption, *A*, where $A = RT\ln(P_0/P)$. In the D-R equation, the distribution of pore sizes (or more correctly, the distribution of the differential molar works of adsorption, *A*) is assumed to be Gaussian. Further, characteristic curves, which are plots of $\theta = W/W_0$ vs *A* are assumed to be invariant with temperature.

A plot of logV, where V is the volume of gas adsorbed at equilibrium (cm^3/g, stp) versus $\log^2(P_0/P)$, referred to as the Dubinin transformed isotherm plot, should yield a straight line if the theory of volume filling of micropores is obeyed. The micropore capacity, V_0, may be obtained from the Y-intercept of the Dubinin transformed isotherm plot. The micropore (monolayer) capacity is related to W_0, the limiting micropore volume, through the relation: $W_0 = V_0XD$, where D is a density conversion factor (cm^3 liquid/cm^3 stp), if it can be assumed that the adsorbate density is equal to the density of the bulk liquid at the adsorption temperature. The micropore surface area may be obtained from the the monolayer capacity by multiplying the monolayer capacity by the cross-sectional area of the adsorbate molecule.

The second equation which is the outcome of TVFM is the Dubinin-Astakhov (D-A) equation (Dubinin and Astakhov, 1971; Dubinin, 1975; Jarionec et al., 1990). The D-A equation is a generalized form of the D-R equation, developed to account for broader pore size distributions than the D-R equation, and may be written as:

2) $$W/W_0 = \theta = \exp\,[\, -(RT/E)^n \ln^n(P_0/P)]$$

where E is the "characteristic free energy of adsorption" which is equal to the differential free energy of adsorption for $\theta = .368$. The free energy of adsorption is believed to be an inverse function of the average micropore size (Stoeckli et al., 1989), and has been related to the half-width of slit-shaped micropores using the radius of gyration obtained from small-angle scattering X-ray techniques (Dubinin and Stoeckli, 1980; Dubinin, 1982; Jaroniec and Choma, 1989).

The energy distribution in the case of the D-A equation is assumed to obey a Weibull distribution (Weibull, 1951; Gregg and Sing, 1982), and the exponent n is optimized to obtain a best fit to the linear regression obtained from the transformed Dubinin plot (plot of logW vs $\log^n(P_0/P)$). For the case of $n = 2$, the D-A equation reduces to the D-R equation. The value of n can give some indication of the nature of the pore size distribution, as discussed in Stoeckli et al. (1989).

In order to obtain a distribution of pore sizes from the Weibull distribution of adsorption energies assumed in Dubinin-Astakhov Theory, certain assumptions must be made (Medek, 1977). Firstly, the total adsorption potential (ϕ) is assumed to obey the following relationship:

3) $$\phi = kz^{-3}$$

where k is referred to as the interaction constant and z is the distance from the adsorbate molecule to the adsorbent surface. Secondly, if the adsorbate molecule is assumed to be adsorbed in a confined space and interacts with adsorbent walls in all directions, then z may be thought of as the average distance to the pore walls and equated to an equivalent pore radius (r_e) in the following equation:

$$z = r_e = 2Q/P$$

where Q is the area and P is the perimeter of the pore in cross-section. Finally, equation 3 is thought to be obeyed over the size range in which volume filling is thought to occur. Equation 3 may then be written as:

4) $$A = \phi = kr_e^{-3}$$

The cumulative distribution function for pore sizes may be obtained by substituting relation 4 into equation 2 and the pore size distribution curve may be obtained differentiating the resulting equation with respect to the equivalent radius (Medek, 1977). Parameters such as the mean equivalent pore diameter may be obtained from the parameters of the Weibull distribution (Medek, 1977).

3.3.2 Langmuir and BET Theory

The classic theory used to describe the Type I isotherm for microporous materials with small external surface area is that based on the Langmuir equation (1916). The Type I isotherm displays a steep increase in adsorption at low relative pressures due to enhanced adsorption caused by the overlapping adsorption potentials between walls of pores whose diameters are commensurate in size with the adsorbate molecule. The Type I isotherm then flattens out into a plateau region at higher relative pressure, which is believed to be due to the completion of a monolayer of adsorbed gas. The micropore volume is then thought to be filled by only a few molecular layers of adsorbate, and further uptake is limited by the dimensions of the micropores.

The Langmuir model assumes that a state of dynamic equilibrium is established between the adsorbate vapour and the adsorbent surface and that adsorption is restricted to a single monolayer (Gregg and Sing, 1982). The adsorbent surface is thought to be composed of a regular array of energetically homogeneous adsorption sites upon which an adsorbed monolayer is assumed to form. The rate of condensation is assumed to be equal to the rate of evaporation from the adsorbed monolayer at a given relative pressure and constant temperature. The Langmuir equation was developed with these assumptions and takes the following form:

$$\frac{P}{V} = \frac{1}{BV_m} + \frac{P}{V_m}$$

where P is the equilibrium pressure, V is the volume of gas adsorbed at equilibrium, V_m is the volume of adsorbate occupying a monolayer, and B is an empirical constant. A plot of P/V vs relative pressure should yield a straight line whose slope will yield V_m from which the surface area may be obtained. As discussed by Gregg and Sing (1982), variance from linearity often occurs. For example, the heat of adsorption of carbon dioxide gas appears to vary with degree of uptake which is contrary to the assumption of constant heat of adsorption with surface coverage made by Langmuir.

The Brunauer, Emmett and Teller (BET) treatment (1938) is simply an extension of the Langmuir kinetic theory of adsorption whereby the dynamic equilibrium discussed above is extended to second and higher layers (multilayer adsorption). Some simplifying assumptions are made in developing the BET equation: the heat of adsorption in second and higher layers is assumed to be equal to the adsorptive heat of liquefaction; condensation occurs only on sites occupied by molecules in a previously adsorbed layer; the number of adsorbed layers at saturation is infinite; and no lateral interaction occurs between adsorbate molecules. The BET equation is:

$$\frac{P}{V(1-P/P_0)} = \frac{1}{V_mC} + \frac{C-1}{V_mC}(P/P_0)$$

where C is the BET constant which is a function of the net heat of adsorption (Chapter 2). A plot of the left side of the equation versus relative pressure will yield a straight line. The values of C and V_m may be obtained from the slope and the intercept. The monolayer volume may be converted to surface area if the adsorbate cross-sectional area is known.

3.4 METHODS

Two sample suites of coal of slightly different rank are used in the current study. The first suite consists of seven samples of the Lower Cretaceous Gates Formation of Northeastern British Columbia (Lamberson and Bustin, 1993) obtained from the Bullmoose Mine C seam and one sample from the A1 seam, approximately 50 m stratigraphically below the C seam. The second suite of eight samples was obtained from a drill core of Cretaceous coals from a locality in Alberta. Each suite represents a wide variation in lithotype composition.

Petrography (maceral and mineral), proximate, sulphur, and low pressure carbon dioxide analyses were performed on both sample suites. In addition, low-temperature ash (LTA), X-ray diffraction (XRD), equilibrium moisture, and high pressure methane adsorption analyses were performed for the Gates sample suite (Lamberson and Bustin, 1993). Petrographic, sulphur, LTA, XRD, and random reflectance procedures used are described in Lamberson and Bustin (1993). Samples were crushed to less than 250 μm screen size for all analyses.

Carbon dioxide adsorption analysis was performed at The University of British Columbia using a Micromeritics ASAP 2000® surface area analyzer. Samples were evacuated at 70°C for at least 16 hours prior to analysis to remove residual volatiles. Each sample (with sample tube) was then transferred to an analysis port on the instrument, back-filled with helium to remove any remaining vapours, and re-evacuated. A preliminary leak test was then performed; this consisted of opening the sample tube to a pressure transducer which monitored pressure buildup due to the release of volatiles from the sample. If a critical pressure increase was not achieved over a 60 second interval, then the analysis was continued. Upon passing the preliminary leak test and further evacuation, a free space analysis was performed using helium gas at the analysis temperature, followed by a more stringent leak test. After the secondary leak test was passed, the sample was cooled to analysis temperature, exposed to fixed doses of Research Grade (99.999%) carbon dioxide, allowed to come to equilibrium, and the adsorbed volume of carbon dioxide gas was measured. The analyses were performed over a relative pressure range of about 0.0006 to 0.01 at 298 K, and 0.0006 to 0.032 at 273 K. No thermal transpiration correction or non-ideality

gas correction was used for carbon dioxide at either temperature. Carbon dioxide adsorption isotherms were obtained for all samples at both 298 and 273 K. A saturation pressure of ~ 6.4196 MPa (48,151 mmHg) and ~ 3.4853 MPa (26,142 mmHg) was used for carbon dioxide at 298 and 273 K, respectively.

The Dubinin-Radushkevich equation was used to obtain carbon dioxide micropore capacities and micropore surface areas from the 298 and 273 K isotherm data. A molecular cross-sectional area of 17.0×10^{-20} m^2 was used for carbon dioxide to obtain the surface areas from the monolayer capacities.

The Dubinin-Astakhov equation was utilized to obtain pore size distribution data. An analysis bath temperature of 273 K was used instead of 298 K due to the larger relative pressure range obtained at the lower temperature (0.0006-0.032 versus 0.0006-0.01). The upper limit for absolute pressure measurements on the ASAP 2000 instrument was 120 kPa (900 mmHg). An affinity coefficient (β) equal to 0.44 (Stoeckli et al., 1993) was used in this study for carbon dioxide at 273 K.

High pressure methane adsorption analyses were performed by Core Laboratories (Calgary, Alberta) using a high pressure volumetric adsorption technique similar to that of Mavor et al. (1990). The procedure for sample preparation is described in Lamberson and Bustin (1993).

3.5 RESULTS

3.5.1 Gates suite

3.5.1.1 Proximate, rank, and petrographic data

Proximate, sulphur, equilibrium moisture, and ash yield data for the Gates suite are presented in Table 3-1. Lithotype classification, LTA and XRD results are presented in Table 3-2. For a discussion of these results, see Lamberson and Bustin (1993).

Random reflectance measurements on samples LTC-1, LTC-15, and LTA1-6 yielded values of 0.97, 0.96, and 1.0 %, respectively. These values indicate a high-volatile A - medium-volatile bituminous rank for the Gates samples (Lamberson and Bustin, 1993). Rank, following American Society of Testing and Materials (ASTM, 1980) procedure, is medium to low volatile bituminous. The ASTM rank determination may be inappropriate for some western Canadian coals, as discussed in Lamberson and Bustin (1993).

Petrographic composition data for the Gates Formation coals is given in Table 3-3 and presented graphically in Figure 3-1. The maceral percentages were calculated on a volume percent, mineral matter-free basis (mmf), and were then recalculated to include mineral matter using the Parr formula (Lamberson and Bustin, 1993). Liptinite content of the Gates suite is very low (0-3 %, mmf), thus the coals are composed mainly of three components: vitrinite, inertinite, and mineral matter. Vitrinite content (mmf) ranges from 18 to 95%, and inertinite from 3 to 81%. On a raw coal basis (mineral matter-inclusive), vitrinite varies from 15 to 90%, inertinite from 3 to 71%, and mineral matter from 2 to 22%. LTC-1 has the highest vitrinite and lowest mineral matter and inertinite content; LTC-5 has the highest inertinite content; LTC-9 has the highest mineral matter content. LTC-5 is a unique sample containing 81% inertinite (mmf), which is mainly structured inertinite. The structured inertinite is interpreted as having been derived from

Table 3-1. Results of proximate, sulphur, and equilibrium moisture analyses.

	Sample	Ash Yield (w%)	Moisture (AR) (w%)	Volatile Matter (w%, dmf)	Fixed Carbon (w%, dmf)	Total Sulphur (w%)	Equ. Mois. (w%)
Gates Suite	LTC-1	8.0	1.1	28.0	72.1	0.7	2.1
	LTC-7	6.8	1.0	24.0	76.0	0.7	1.7
	LTC-15	9.6	0.7	25.9	74.1	0.8	1.7
	LTA1-6	3.6	0.9	23.7	76.3	0.4	2.0
	LTC-11	20.5	0.9	21.5	78.5	0.4	1.6
	LTC-14	17.6	0.7	21.3	78.8	0.5	1.4
	LTC-9	33.8	0.8	17.4	82.6	0.3	1.5
	LTC-5	22.2	0.5	30.5	69.5	0.2	1.4
Alberta Suite	ACCC-27	4.3	0.1	35.1	64.9	0.6	-
	ACCC-29	1.6	0.2	35.1	64.8	0.5	-
	ACCC-1	6.3	0.4	33.1	66.9	3.0	-
	ACCC-5	4.4	0.3	34.3	65.6	1.5	-
	ACCC-6	2.9	0.1	35.5	64.5	1.3	-
	ACCC-35	10.6	0.5	33.5	66.5	0.5	-
	ACCC-13	1.2	0.4	23.1	76.9	1.0	-
	*ACCC	4.6	0.1	33.8	66.1	0.9	-

w % = weight percent
AR = As received

dmf = dry, mineral matter free (ASTM)
Equ. Mois. = equilibrium moisture

Table 3-2. Lithotype classification, low-temperature ash and x-ray diffraction results for the Gates suite. Modified from Lamberson and Bustin (1993).

Sample	* Lithotype	Low-temp ash yield (weight %)	Quartz	Kaolinite	Dolomite	Ferroan Dolomite
LTC-1	Bright	7.20	major	major	-	minor
LTC-7	Banded bright	7.51	major	major	-	minor
LTC-15	Banded coal	11.28	major	major	minor	-
LTA1-6	Banded dull	2.83	dominant	minor	-	minor
LTC-11	Banded dull	18.57	major	major	-	minor
LTC-14	Dull	19.15	major	minor	minor	-
LTC-9	Dull	37.59	major	minor	-	-
LTC-5	Fibrous	33.43	minor	-	dominant	-

Dominant: essentially monomineralic.
Major: strong peak intensity (15 -40% ?).
Minor: weak peak intensity (5-15% ?).
* Lithotype classification is a modified Australian classification (Diessel, 1965).

Table 3-3. Gates and Alberta suite petrography data.

GATES SUITE

	Maceral	LTC-1	LTC-7	LTC-15	LTA1-6	LTC-11	LTC-14	LTC-9	LTC-5
Volume %, Mineral-Free	Structured Vitrinite	79	50	46	41	22	13	6	11
	Desmocollinite	6	12	9	17	7	2	0	6
	Vitrodetrinite	11	1	5	1	7	14	13	1
	Semifusinite	1	24	21	26	38	37	23	20
	Fusinite	1	9	8	4	3	4	1	53
	Other Inertinite	2	4	10	11	23	29	54	8
	Total Liptinite	1	0	0	0	1	1	3	1
	Total Vitrinite	95	63	61	59	35	29	19	18
	Total Inertinite	3	37	39	41	64	70	78	81
	Struct:Deg Vit *	5	4	3	2	2	1	1	2
	Struct:Deg Inert**	1	9	3	3	2	11	0	9
Volume %, Raw Coal	Structured Vitrinite	75	48	43	40	20	12	5	10
	Desmocollinite	5	11	9	16	6	2	0	5
	Vitrodetrinite	10	1	5	1	6	13	10	1
	Semifusinite	1	23	20	25	34	33	18	18
	Fusinite	1	9	7	4	3	4	1	46
	Other Inertinite	2	4	9	10	21	26	43	7
	Total Liptinite	1	0	0	0	1	1	2	1
	Total Vitrinite	90	61	57	58	32	26	15	16
	Total Inertinite	3	35	37	40	57	63	61	71
	Ash Yield (vol.%)	5	4	6	2	10	10	22	12

ALBERTA SUITE

		ACCC-27	ACCC-29	ACCC-1	ACCC-5	ACCC-6	ACCC-35	ACCC-13	*ACCC
Volume %, Mineral-Free	Structured Vitrinite	77	73	49	49	34	34	19	13
	Desmocollinite	9	9	14	23	19	17	30	22
	Vitrodetrinite	2	0	6	3	9	5	3	1
	Semifusinite	3	5	19	14	23	25	31	34
	Fusinite	5	3	8	6	11	16	10	3
	Other Inertinite	2	8	2	3	3	2	5	25
	Total Liptinite	2	2	2	2	1	1	2	1
	Total Vitrinite	88	83	69	75	63	55	52	37
	Total Inertinite	10	16	29	23	37	44	46	62
	Struct:Deg Vit	7	8	2	2	1	2	1	1
	Struct:Deg Inert	4	1	13	7	13	18	8	1
Volume %, Raw Coal	Structured Vitrinite	75	73	47	47	33	32	18	13
	Desmocollinite	8	9	13	23	19	16	30	21
	Vitrodetrinite	2	0	6	3	9	4	3	1
	Semifusinite	3	5	18	13	22	24	31	33
	Fusinite	5	3	7	5	11	15	10	3
	Other Inertinite	2	8	2	3	3	2	5	25
	Total Liptinite	2	2	2	2	1	1	2	1
	Total Vitrinite	85	82	66	73	61	52	51	36
	Total Inertinite	10	15	27	22	36	41	46	60
	Ash Yield (vol.%)	2	1	4	3	2	6	1	3

* Structured Vitrinite : Degraded Vitrinite

** Structured Inertinite : Degraded Inertinite

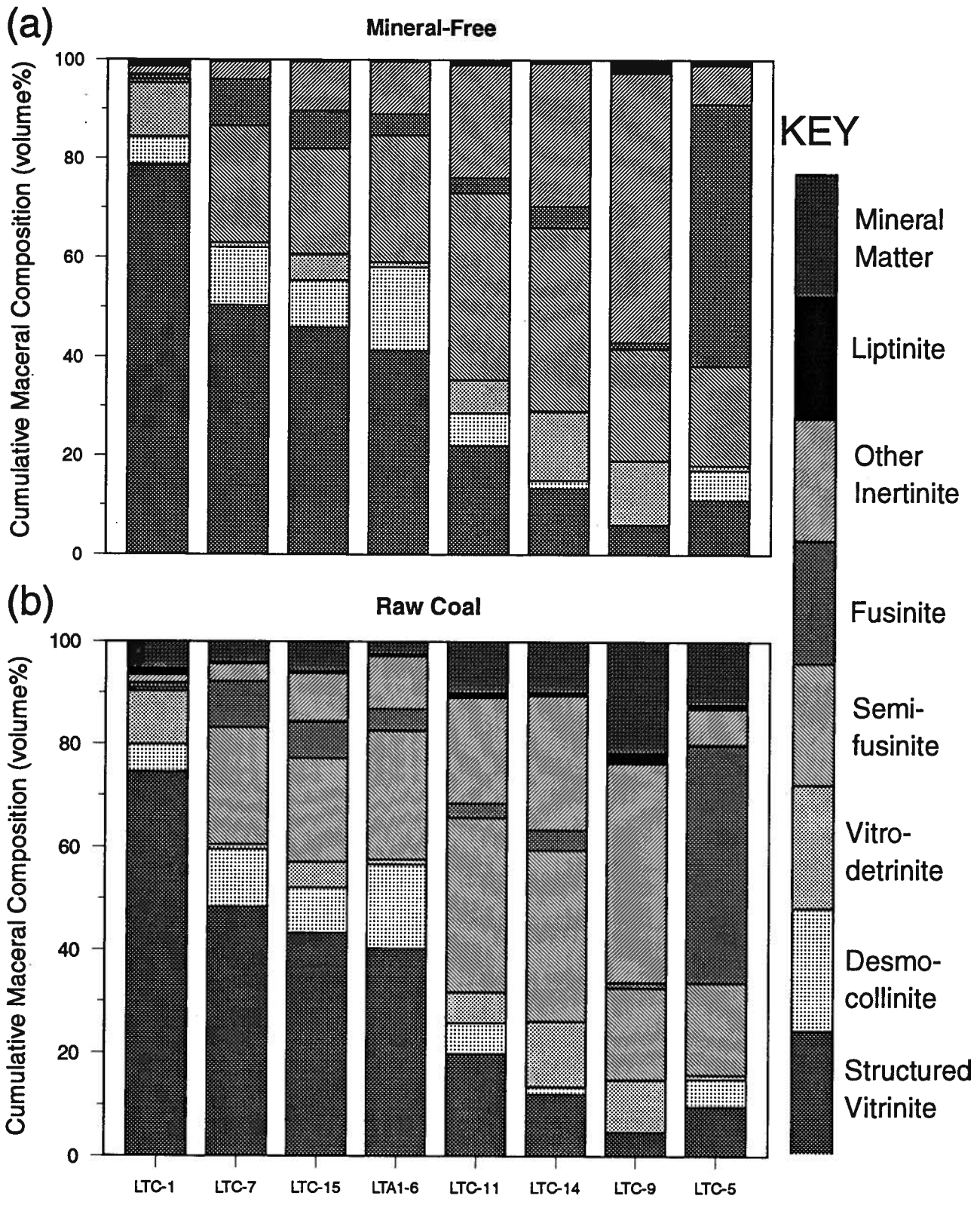

Figure 3-1. Gates coal petrography data. Samples analysed on a mineral-free (a) and raw-coal (b) basis. Maceral and mineral contents expressed as volume %. Modified from Lamberson and Bustin (1993).

fires (charcoal) (Lamberson, 1993). The Gates therefore contains a broad range of compositions with respect to the three main components vitrinite, inertinite, and mineral matter.

Ratios of structured to unstructured vitrinite and inertinite are presented in Table 3-3. Structured vitrinite (telocollinite, telinite, pseudovitrinite) increases with decreasing in mineral matter content. The higher ash yield samples are enriched in degraded (unstructured) vitrinite (i.e., vitrodetrinite) and inertinite. In general (with exception of LTC-5), the structured vitrinite content decreases with decreases in total vitrinite content. Structured inertinite (semifusinite and fusinite) appears to decrease with an increase in total inertinite, with the exception of LTC-1 and LTC-5. For a discussion of the impact of depositional environment and original vegetation on these compositional trends, see Lamberson and Bustin (1993).

3.5.1.2 Gas Adsorption

Plots of carbon dioxide monolayer capacities (calculated from D-R equation) versus vitrinite content on a mineral matter-free (calculated from Parr formula) and raw coal basis are shown in Figure 3-2. Micropore capacities are corrected to a volume percent, mineral matter-free basis using the Parr mineral formula (Lamberson, 1993). Both the 298 K and 273 K data is displayed in Table 3-4.

The 298 K carbon dioxide surface areas (Table 3-5) and micropore capacities (raw coal basis) vary from 87.1 to 176 m^2/g and 19.1 to 38.6 cm^3/g, respectively. The 273 K carbon dioxide values range from 94.9 to 192 m^2/g and 20.8 to 40.1 cm^3/g, respectively. Experimental error associated with these values is +/- 10%. The correlation between the micropore capacities and total vitrinite content appears to be logarithmic. For the raw coal data, the correlation between mineral matter and micropore capacities appears to be linear but a logarithmic correlation also yields a high correlation coefficient.

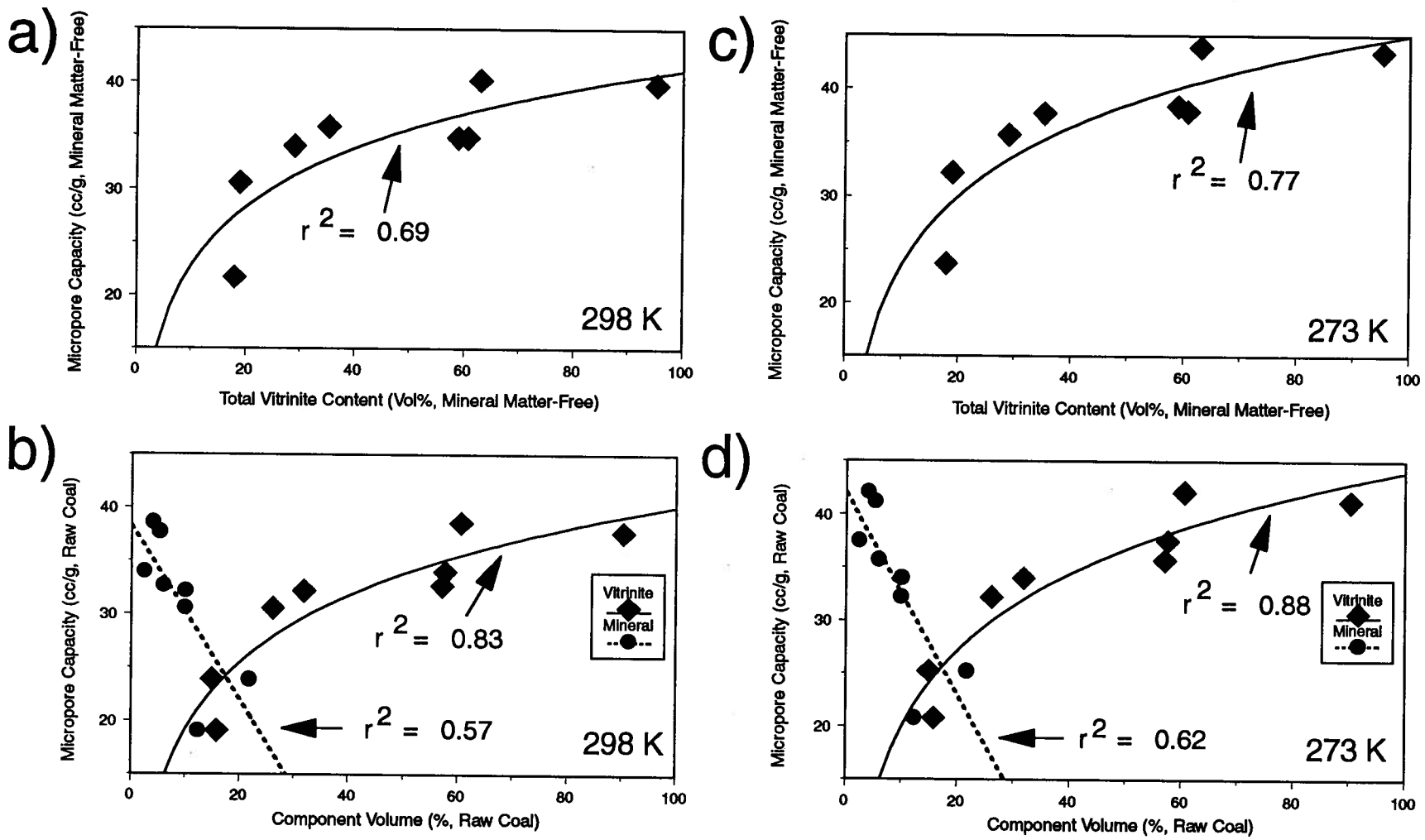

Figure 3-2. Plots of carbon dioxide micropore capacities versus Gates suite coal composition on a raw coal (b, d) and mineral-free (a, c) basis at 298 K (a, b) and 273 K (c, d). Mineral-free micropore capacities calculated using the Parr Formula.

Table 3-4. Carbon dioxide Dubinin-Radushkevich (D-R) micropore capacities, Langmuir and BET monolayer volumes presented on a raw coal and mineral matter-free (see text) basis. Data obtained from 298 and 273 Kelvin isotherms.

		D-R Micropore Capacity (cc/g)				Langmuir Monolayer Volume (cc/g)				BET Monolayer Volume (cc/g)			
		Raw Coal		** Min. Free		Raw Coal		** Min. Free		Raw Coal		** Min. Free	
		298 K	273 K	298 K	273 K	298 K	273 K	298 K	273 K	298 K	273 K	298 K	273 K
Gates Suite	LTC-1	37.7	41.2	39.8	43.4	24.3	30.6	25.6	32.3	22.9	27.8	24.1	29.3
	LTC-7	38.6	42.1	40.2	43.9	27.6	32.2	28.7	33.5	25.9	29.1	27.0	30.3
	LTC-15	32.7	35.7	34.8	37.9	21.1	29.8	22.4	31.7	19.9	26.6	21.1	28.3
	LTA1-6	34.0	37.5	34.8	38.4	24.0	29.8	24.6	30.5	22.6	26.9	23.1	27.6
	LTC-11	32.2	34.0	35.8	37.7	24.2	29.7	26.8	33.0	22.4	25.8	24.9	28.7
	LTC-14	30.6	32.2	34.0	35.7	20.0	29.3	22.2	32.5	18.8	25.4	20.9	28.2
	LTC-9	23.9	25.2	30.6	32.2	16.1	21.9	20.6	28.0	15.1	19.5	19.3	24.9
	LTC-5	19.1	20.8	21.7	23.7	12.8	21.3	14.6	24.3	12.1	18.6	13.8	21.2
Alberta Suite	ACCC-27	46.4	50.2	47.6	51.5	27.3	40.2	28.0	41.2	25.8	35.7	26.5	36.6
	ACCC-29	49.2	54.2	49.7	54.7	30.5	43.2	30.8	43.6	28.9	38.2	29.2	38.6
	ACCC-1	36.2	40.3	37.8	42.1	20.5	33.4	21.4	34.9	19.6	29.8	20.4	31.1
	ACCC-5	36.2	40.3	37.2	41.4	23.5	36.6	24.1	37.6	22.4	32.7	23.0	33.6
	ACCC-6	37.8	42.4	38.5	43.2	22.2	35.8	22.6	36.5	20.8	32.0	21.2	32.6
	ACCC-35	35.6	38.8	37.9	41.3	20.0	32.8	21.3	34.9	19.2	29.6	20.4	31.5
	ACCC-13	33.8	38.2	34.1	38.5	20.5	33.8	20.7	34.1	19.7	30.6	19.9	30.9
	*ACCC	33.4	36.0	34.3	37.0	19.4	32.8	19.9	33.7	18.7	29.6	19.2	30.4

** Min. Free = Mineral Free

Table 3-5. Carbon dioxide Dubinin-Radushkevich (D-R), Langmuir and BET equivalent surface areas presented on a raw coal and mineral matter-free (see text) basis. Data obtained from 298 and 273 Kelvin isotherms. Also included are BET C values mesured at 298 Kelvin.

		D-R Surface Area (sq. m/g)				Langmuir Surface Area (sq. m/g)				BET Surface Area (sq. m/g)				BET C Value
		Raw Coal		** Min.	Free	Raw Coal		** Min.	Free	Raw Coal		** Min.	Free	
		298 K	273 K	298 K	273 K	298 K	273 K	298 K	273 K	298 K	273 K	298 K	273 K	298 K
Gates Suite	LTC-1	172.2	188.2	181.7	198.5	110.9	139.9	117.0	147.6	104.7	127.1	110.4	134.1	46
	LTC-7	176.3	192.3	183.6	200.3	125.9	147.1	131.1	153.2	118.2	132.9	123.1	138.4	42
	LTC-15	149.6	163.3	158.9	173.5	96.5	136.1	102.5	144.6	90.8	121.6	96.5	129.2	45
	LTA1-6	155.1	171.4	158.9	175.6	109.7	136.3	112.4	139.6	103.0	123.1	105.5	126.1	43
	LTC-11	147.2	155.6	163.5	172.9	110.7	135.7	123.0	150.8	102.4	118.0	113.8	131.1	35
	LTC-14	139.8	147.0	155.2	163.1	91.6	133.7	101.7	148.3	85.8	116.1	95.2	128.8	44
	LTC-9	109.3	115.0	139.6	146.9	73.7	100.1	94.1	127.8	69.2	89.0	88.4	113.7	44
	LTC-5	87.1	94.9	99.2	108.2	58.3	97.5	66.5	111.1	55.3	85.1	63.0	97.0	53
Alberta Suite	ACCC-27	211.8	229.3	217.2	235.2	124.5	183.4	127.7	188.1	118.0	163.1	121.0	167.3	53
	ACCC-29	224.6	247.7	226.9	250.2	139.3	197.3	140.7	199.3	131.9	174.7	133.2	176.5	50
	ACCC-1	165.4	184.3	172.6	192.3	93.6	152.5	97.7	159.2	89.7	136.0	93.6	142.0	71
	ACCC-5	165.2	184.3	169.8	189.4	107.4	167.0	110.4	171.6	102.5	149.6	105.3	153.7	67
	ACCC-6	172.9	193.7	176.2	197.4	101.3	163.7	103.3	166.9	96.9	146.2	98.8	149.0	69
	ACCC-35	162.5	177.3	172.9	188.6	91.4	149.6	97.2	159.1	87.8	135.1	93.4	143.7	76
	ACCC-13	154.5	174.4	155.9	176.0	93.6	154.4	94.4	155.8	88.7	139.6	89.5	140.9	87
	*ACCC	152.5	164.4	156.7	169.0	88.6	149.7	91.0	153.8	85.3	135.2	87.7	138.9	80

** Min. Free = Mineral Free

Plots of Langmuir and BET monolayer volumes (calculated from the Langmuir and BET equations, respectively) versus vitrinite content on a raw coal and mineral matter-free basis (at 298 and 273 K) are shown in Figures 3-3 and 3-4 and are presented in Table 3-4. The corresponding surface areas and BET C values are given in Table 3-5. The relationship between the BET and Langmuir monolayer volumes and vitrinite content is similar to that observed for the D-R monolayer volume.

High pressure methane monolayer capacities (Table 3-6), determined at 295 K using the Langmuir equation (Lamberson and Bustin, 1993), and plotted versus vitrinite content (mineral matter-free and raw coal basis) are given in Figure 3-5. Like the carbon dioxide data, a logarithmic correlation occurs. The low pressure carbon dioxide monolayer capacities are plotted versus methane monolayer capacities in Figure 3-6 and are given an exponential correlation but a linear correlation also applies.

3.5.2 Alberta suite

3.5.2.1 Proximate, rank, and petrographic data

Proximate and sulphur analysis results are summarized in Table 3-1. Sulphur contents vary from 0.5 (ACCC-29) to 3.1 wt% (ACCC-1). Volatile matter content (weight %, dmmf) varies from 23.1% (ACCC-13) to 35.5% (ACCC-6). Ash yields (wt %) range from 1.2% (ACCC-13) to 10.6% (ACCC-35). The average ash content of the Alberta suite (4.4%) is much lower than the average for the Gates suite (15.3%). The moisture contents (as-received) of the Alberta suite vary from 0.1% (ACCC-27) to 0.5 % (ACCC-35) and are lower on average than the Gates suite (0.2 % vs 0.8 %, respectively).

Random reflectance values for the Alberta suite range from 0.50 to 0.65, which span the sub-bituminous A/high volatile bituminous C boundary. The reflectance values may be suppressed by the high degree of resinite impregnation in the vitrinite macerals, leading to a lower rank determination. The ASTM ranking for the coals is high volatile A bituminous, with the

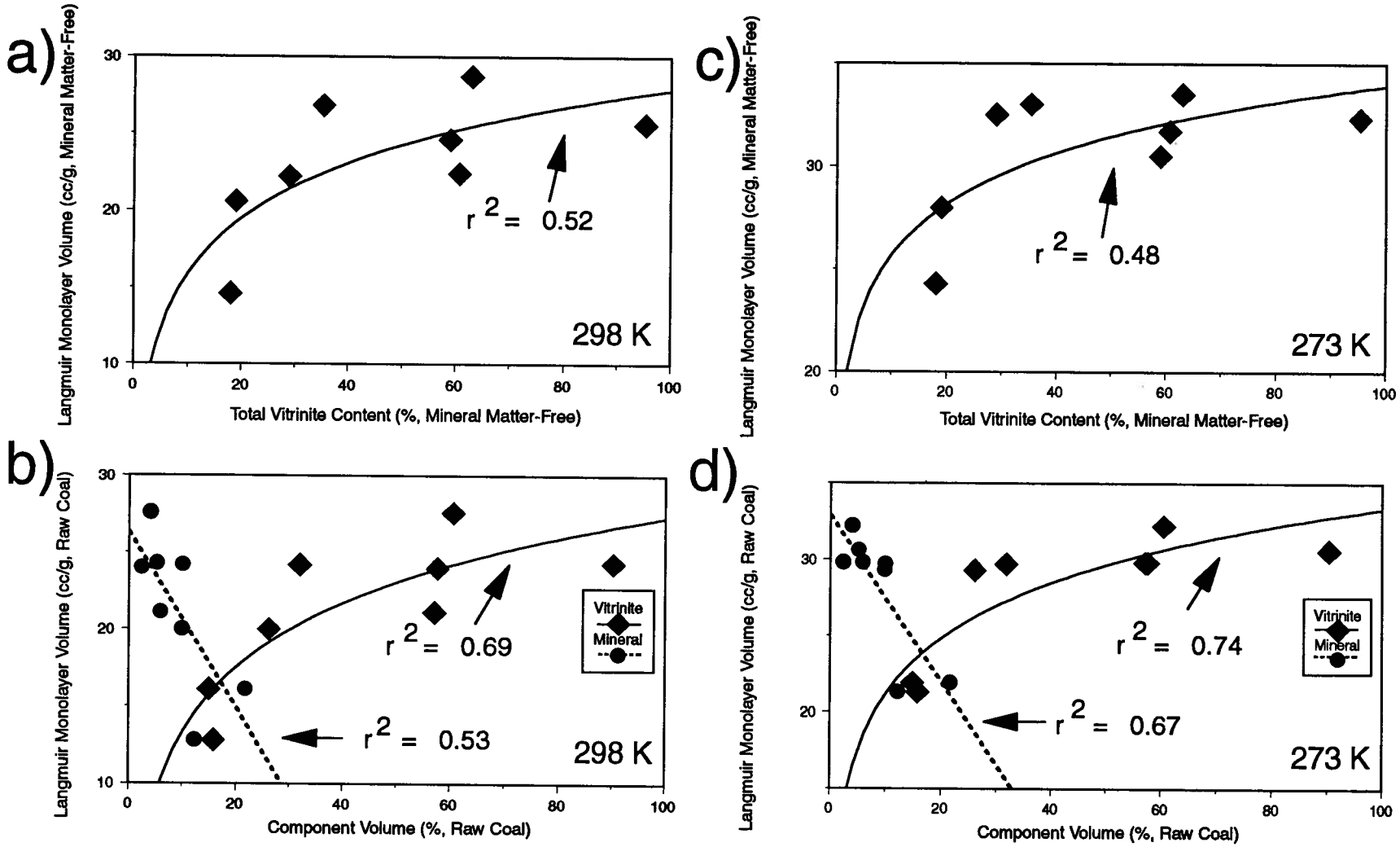

Figure 3-3. Plots of carbon dioxide Langmuir monolayer volumes versus Gates suite coal composition on a raw coal (b, d) and mineral-free (a, c) basis at 298 K (a, b) and 273 K (c, d). Mineral-free monolayer volumes calculated using the Parr Formula.

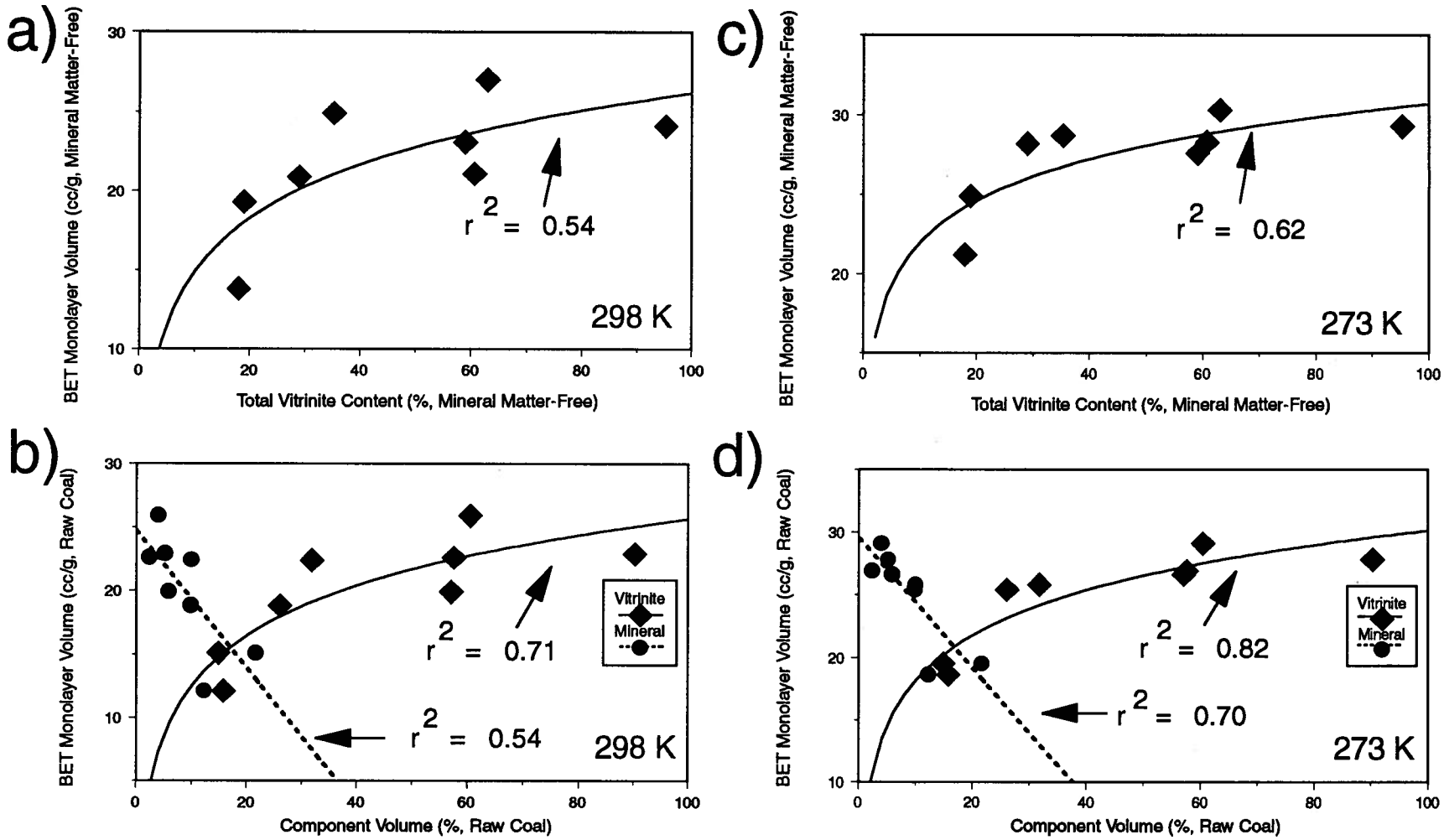

Figure 3-4. Plots of carbon dioxide BET monolayer volumes versus Gates suite coal composition on a raw coal (b, d) and mineral-free (a, c) basis at 298 K (a, b) and 273 K (c, d). Mineral-free monolayer volumes calculated using the Parr Formula.

Table 3-6 . High pressure methane monolayer volumes measured for the Gates suite.

Sample	Monolayer Volume (cc/g) Raw Coal	Ash-Free *	Mineral-Free
LTC-1	19.3	21.3	20.4
LTC-7	22.0	23.7	22.9
LTC-15	20.5	22.9	21.8
LTA1-6	18.7	19.5	19.1
LTC-11	12.3	14.8	13.6
LTC-14	15.5	18.6	17.2
LTC-9	7.9	11.8	10.0
LTC-5	8.1	10.2	9.2

* Corrected using ash yield (weight %)

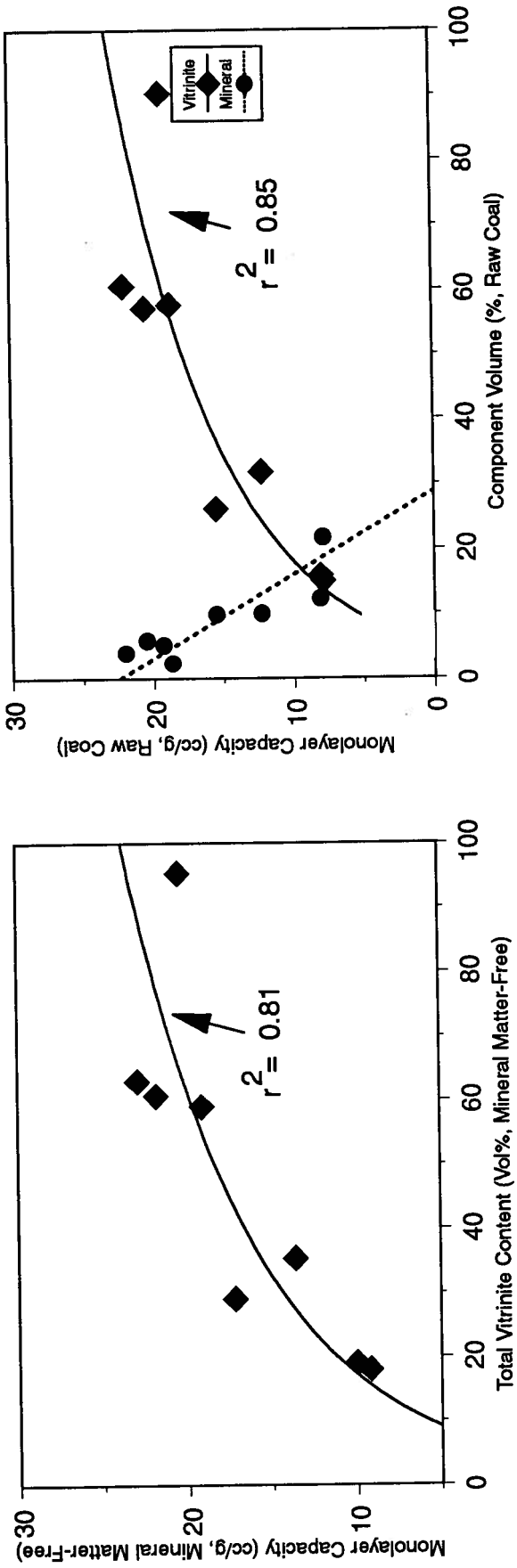

Figure 3-5. Plots of methane Langmuir monolayer capacities versus Gates suite coal composition on a mineral-free (a) and raw coal (b) basis. Modified from Lamberson and Bustin, (1993).

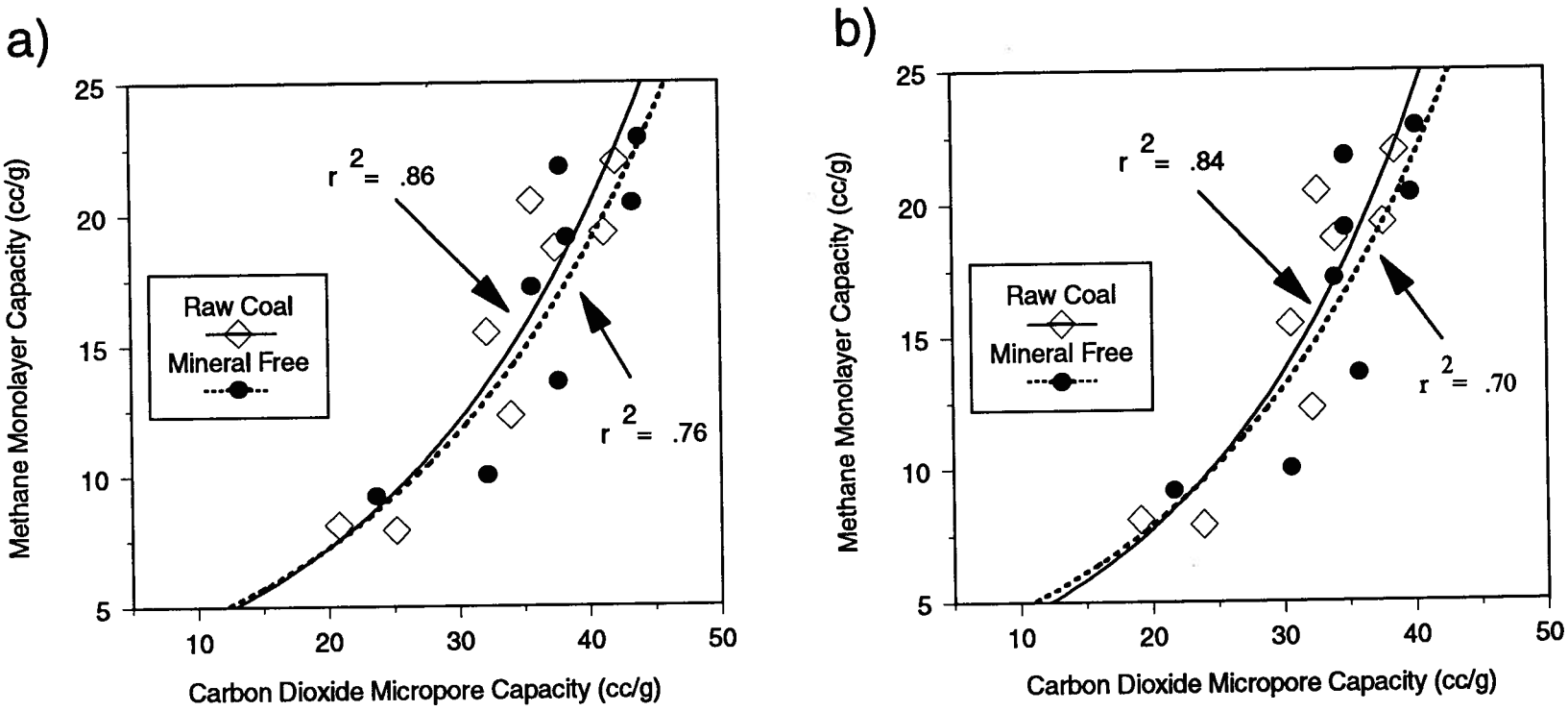

Figure 3-6. Plots of Gates suite carbon dioxide D-R micropore capacities versus methane monolayer capacities on a raw coal and mineral-free basis. D-R micropore capacities calculated from the 273 K isotherm (a), and the 298 K isotherm (b). An exponential regression was used in each case.

exception of ACCC-13, which is medium volatile bituminous in rank. The rank of the Albertan coals is therefore between high volatile bituminous C and A in rank.

Petrographic composition data for the Alberta suite are shown in Table 3-3 and presented graphically in Figure 3-7. Maceral percentages were calculated in the same fashion as for the Gates suite. Liptinite content is slightly higher than the Gates suite (1 to 2% vs 0-3% mmf). Mineral matter-free (mmf) vitrinite composition (volume %) varies from 37 to 88%, and inertinite from 10 to 62%. The average mmf vitrinite content is higher for the Alberta coals (67%) than the Gates (47%), whereas the total inertinite content is lower (31% vs 52%). On a raw coal basis, vitrinite varies from 36 to 85%, and inertinite from 10 to 60%. ACCC-27 has the highest vitrinite and lowest inertinite content, and *ACCC has the lowest vitrinite and highest inertinite content. Samples ACCC-35 and ACCC-13 have the highest and lowest ash contents, respectively.

Ratios of structured vitrinite and inertinite to degraded vitrinite and inertinite, respectively, are given in Table 3-3. With one exception (ACCC-5), the total vitrinite content decreases with declining structured vitrinite abundance. The structured vitrinite also decreases with increases in total inertinite content, with the exception of ACCC-5. As stated by Lamberson and Bustin (1993), the relationship between the structured vitrinite and total inertinite contents appears to be due to the original depositional environment and vegetation. The structured vitrinite-rich coals probably formed from woody peats, whereas the duller coal (inertinite-rich) formed in more herbaceous (less resistant) wetlands or wetlands subjected to higher fire frequency.

The semifusinite (mostly high reflecting) contents of the Alberta coals decreases with an increase in structured vitrinite content, which may also be related to fire frequency in wetlands. The partial burning and charring of the semifusinite precursor, i.e. structured vitrinite, would lead to an increase in abundance of high reflecting semifusinite. The sample with the highest semifusinite content (*ACCC) also has the highest inertodetrinite content, which is probably due to brittleness of inertinite macerals derived from burning and charring of their precursors.

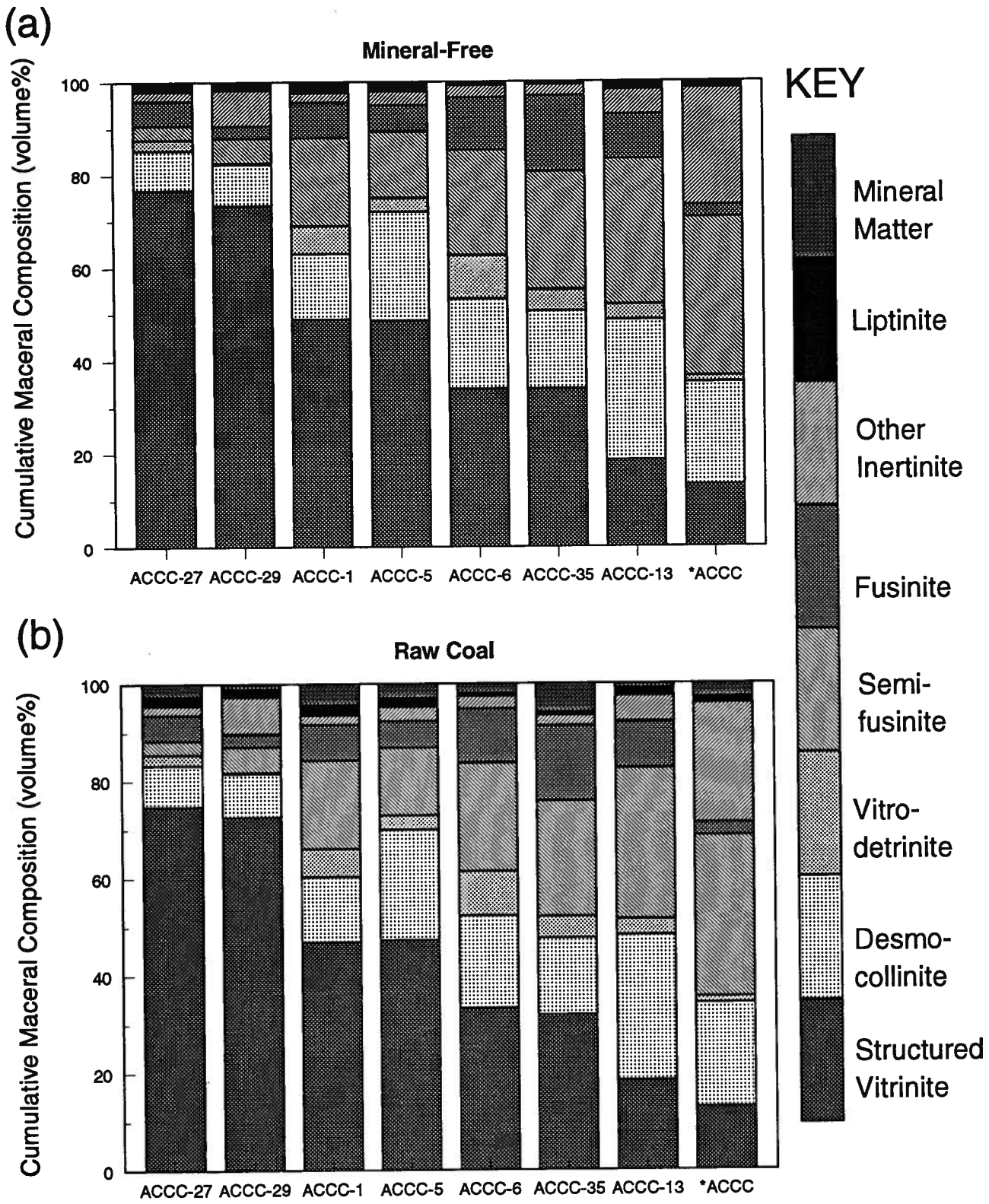

Figure 3-7. Alberta suite petrography data. Samples analysed on a mineral-free (a) and raw-coal (b) basis. Maceral and mineral contents expressed as volume %.

3.5.2.2 Gas adsorption

Plots of carbon dioxide micropore capacities versus vitrinite content on a mineral matter-free and raw coal basis at 298 and 273 K are given in Figure 3-8. The 298 K surface areas (Table 3-5) and micropore capacities (raw coal basis) vary from 152 to 224 m^2/g and 33.4 to 49.2 cm^3/g, respectively. The 273 K surface areas and micropore volumes (raw coal basis) for the Alberta suite range from 164 to 247 m^2/g and 36.0 to 50.2 cm^3/g, respectively.

A linear correlation best fits the relation between carbon dioxide micropore capacities and total vitrinite content as opposed to a logarithmic correlation found for the Gates suite. For the Gates suite, the correlation approaches linearity for values of total vitrinite greater than 30% (raw coal basis). The total vitrinite contents (raw coal basis) of all samples in the Alberta suite are greater than 30%, therefore it is no surprise that the correlation is linear. A better correlation, however, is obtained if the carbon dioxide micropore capacities are plotted against structured vitrinite content as opposed to total vitrinite content (Figure 3-9).

Plots of Langmuir and BET monolayer volumes versus total vitrinite content at 298 and 273 K are shown in Figures 3-10 and 3-11. A relationship similar to the plots of D-R micropore capacities versus vitrinite (total and structured) content was again achieved. Plots of BET and Langmuir monolayer volumes versus structured vitrinite also yield better correlations than monolayer volume versus total vitrinite (Figures 3-12, 3-13).

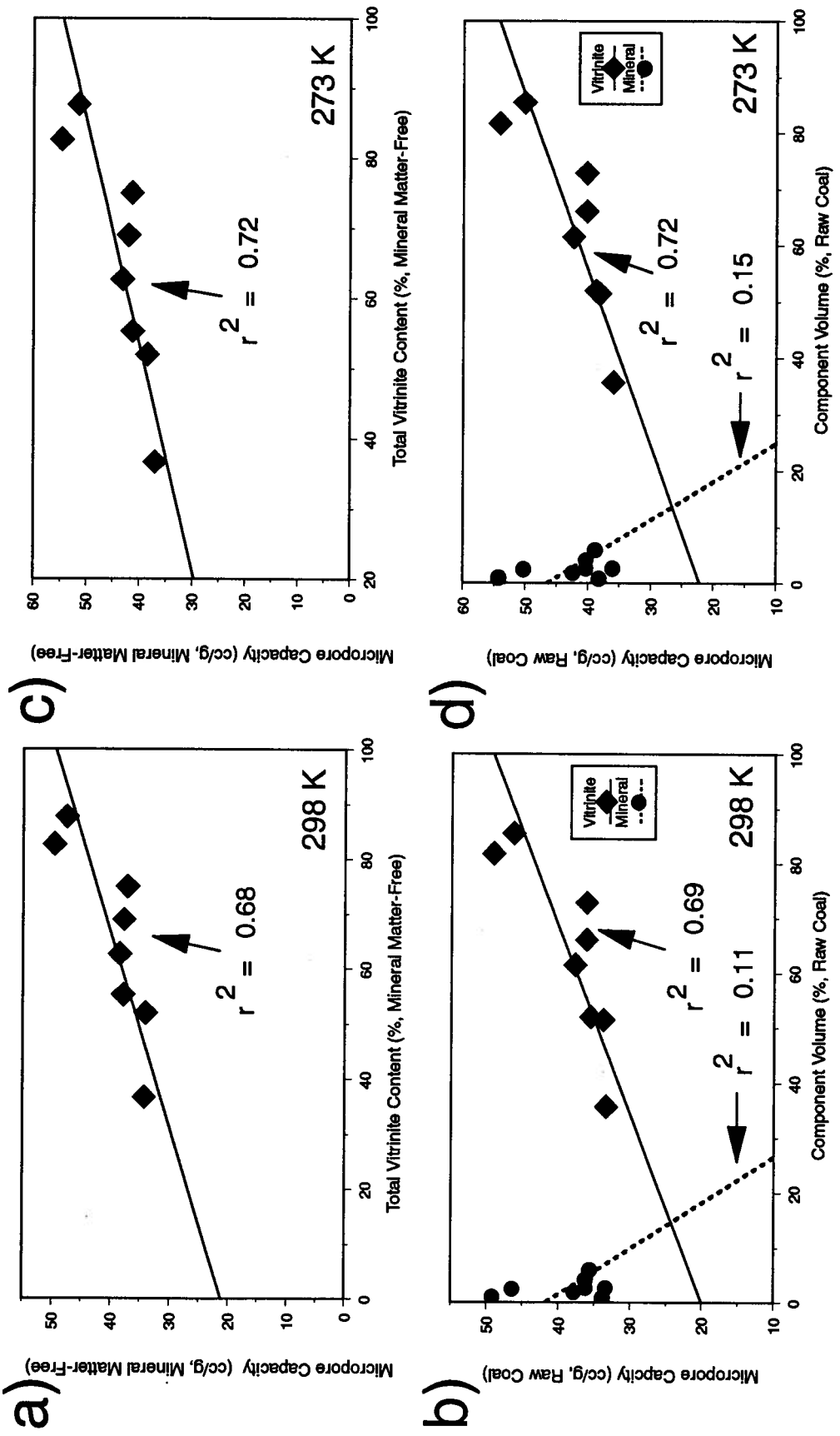

Figure 3-8 . Plots of carbon dioxide D-R micropore capacities versus Alberta suite coal composition on a raw coal (b, d) and mineral-free (a, c) basis at 298 K (a, b) and 273 K (c, d). Mineral-free micropore capacities calculated using the Parr Formula.

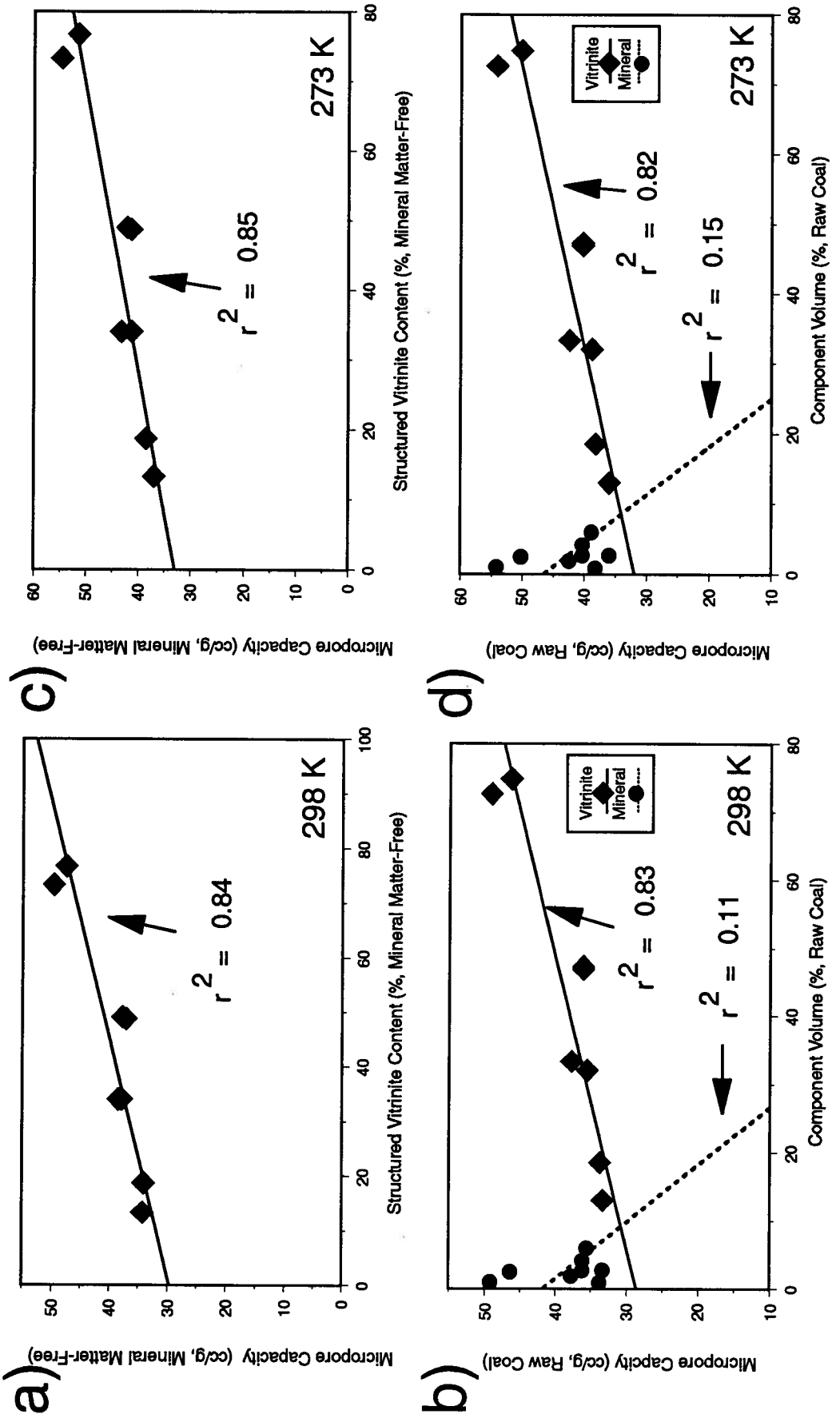

Figure 3-9. Plots of carbon dioxide D-R micropore capacities versus Alberta suite coal composition on a raw coal (b, d) and mineral-free (a, c) basis at 298 K (a, b) and 273 K (c, d). Mineral-free micropore capacities calculated using the Parr Formula.

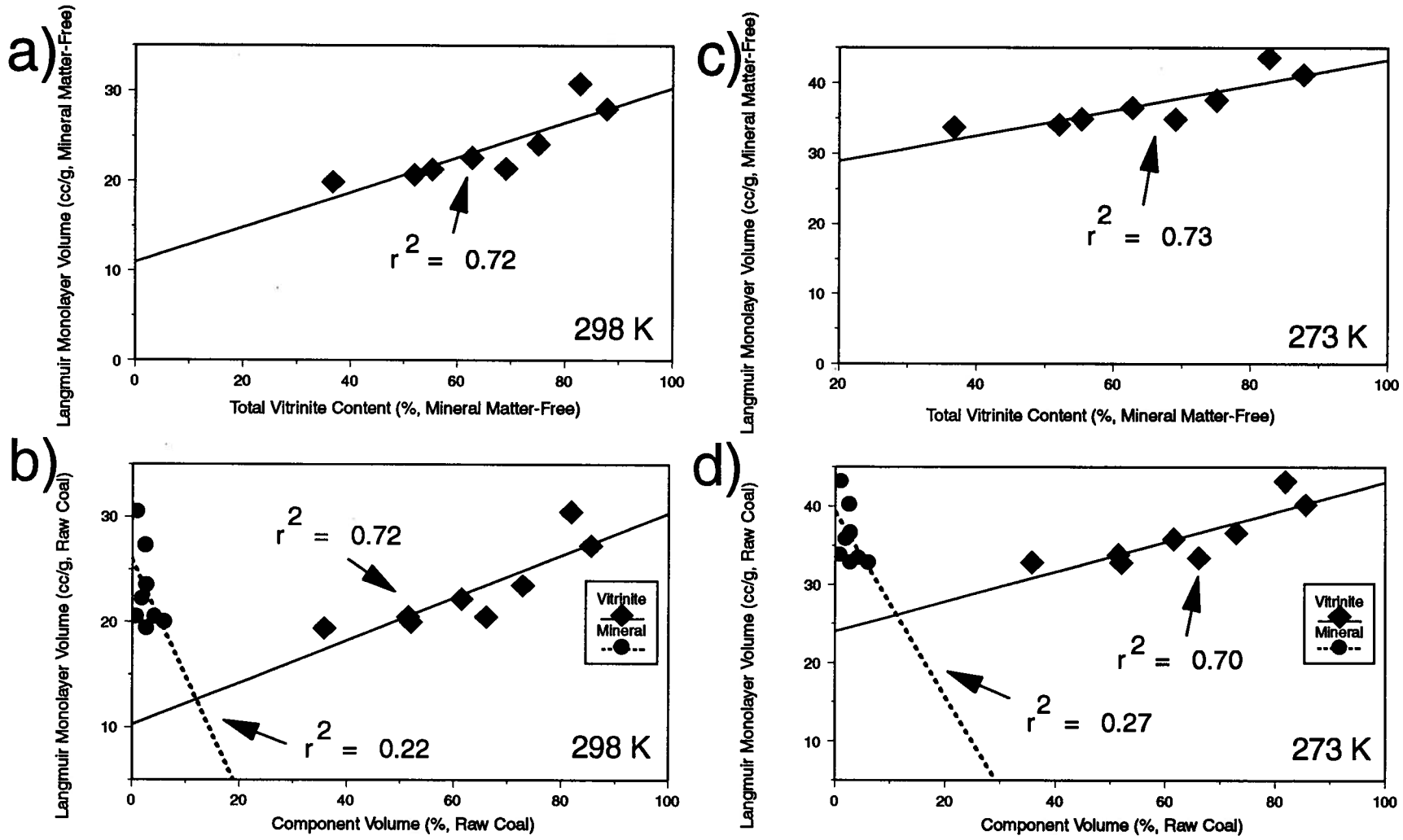

Figure 3-10. Plots of carbon dioxide Langmuir monolayer volumes versus Alberta suite coal composition on a raw coal (b, d) and mineral-free (a, c) basis at 298 K (a, b) and 273 K (c, d). Mineral-free monolayer volumes calculated using the Parr Formula.

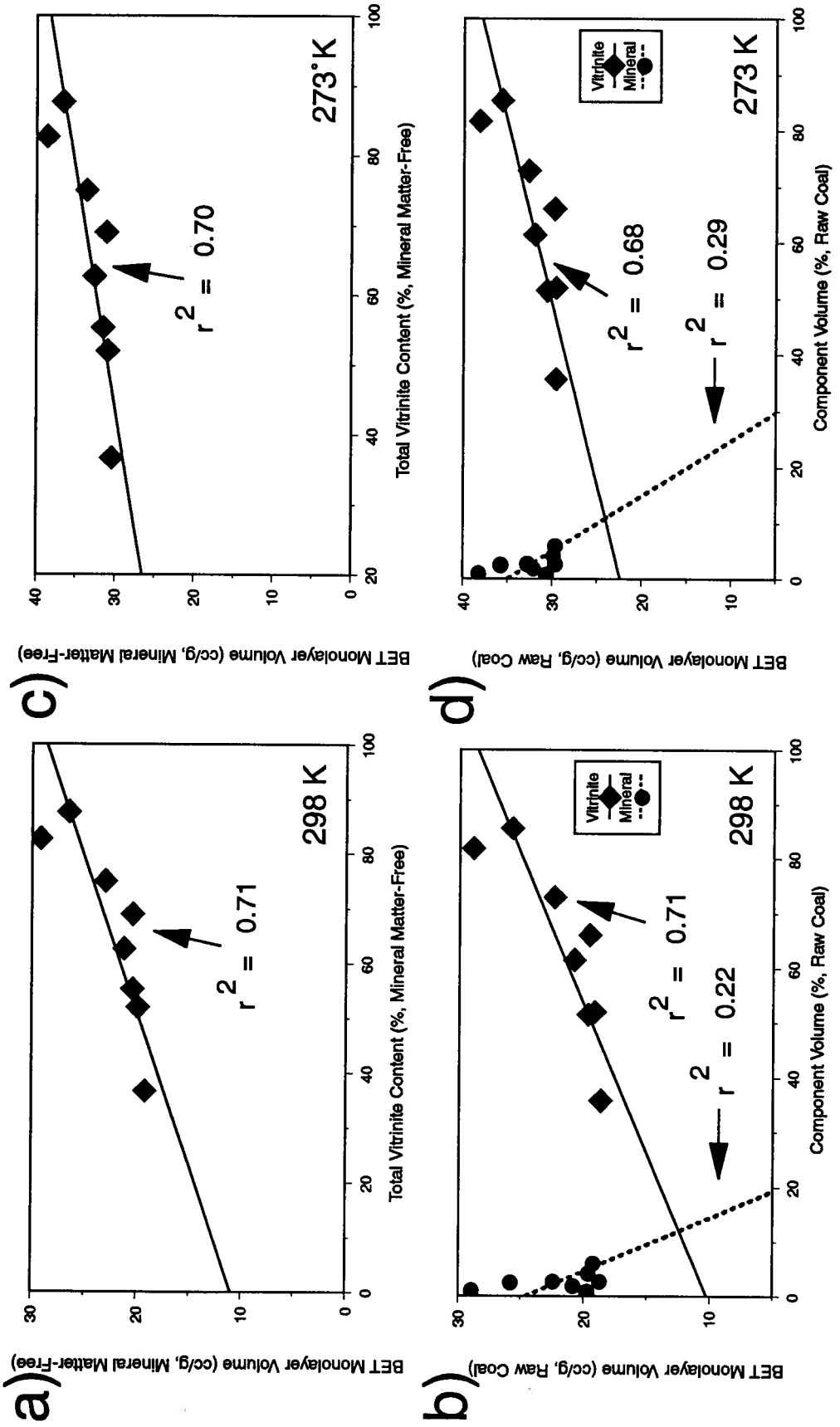

Figure 3-11. Plots of carbon dioxide BET monolayer volumes versus Alberta suite coal composition on a raw coal (b, d) and mineral-free (a, c) basis at 298 K (a, b) and 273 K (c, d). Mineral-free monolayer volumes calculated using the Parr Formula.

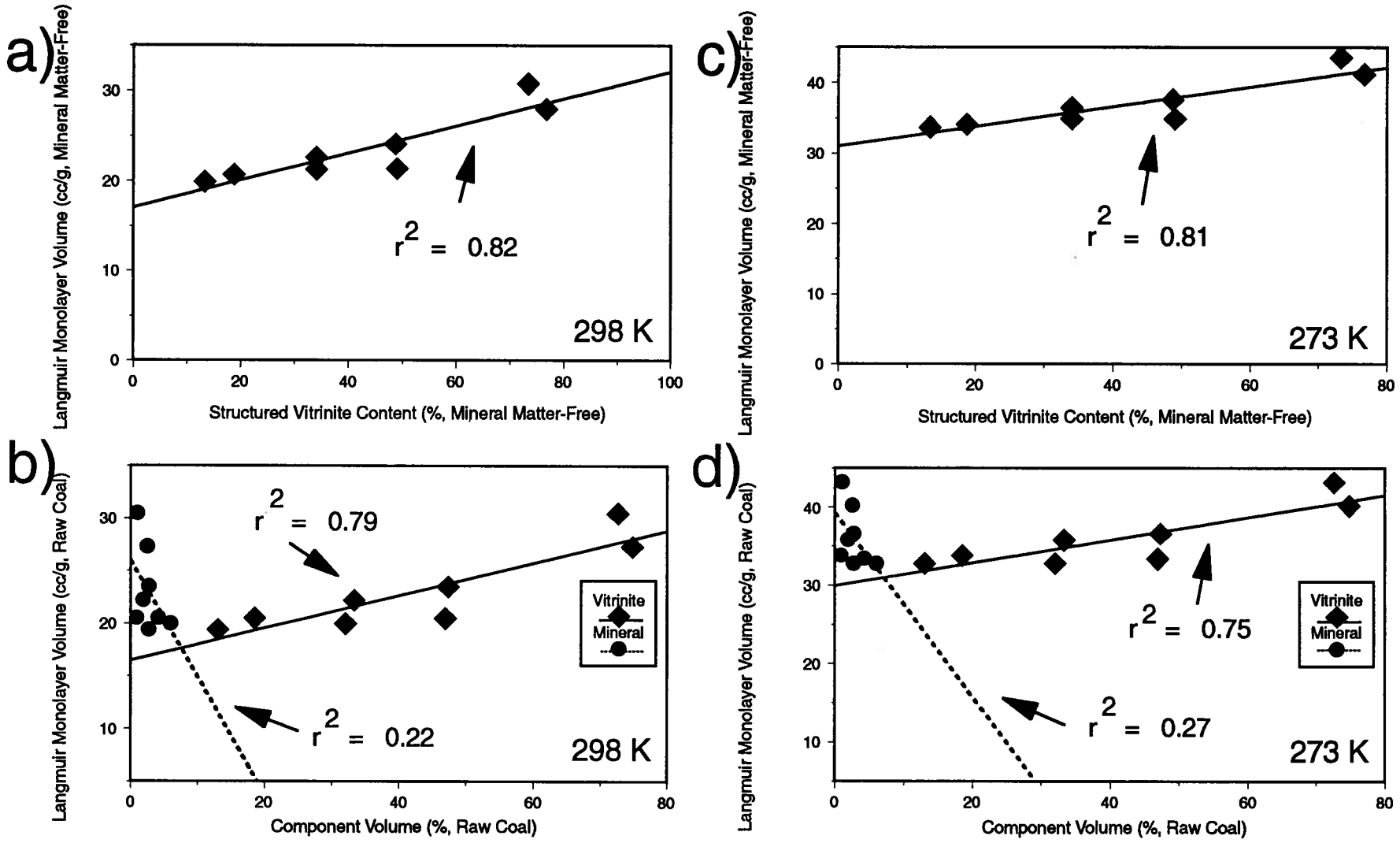

Figure 3-12. Plots of carbon dioxide Langmuir monolayer volumes versus Alberta suite coal composition on a raw coal (b, d) and mineral-free (a, c) basis at 298 K (a, b) and 273 K (c, d). Mineral-free monolayer volumes calculated using the Parr Formula.

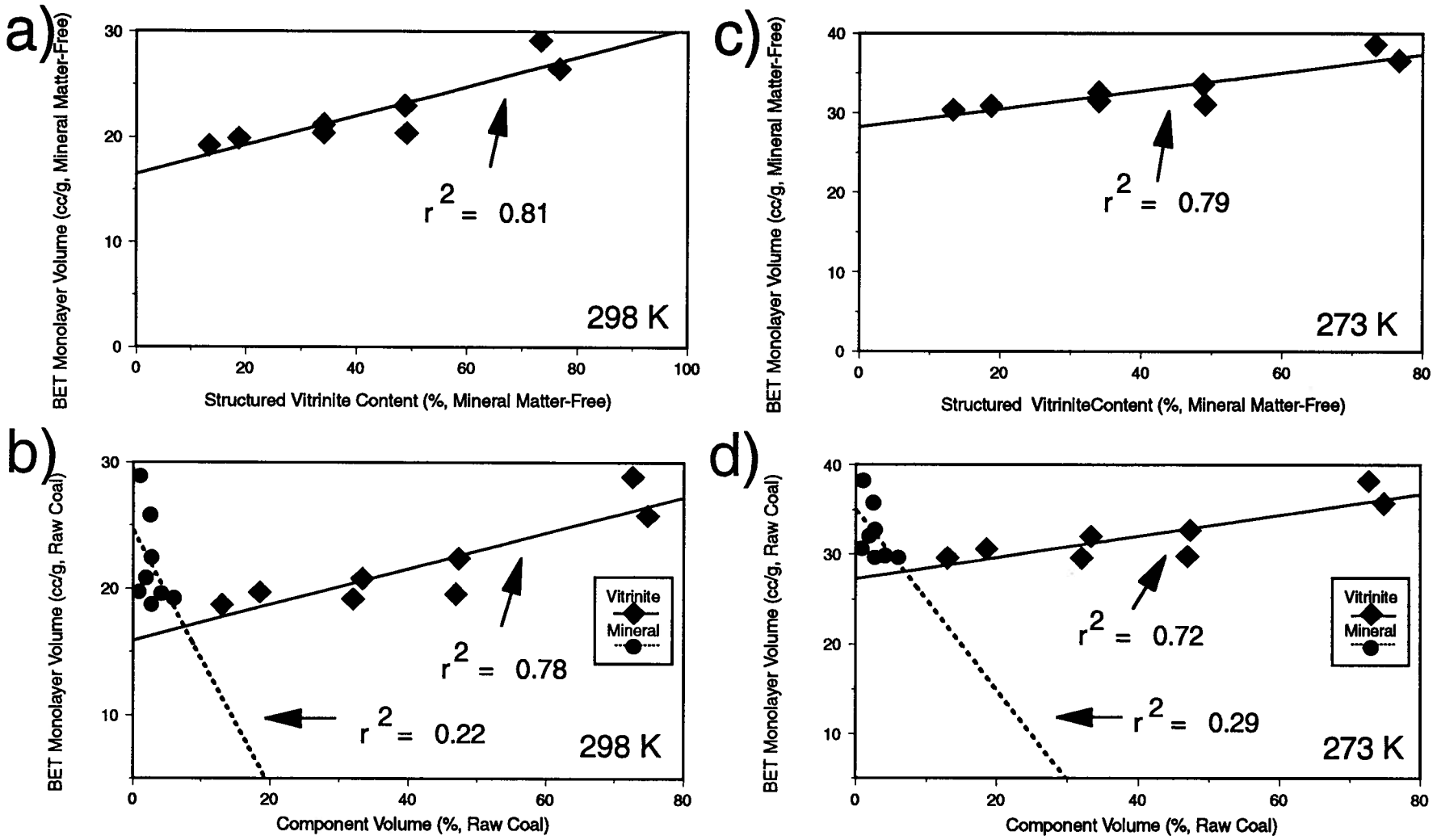

Figure 3-13. Plots of carbon dioxide BET monolayer volumes versus Alberta suite coal composition on a raw coal (b, d) and mineral-free (a, c) basis at 298 K (a, b) and 273 K (c, d). Mineral-free monolayer volumes calculated using the Parr Formula.

3.6 DISCUSSION

The adsorption characteristics of the two coal suites studied are determined by their petrographic compositions. The composition of the coals affects the pore structure and resulting micropore capacity, which in turn determines the ultimate gas capacity. Details about the micropore structure and adsorbate-adsorbent interactions may be obtained through the study of the Dubinin parameters and plots.

In the following discussion, factors affecting the gas adsorption characteristics of the coal suites are discussed, and the Dubinin plots examined in detail in an attempt to elucidate the effect of coal composition upon pore structure. Langmuir and BET plots for both suites are used to obtain further information concerning the effect of coal composition upon gas adsorption characteristics of the coals. The variation of equilibrium moisture content with composition for the Gates coals is examined and the implications for methane gas adsorption discussed. Finally, the origin of microporosity with respect to coal structure will be discussed.

3.6.1 Gates Suite

For the Gates suite, the low pressure carbon dioxide (Figure 3-2) and high pressure methane monolayer (Figure 3-5) capacities show a general decrease with increased mineral matter or inertinite content. Conversely carbon dioxide and methane monolayer capacities increase with increased total vitrinite content. The high pressure methane monolayer capacities are smaller but correlatable with the carbon dioxide micropore capacities (Figure 3-6). The smaller carbon dioxide micropore capacities may be due to the quadrupolar nature of the carbon dioxide molecule which may allow it to assume a more closely packed arrangement within the micropores compared to methane (Lamberson and Bustin, 1993). The polar carbon dioxide molecule may also interact more strongly with polar groups at the micropore surface than methane. Finally, the high pressure methane analyses were performed at equilibrium moisture whereas the carbon dioxide analyses were performed on evacuated samples. Previous studies (Joubert et al., 1973)

have shown that sorption of methane decreases with an increase in moisture up to a critical moisture content; this may also explain the lower high pressure methane monolayer capacities.

The sample with the smallest carbon dioxide micropore capacity is the sample with the highest total inertinite content. The most abundant inertinite maceral in LTC-5 is fusinite, which appears to suppress the amount of gas adsorbed.

The increase in carbon dioxide micropore capacity (and micropore surface area) with vitrinite content is due to an associated increase in the total amount of microporosity (Figure 3-15). These results support earlier conclusions that vitrinite is essentially microporous whereas inertinite is mainly meso-macroporous (Harris and Yust, 1979). The coals in the Gates suite have similar mean micropore sizes, but differing micropore capacities, which are dependant upon vitrinite content.

The sample with the largest carbon dioxide and methane monolayer capacity, however, is LTC-7 which does not have the highest total vitrinite content, but a mixture of vitrinite and inertinite. The inertinite in LTC-7 is mostly in the form of semifusinite, a submaceral interpreted to be created by the partial burning (charring) of vitrinite precursors. It is possible that the burning of vitrinite precursors creates microporosity. The loss of volatile matter as a result of charring may open up the pore structure, allowing additional adsorption. The process may be analogous to that described by Dubinin (1982) for strongly or overactivated carbons, whereby microporosity is thought to be created by the removal of walls between adjacent micropores through burning (Dubinin and Stoeckli, 1980). Dubinin (1966) proposed a two-term D-R equation to account for two linear segments of the transformed plot in active carbons subjected to varying degrees of burnout. The steeper sloped linear segment was believed to be due to the existance of supermicroporosity (< 1.4 - 3.2 nm diameter) created by burnout of the activated carbon and the shallower segment due to inherent microporosity. In the D-R transformed isotherms given for the Gates samples (Figure 3-14), only one linear segment is observed, however. That burning creates microporosity in semifusinite is supported by the fact that LTC-7

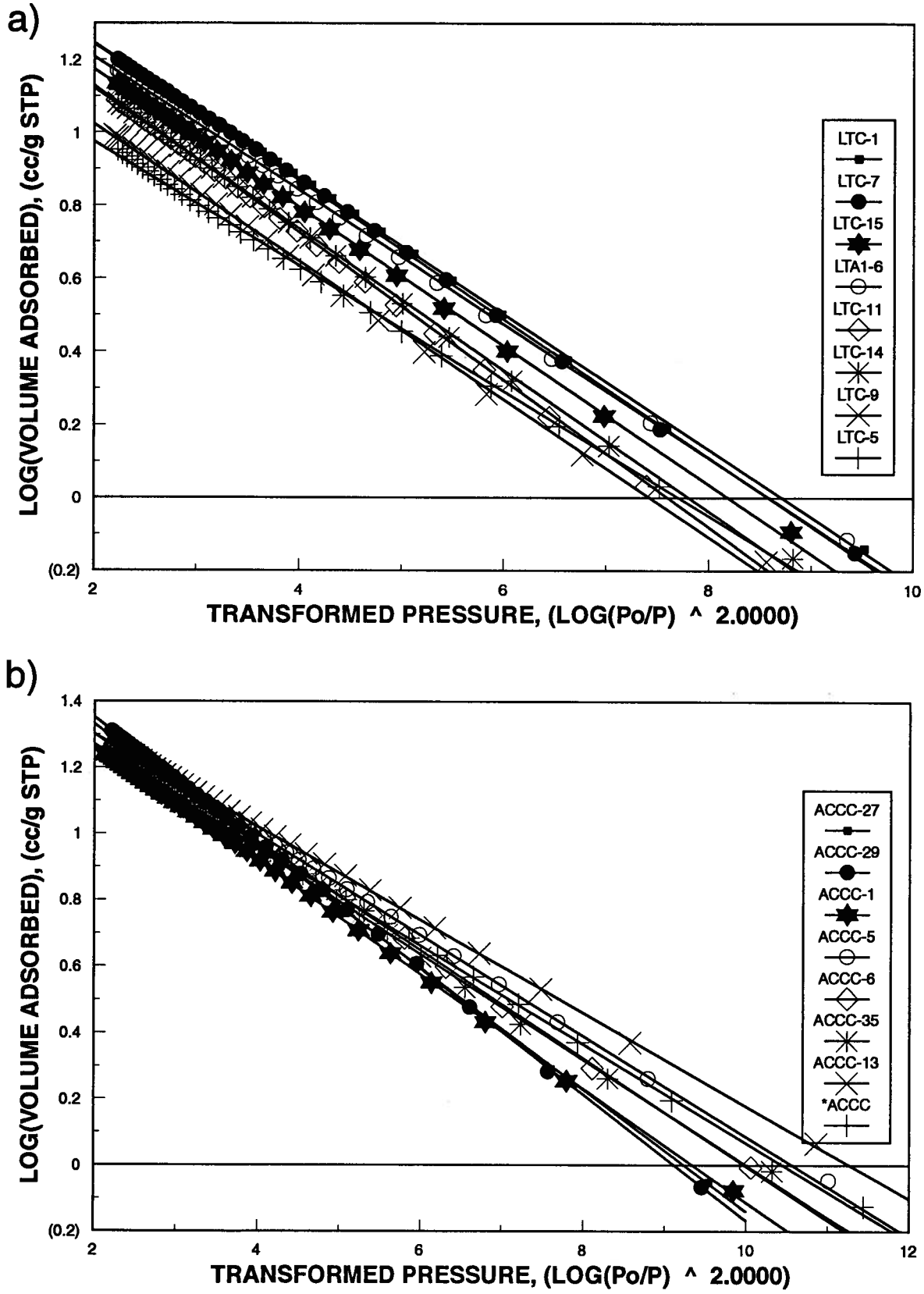

Figure 3-14. Dubinin-Radushkevich transformed isotherm plots for the Gates (a) and Alberta (b) suites. Calculations were made using the 273 K carbon dioxide isotherm.

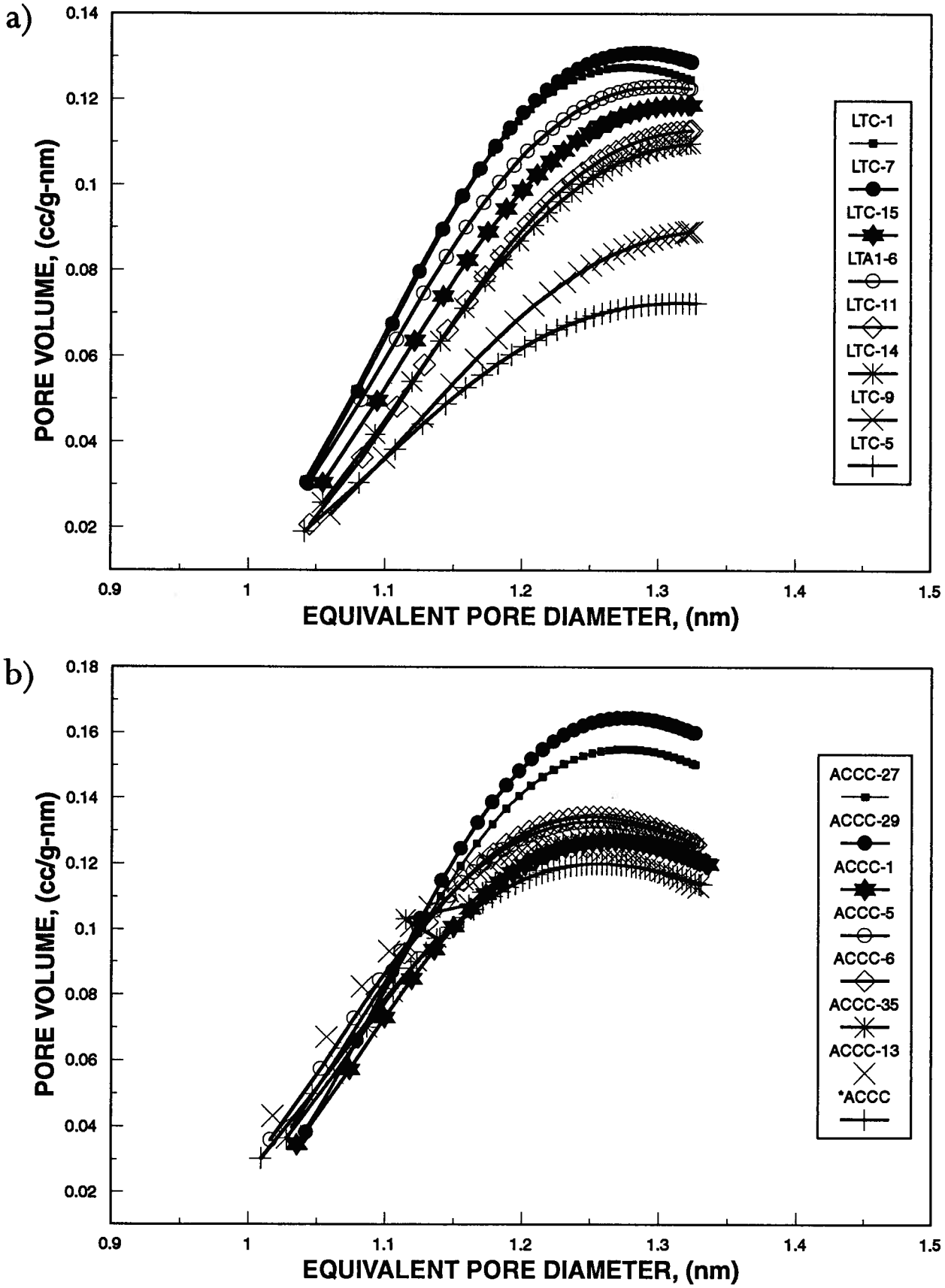

Figure 3-15. Dubinin-Astakhov differential pore volume plots for the Gates (a) and Alberta (b) suites. Calculations were made using the 273 Kelvin carbon dioxide isotherm.

has the greatest total number of micropores (Figure 3-15) even though it does not have the highest total vitrinite content.

The increased adsorption within the semifusinite and vitrinite-rich coal could be also be attributed to the swelling properties of semifusinite. Semifusinite has been demonstrated to swell in water to a greater extent than vitrinite and may swell more than vitrinite when carbon dioxide is adsorbed, creating more accessable surface area (Unsworth et al., 1989).

Semifusinite content appears to be an important factor controlling gas yield determined from canister desorption studies of western Canadian coals. Potter (1993) noted that gas yield is greatest in coals of the Mist Mountain Formation (Southeastern Alberta) with semifusinite as the dominant inertinite maceral. Gas desorption results from this same formation are correlated with micropore capacities later in this chapter.

3.6.1.1 Dubinin-Radushkevich Plots

D-R plots (Figure 3-14) reveal information about the nature of porosity and adsorbate-adsorbent interactions in the Gates coals. The plots have similar slopes but differing intercepts. The coals have differing micropore capacities (obtained from Y-intercept) depending on composition as discussed above.

The linearity of these plots suggests that the assumption that adsorption energies in micropores of the Gates coals obey a Gaussian distribution is satisfactory. Further, deviations from linearity due to the presence of polar-polar adsorbate-adsorbent interactions does not occur as might be expected for the interaction of the quadrupolar carbon dioxide molecule with functional groups of the coal surface. Marsh states (1987) however, that with polar adsorbates, the gradient of the D-R plot should decrease with increasing temperature due to the temperature dependance of polar adsorbate adsorption. The Gates 273 K D-R plots do have a higher average gradient than the 298 K D-R plots, suggesting that the quadrupolar carbon dioxide adsorbate is not strictly being adsorbed to the coal surface through temperature invariant van der Waals

forces. The increased gradient at lower temperatures accounts for the higher micropore capacities at 273 K.

The consistancy of the gradient at each temperature of the D-R plots suggests that the average pore size of the Gates coals is similar, as revealed by the pore size distribution plots (Figure 3-15). According to Marsh (1987), for adsorbents of similar type, lower gradients indicate narrow pores, and higher gradients represent wider pores. The mean equivalent pore diameter as determined from the Dubinin-Astakhov treatment, however, does decrease slightly with total vitrinite content and increase with mineral matter content (Figure 3-16).

3.6.1.2 Dubinin-Astakhov Differential Pore Volume Plots

The Dubinin-Astakhov differential pore volume plots for the Gates suite are shown in Figure 3-15. The pore size distributions are fit to a Weibull distribution as opposed to a Gaussian distribution assumed for the Dubinin-Radushkevich equation. In the Dubinin-Astakhov treatment, the exponent 'n' is optimized, whereas for the Dubinin-Radushkevich treatment the exponent is assumed to be equal to 2. The value of 'n' is believed to reflect the nature of the pore size distribution.

The exponent 'n' for the Gates suite appears to increase linearly with vitrinite and decrease with inertinite and mineral matter content (Figure 3-16), although the value does not vary much from 2 (Table 3-7). Dubinin (1966) states that a value of n = 2 is indicative of a carbonaceous adsorbent with a homogeneous micropore distribution. Stoeckli (1989), however, states that homogeneous active carbons should have an exponent 'n' equal to 3, and that the degree of heterogeneity of the micropore system increases as 'n' decreases. The value of 'n' for the Gates coals is for the most part less than 2, so they do not qualify as truly homogeneous molecular sieve materials. The decreasing value of 'n' with decreasing vitrinite content and increasing inertinite content suggests that the degree of heterogeneity of the micropore system increases with decreasing vitrinite and increasing inertinite content. This follows because the two maceral groups have different ranges of pore sizes.

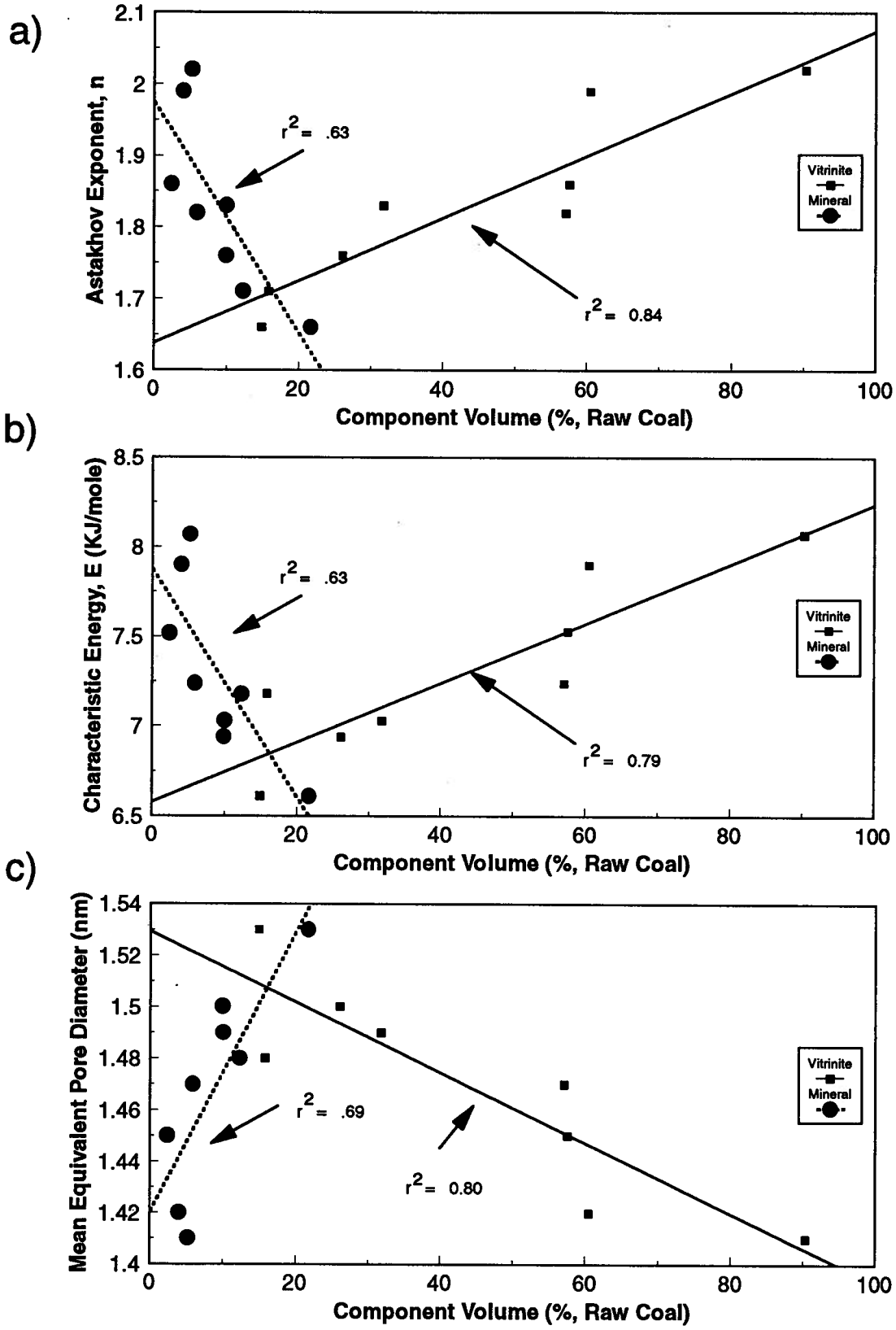

Figure 3-16. Plots of Astakhov exponent (a), characteristic energy (b) and mean equivalent pore diamter (c) versus Gates coal composition on a raw coal basis. The 273 K isotherm was used.

Table 3-7. Astakhov exponents, characteristic energies, and mean equivalent pore diameters calculated from 273 K carbon dioxide isotherm.

	Sample	Astakhov Exponent n	Characteristic Energy E (KJ/mole)	Mean Equivalent Pore Diameter (nm)
Gates Suite	LTC-1	2.02	8.07	1.41
	LTC-7	1.99	7.90	1.42
	LTC-15	1.82	7.24	1.47
	LTA1-6	1.86	7.52	1.45
	LTC-11	1.83	7.03	1.49
	LTC-14	1.76	6.94	1.50
	LTC-9	1.66	6.61	1.53
	LTC-5	1.70	7.18	1.48
Alberta Suite	ACCC-27	2.03	8.14	1.41
	ACCC-29	2.07	8.13	1.41
	ACCC-1	2.00	8.33	1.40
	ACCC-5	1.89	8.44	1.40
	ACCC-6	2.01	8.59	1.38
	ACCC-35	1.85	8.08	1.42
	ACCC-13	1.94	9.00	1.36
	*ACCC	1.85	8.38	1.40

3.6.1.3 Langmuir and BET Analysis

Carbon dioxide monolayer volumes were obtained in the low relative pressure range, using Langmuir and BET theories, to determine the relationship between these values and carbon dioxide D-R micropore capacities. Langmuir and BET monolayer volumes were obtained by extrapolation from the linear portion of the plot, at relative pressures greater than .004, to the Y axis. At lower relative pressures (< .004) the plot deviates upward from linearity. The cause for this deviation from linearity for carbon dioxide at relative pressures lower than 0.004 is uncertain, but may be related to the polarity of the carbon dioxide molecule and interaction with surface groups of the coal.

The BET equation is normally assumed to be valid over the relative pressure range 0.05 to 0.30, although Dubinin (1969) obtained a linear plot for nitrogen on carbon black at relative pressures from .005 to 0.15 which is similar to the range of linearity obtained in the current study. The cause for linearity of the obtained plots at relative pressures below 0.1 is believed to be due to enhanced adsorption potential in micropores which may lead to condensation at lower relative pressures. BET C values for the Gates suite are relatively small compared to values recorded for microporous materials (Table 3-5), but low values of C are not uncommon with carbon dioxide as an adsorbent (Gregg and Sing, 1982).

A linear relationship exists between the Langmuir monolayer volumes found in the above range of relative pressures and the D-R micropore capacities for the Gates suite. Kobayashi et al. (1993) have shown that for several adsorbates on a variety of carbons V_0 and V_m obey the relationship:

$$V_0 = KV_m$$

where K is a constant. For carbon dioxide (at 298 K) on a variety of carbons, the constant K was found to be equal to 1.145. For the Gates coal suite, this constant was found to be equal to 1.470.

3.6.1.4 Equilibrium Moisture

Joubert et al. (1973) noted that adsorption of methane is a function of moisture content up to a 'critical value' of moisture content. Equilibrium moisture (EM) contents (wt %) of the Gates coals appear to increase linearly with total vitrinite content (vol %, raw coal) (Figure 3-17). Unsworth et al. (1989) suggest that the difference in EM of inertinites and vitrinites found by previous studies is due to the fact that inertinite is mainly meso-macroporous and vitrinite is mainly microporous. Unsworth et al., however found that there is no clear dependance of EM and total porosity upon vitrinite content in coals.

In addition to differences in pore structure between inertinite and vitrinite-rich coal, differences in surface chemistry such as a lack of primary sites for adsorption at low relative pressures for the inertinite-rich coals relative to vitrinite-rich coal may also account for the variation in adsorbed water (Evans, 1986). Joubert et al. (1973) found that the moisture content of coal increases with oxygen content of coal in a general way. Vitrinite has a larger number of oxygen-containing surface complexes that act as primary adsorption sites for the polar water molecule. Because vitrinite usually has a higher average oxygen content than inertinite (Greene et al., 1982), it follows that that vitrinite-rich coals should also have a higher equilibrium moisture content than inertinite-rich coals. The vitrinite-rich coals have higher equilibrium moisture contents despite the fact that inertinite is more hydrophilic than vitrinite on a macroscopic surface (Arnold and Aplan, 1989). The increase in equilibrium moisture with vitrinite content therefore appears to be due to both the pore structure and surface chemistry of the vitrinite maceral group.

Although equilibrium moisture varies with total vitrinite content of the Gates, increase in methane adsorption measured at equilibrium moisture with vitrinite content still occurs.

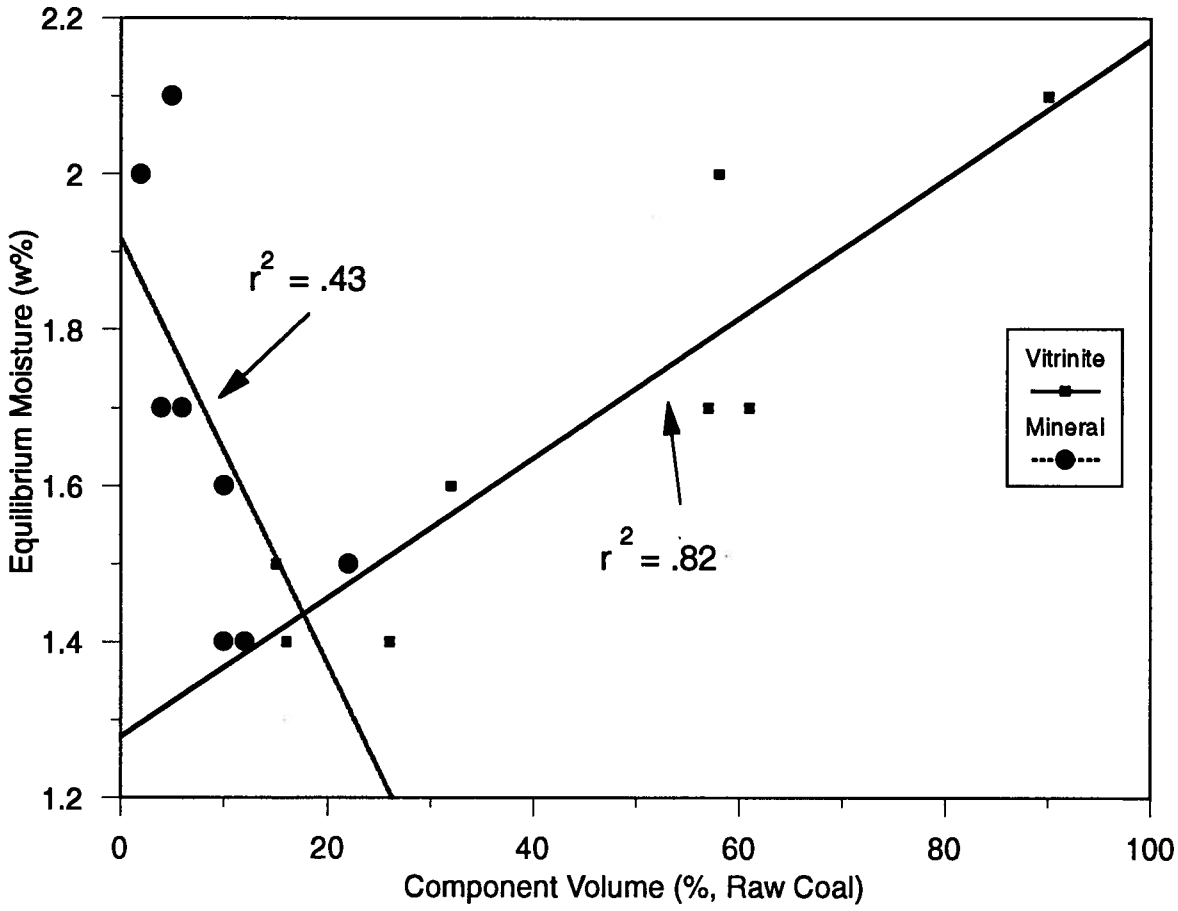

Figure 3-17. Plot of equilibrium moisture versus Gates coal composition on a raw coal basis.

3.6.2 Alberta Suite

The Alberta suite coals yield a linear relationship between carbon dioxide micropore capacity and total and structured vitrinite (Figures 3-8, 3-9). The micropore capacities increase with an increase in vitrinite content and decrease with inertinite content. A poor correlation, however, is achieved between micropore capacity and mineral matter content for the Alberta suite. No XRD analysis was performed on the Alberta suite so it is difficult to assess the contribution of the mineral matter to the total surface area of the coals. The mineral matter content of the Alberta suite is less variable than the Gates, which might explain the poor correlation with monolayer capacities.

Samples ACCC-27 and ACCC-29 yield the largest micropore capacities due to their high vitrinite content. ACCC-29 has a larger micropore capacity than ACCC-27 even though the former has a lower vitrinite content.

Semifusinite does not appear to be a significant contributor to the surface area of the Alberta suite. Semifusinite content is greatest in the coals (*ACCC and ACCC-13) with the lowest carbon dioxide micropore capacity. These two samples, however, have a high total inertinite content which suppresses adsorption.

Plots of the carbon dioxide micropore capacity versus vitrinite content for both the Gates and Alberta suites is given in Figure 3-18. Because the two sample suites are similar in rank, the variation between suites is mainly due to composition. The Alberta suite has a higher average vitrinite content and lower mineral matter content, which may explain the higher average carbon dioxide micropore capacities for the Alberta suite.

The effects of rank cannot be excluded, however. The Alberta suite is of lower rank and may contain a higher amount of micropore surface polarity or smaller average micropore mean size (see later) due to this fact. Both factors would lead to greater apparent micropore capacities for the Alberta suite.

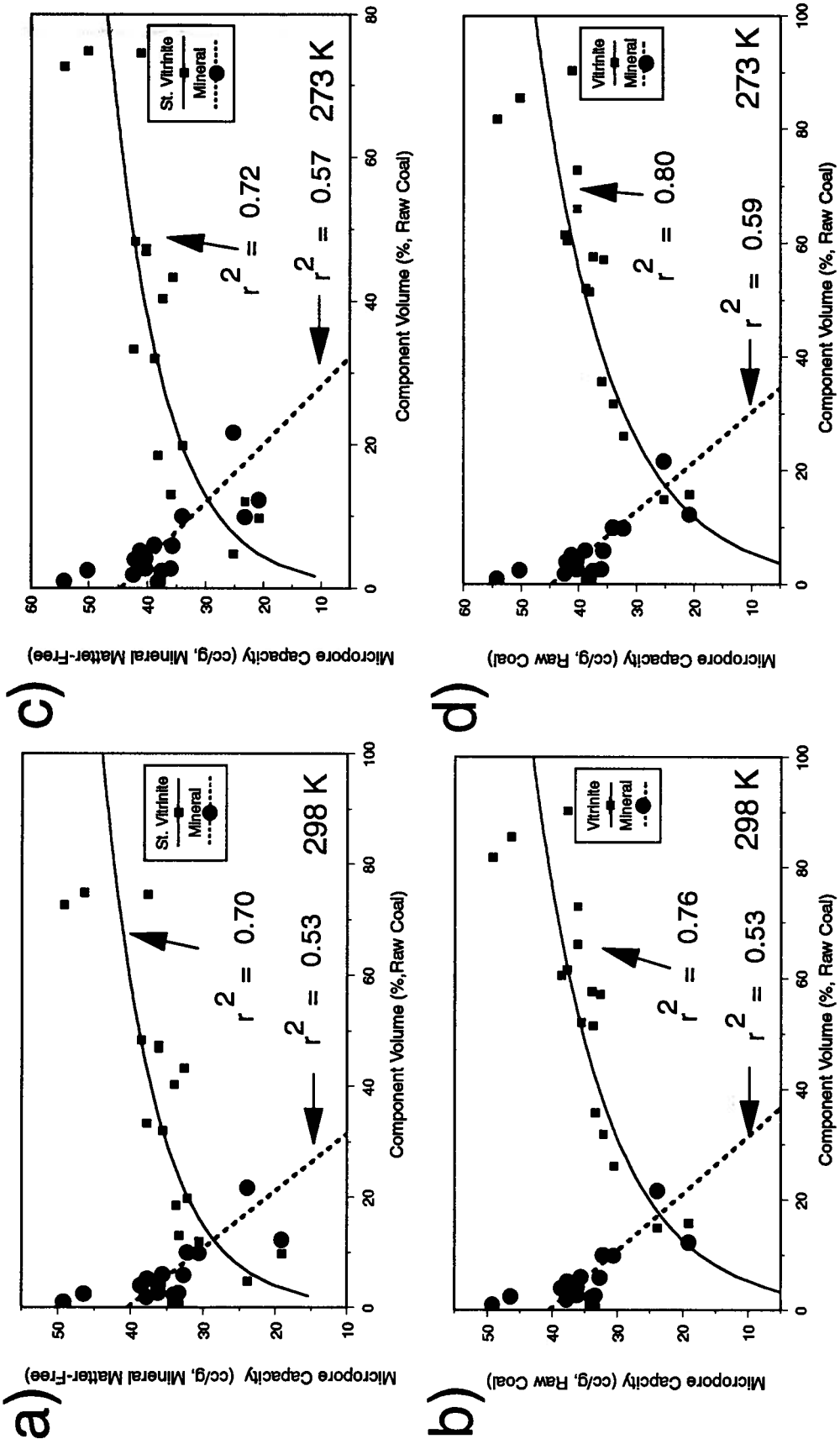

Figure 3-18. Plots of carbon dioxide D-R micropore capacities versus Gates and Alberta suite coal composition, on a raw coal basis, calculated from a 298 K isotherm (a,b) and a 273 K isotherm (c, d). Total vitrinite versus micropore capacity is plotted in b) and d); Structured vitrinite versus micropore capacity in a) and c).

3.6.2.1 D-R Plots

D-R plots for the Alberta suite (Figure 3-14) are linear, which shows that the adsorption energies obey a Gaussian distribution. Gradients increase with a decrease in temperature (as with the Gates suite) due to the polar interaction of the carbon dioxide molecule with the coal surface. The gradients of the plots, unlike the Gates suite, are not uniform, which may be due to a greater variation in mean pore size of the samples. The gradients for the low total vitrinite content samples are slightly lower than those for higher vitrinite samples. The mean equivalent pore diameter, as determined from D-A treatment, does not decrease in a consistant manner with vitrinite content as with the Gates suite, however.

3.6.2.2 D-A Differential Pore Volume Plots

Dubinin-Astakhov differential pore volume plots for the Alberta suite are given in Figure 3-15. The two samples that have the largest carbon dioxide monolayer capacities and total vitrinite contents (ACCC-29 and ACCC-27) have the largest number of micropores. The number of micropores, like the Gates suite, appear to increase, in a general way, with vitrinite content.

The exponent 'n' for the Alberta suite does not vary much from the value of 2, but does decrease slightly with a decrease in vitrinite content. An increase in degree of heterogeneity of pore size with decrease in vitrinite content thus occurs in both suites. The higher average value of 'n' for the Alberta suite (1.9 versus 1.8) is indicative of smaller pore sizes.

The mean equivalent pore diameter of the Alberta suite is slightly smaller than that of the Gates suite (1.40 nm and 1.47 nm, respectively) which may be due to: a) higher average vitrinite content of the Alberta suite; b) the difference in rank c); resinite impregnation in structured vitrinite of the Alberta suite; or d) mineral matter composition. Resinite impregnation may constrict pore access analogous the situation of active carbon impregnation with cobalt and nitrate solutions (Alvim Ferraz, 1989). Pore constriction due to resin impregnation may decrease the average micropore size in vitrinite. This may exlain why ACCC-27 and ACCC-29 have higher

micropore surface areas than LTC-7 or LTC-1 of the Gates suite, despite the fact the two Alberta suite coals have lower total vitrinite contents.

Another possible cause of the difference in mean pore sizes between suites may be due to the type of mineral matter present in the coals. The Alberta suite may contain more mixed layer clay which could increase the micropore volume. The Gates suite contains little or no mixed layer clays, whereas the mixed layer clay content of the Alberta suite is not known. The interlayer of such clays could possibly provide additional adsorption space for carbon dioxide. For example, the basal (001) spacing of the phyllosilicate vermiculite is 1.4 nm, which is close to the mean equivalent pore diameter of the Alberta suite. The accessibility of the adsorption space between interlayers depends on the amount of adsorbed water left in the interlayer after degassing under the conditions specified earlier. Under the conditions of degassing used, most of the adsorbed water in the interlayer would likely still be present and the interlayer may not be accessible for the physisorption of carbon dioxide, although some carbon dioxide gas may be dissolved in interlayer water. Further research is required on this point.

3.6.2.3 Langmuir and BET Analysis

A linear relationship between the Langmuir monolayer volume (Vm) and the D-R micropore capacity (Vo) also occurs for the Alberta suite. The value of K is 1.68 compared to 1.47 for the Gates suite.

BET C values range from 87 to 50 for the Alberta suite and are higher on average than the Gates suite, which is consistant with the higher average micropore capacity of the Alberta suite.

3.6.3 Comment on the Origin and Nature of Microporosity in Coals

A generally accepted view of coal structure is that it consists of a three-dimensional cross-linked macromolecular framework (Greene et al., 1982). Derbyshire et al. (1989) have suggested that there may, in fact, be two components of coal including a three-dimensional cross-linked macromolecular structure and a molecular phase trapped within this structure

Some authors (Dryden, 1963; Fuller, 1981; and Given, 1984) suggest that microporosity is not necessarily a fixed property of coal structure and argue that gas sorption in coal may either be modeled as adsorption within the molecular structure of the coal or as dissolution of the sorbate within the molecular structure. Marsh (1987) states that microporosity exists as "space of low electron density between the macromolecules of the cross-linked entanglements". The cross-link density has been shown to change with rank: the initial predominantly oxygen cross-links (primarily ethers?) decrease in density to a minimum at ca. 86% carbon (medium volatile bituminous stage) after which carbon-carbon cross-links are formed. The trend in carbon dioxide surface areas and micropore volumes of vitrinite-rich coals appears to mimic the trend in cross-link density. These values have been found to decrease with rank to about 85% carbon content and increase for higher carbon content (Mahajan, 1982). As the cross-link density decreases with rank below 85% carbon content, the adsorption capacity of the coal would decrease due to a decrease in adsorption potential in the pore space. An additional consideration is that the oxygen content of the whole coal decreases with coalification, and that the interaction of the polar carbon dioxide molecule with the oxygen containing functional groups may decrease to the minimum at 85% carbon. Polar interactions of the carbon dioxide molecule in lignites is not considered significant.

Increase in carbon dioxide surface areas at carbon contents greater than 85% may be related to the formation of carbon-carbon cross-links. Toda et al. (1971) have shown, however, that the carbon dioxide micropore volumes and apparent size increase with the amount of aliphatic, alicyclic, and aromatic CH hydrogen.

The trend in carbon dioxide micropore surface areas and volumes with organic composition, demonstrated in the current study, must similarly be linked to the structure and surface chemistry of the macromolecular network of the coal. Vitrinite-rich coals have been shown to have a greater amount of microporosity, and hence, larger monolayer capacities than vitrinite-poor coals of the same rank. The vitrinitic components may possess a greater density of cross-linking and possess a different structural orientation than inertinitic components. Further, differences in surface functionality of the respective maceral groups may account for differences in gas adsorption characteristics. For example, vitrinite possesses a greater oxygen content than inertinite macerals, and this may lead to a greater interaction of polar adsorbates such as carbon dioxide with the micropore surface in coals rich in vitrinite. Functional group type, density and orientation may similarly account for differences in gas adsorption characteristics of coals of varying composition.

Ultimately a true understanding of the trends in gas adsorption characteristics of coals of varying composition is dependant upon the understanding of coal structure and chemistry which continue to be debated (Derbyshire et al., 1989).

3.7 CONCLUSIONS

The current study has focused on the gas adsorption, particularly low pressure carbon dioxide adsorption, characteristics of two coals suites representing a large range in composition. Several important conclusions have been reached through the current study:

1) For both suites, Dubinin-Radushkevich carbon dioxide micropore (monolayer) capacities increase with total vitrinite content and decrease in a general way with mineral matter content. A better correlation was acheived between structured vitrinite composition and micropore capacity for the Alberta suite than for total vitrinite. For the Gates suite, high pressure methane monolayer capacities, as determined from the Langmuir equation, display a similar relationship to coal composition as carbon dioxide micropore capacities and are correlative but smaller than the carbon dioxide monolayer capacities.

2) For both suites, a general increase in the total number of micropores occurs with an increase in vitrinite content which, in turn, leads to an overall increase in carbon dioxide micropore capacities with vitrinite content. Microporosity correspondingly decreases with an increase in total (structured, unstructured and degraded) inertinite and mineral matter content.

3) Carbon dioxide micropore capacities of the Alberta suite are larger on average than the Gates micropore capacities. Such differences are attributed to the higher average vitrinite content of the Alberta suite and differences in rank.

4) For the Gates suite, a sample (LTC-7) with a high vitrinite and semifusinite content has the largest carbon dioxide monolayer capacity and total number of micropores. Semifusinite may contribute to the large number of micropores in this sample due to the creation of microporosity through charring of vitrinitic precursors. Swelling due to the adsorption of carbon dioxide gas upon vitrinite and semifusinite-rich coals may contribute to the large micropore capacities of such coals, but this effect requires investigation.

5) Carbon dioxide BET and Langmuir monolayer volumes show a similar relationship to coal composition as Dubinin-Radushkevich micropore capacities. Langmuir monolayer volumes are larger than the corresponding Dubinin-Radushkevich micropore capacities but the two are correlative.

6) Dubinin micropore capacities and Langmuir and BET monolayer capacities obtained at 273 K are larger than the corresponding values at 298 K which appears to indicate that polar interaction between the quadrupolar carbon dioxide molecule and polar surface groups is occurring.

7) For both suites, micropore heterogeneity appears to increase with total inertinite and mineral content, as indicated by a general increase in the Astakhov exponent 'n'.

8) For both suites, adsorption energies and hence micropore diameters appear to obey a Gaussian and Weibull distribution.

9) For the Gates suite, mean equivalent pore diameter decreases slightly with an increase in total vitrinite content and decrease in total inertinite and mineral matter content.

10) For the Gates suite, equilbrium moisture content generally increases with total vitrinite content due to an increase in microporosity with vitrinite. High pressure Langmuir methane monolayer capacities do generally increase with vitrinite content despite this fact.

From the above conclusions it is obvious that composition, as well as rank, has a definite control upon the pore structure and adsorption capacity of coal. In fact, the variation of methane adsorption capacities within one suite of compositionally variable coals may be just as large as the variation observed between coals of varying rank.

3.8 REFERENCES

Alvim Ferraz, M.C., 1989. Micropore volume determination in activated carbon. Fuel, 68: 635-640.

Arnold, B.J., and Aplan, F.F., 1989. The hydrophobicity of coal macerals. Fuel, 68: 651-658.

Ayers, W.B., Jr., and Kaiser, W.R., 1992. Coalbed methane occurrence and producibility, Fruitland Formation, Navajo Lake Area, San Juan Basin, New Mexico. In: Proceedings of the Canadian Coal and Coalbed Methane Geoscience Forum, Parksville, British Columbia, February 2-5th, 1992. pp. 3-20.

Brunauer, S., Emmett, P.H., and Teller, E., 1938. Adsorption of gases in multimolecular layers. The Journal of the American Chemical Society., 60: 309-319.

Dawson, F.M., and Clow, J.T., 1992. Coalbed methane research Elk Valley Coalfield. In: Proceedings of the Canadian Coal and Coalbed Methane Geoscience Forum, Parksville, British Columbia, February 2-5th, 1992. pp. 57-71.

Deissel, C.F.K., 1965. Correlation of macro- and micropetrography of some New South Wales coals. In: J.T. Woodcock, R.T. Madigan and R.G. Thomas (Editors), Proceedings 8th Commonwealth Mining and Metallurgical Congress, 6: 669-667.

Derbyshire, F., Marzec, A., Schulten, H., Wilson, M., Davis, A., Tekely, P., Delpuech, J., Jurkiewicz, A., Bronnimann, C.E., Wind, R.A., Maciel, G.E., Narayan, R., Bartle, K., Snape, C., 1989. Molecular structure of coals: a debate. Fuel, 68: 1091-1106.

Dryden, I.G.C., 1963. Chemical constitution and reaction of coal. In: H.H. Lowry (Editor), Chemistry of Coal Utilization Supplementary Volume. New York, John & Sons, pp 232-295.

Dubinin, M.M., 1965. Theory of the bulk saturation of microporous activated charcoals during adsorption of gases and vapours. Russian Journal of Physical Chemistry, 39: 697-704.

Dubinin, M.M., 1966. Porous structure and adsorption properties of active carbons. In: P.L. Walker, Jr. (Editor), Chemistry and Physics of Carbon, Volume 2. Edward Arnold, Ltd., New York. pp. 51-120.

Dubinin, M.M., 1975. Physical adsorption of gases and vapors in micropores. In: D.A.Cadenhead, J.F. Danielli, and M.D. Rosenberg (Editors), Progress in surface and membrane science, Volume 9. Academic press, New York. pp. 1-70.

Dubinin, M.M., 1982. Microporous structures of carbonaceous adsorbents. Carbon, 20: 195-200.

Dubinin, M.M., 1983. Microporous structures and absorption properties of carbonaceous adsorbents. Carbon, 21: 359-366.

Dubinin, M.M., 1985. Generalization of the Theory of Volume Filling of Micropores to nonhomogeneous microporous structures. Carbon, 23: 373-380.

Dubinin, M.M., 1989. Fundamentals of the theory of adsorption in micropores of carbon adsorbents: characteristics of their adsorption properties and microporous structures. Carbon, 27: 457-467.

Dubinin, M.M., and Astakhov, V.A., 1971. Advances in Chemistry Series. No. 102: p102.

Dubinin, M.M., and Stoeckli, H.F., 1980. Homogeneous and heterogeneous micropore structures in carbonaceous adsorbents. Journal of Colloid and Interface Science, 75: pp. 34-42.

Ertekin, T., Sung, W., and Bilgesu, H.I., 1991. Structural properties of coal that control coalbed methane production. In: D.C. Peters (Editor), Geology in Coal Resource Utilization. pp. 105-124.

Evans, M.J.B., 1987. The adsorption of water by oxidized microporous carbon. Carbon, 25: 81-83.

Fassett, J.E., 1987. Geometry and depositional environments of Fruitland Formation coalbeds, San Juan Basin, New Mexico and Colorado: anatomy of a giant coalbed methane deposit. In: Proceedings of the 1987 Coalbed Methane Symposium, Tuscaloosa, Alabama, Nov. 16-19, 1987. pp. 19-35.

Fuller, E.L., Jr., 1981. Physical and chemical structure of coals: sorption studies. In: M.L. Gobarty, and K. Ouchy (Editors), Coal structure: Advances in Chemistry Series 192, Washington, D.C., American Chemical Society, pp. 293-209.

Gan, H., Nandi, S.P., and Walker, P.L., Jr., 1972. Nature of the porosity in American coals. Fuel, 51: 272-277.

Given, P.H., 1984. An essay on the organic geochemistry of coal. In: M.L. Gobarty et al. (Editors), Coal Science, v.3 New York Academic Press, pp. 63-252, 339-341.

Greene, T., Kovac, J., Brenner, D., and Larsen, J.W. The macromolecular structure of coals. In: R.A. Meyers (Editor), Coal Structure. Academic Press. pp. 199-282.

Gregg, S.J., and Sing, K.S.W., 1982. Adsorption, Surface Area and Porosity, Second Edition. Academic Press, New York. 303 pp.

Harris, L.A., and Yust, C.S., 1976. Transmission electron microscope observations of porosity in coal. Fuel, 55: 233-236.

Harris, L.A., and Yust, C.S., 1979. Ultrafine structure of coal determined by electron microscopy. Preprint paper, American Chemical Society, Division of Fuel Chemicals , 24: 210-217.

Jaroniec, M., and Choma, J., 1989. Theory of gas adsorption on structurally heterogeneous solids and its application for characterizing activated carbons. In: P.A. Thrower (Editor), Chemistry and Physics of Carbon, Volume 22. Marcel Dekker, Inc., New York and Basel. pp. 197-243.

Jaroniec, M., Lu, X., Madey, R., and Choma, J., 1990. Comparitive studies of the overall adsorption isotherm associated with the Dubinin-Astakhov equation. Carbon, 28: 243-245.

Joubert, J.I., Grein, C.T., and Bienstock, D., 1973. Sorption of methane on moist coal. Fuel, 52: 181-185.

Kim, A.G., 1977. Estimating methane content of bituminous coalbeds from adsorption data. U.S. Bureau of Mines Report of Investigations 8245, 22p.

Kobayashi, M., Ishikawa, E., and Toda, Y., 1993. Experimental relation between the Dubinin-Radushkevich equation and Langmuir equation for various adsorbates on many carbons. Carbon, 31: 990-992.

Lamberson, M.N., and Bustin, R.M., 1993. Coalbed methane characteristics of the Gates Formation coals, northeastern British Columbia: effect of maceral composition. In press.

Langmuir, I., 1916. The constitution and fundamental properties of solids and liquids. Journal of the American Chemical Society, 38: 2221-2295.

Levine, J.R., 1993. Coalification: the evolution of coal as source rock and reservoir rock for oil and gas. In : B.E. Law and D.D. Rice (Editors), Hydrocarbons from coal, AAPG Studies in Geology # 38, pp. 39-77.

Lowell, S., and Shields, J.E., 1984. Powder Surface Area and Porosity, Second Edition. Chapman and Hall, London, 234 pp.

Mahajan, O.P., 1982. Coal porosity. In: R.A. Meyers (Editor), Coal Structure. Academic Press. pp. 51-86.

Mahajan, O.P., 1991. CO_2 surface area of coals: the 25 year paradox. Carbon, 29: 735-742.

Mahajan, O.P., and Walker, P.L., Jr. 1978. Porosity of coal and coal products. In: C. Karr, Jr (Editor), Analytical Methods for Coal and Coal Products, Volume I. Academic Press, New York. pp. 125-162.

Marsh, H., 1987. Adsorption methods to study microporosity in coals and carbon - a critique. Carbon, 25: 49-58.

Mavor, M.J., Owen, L.B., and Pratt, T.J., 1990. Measurement and evaluation of isotherm data; Proceedings of 65th Annual Technical Conference and Exhibition of the Society of Petroleum Engineers, SPE 20728: 157-170.

McEnaney, B., 1987. Estimation of the dimensions of micropores in active carbons using the Dubinin-Radushkevich equation. Carbon, 25: 69-75.

Medek, J., 1977. Possibility of micropore analysis of coal and coke from the carbon dioxide isotherm. Fuel, 56: 131-133.

Meissner, F.F., 1984. Cretaceous and lower Tertiary coals as sources for gas accumulations in the Rocky Mountain area. Source rocks of the Rocky Mountain Region, 1984 Guidebook, Rocky Mountain Association of Geologists, pp. 401-431.

Potter, J., 1993. Coalbed methane potential and the effects of coal composition and fractures in medium-volatile bituminous coals from the Mist Mountain Formation, southwestern Alberta (abstract). Geological Association of Canada/Mineralogical Association of Canada, Joint Annual Meeting, Program and Abstracts, p. A-84.

Rice, D.D., 1993. Composition and origin of coalbed gas. In: B.E. Law and D.D. Rice (Editors), Hydrocarbons from Coal, AAPG Studies in Geology # 38, pp. 159-184.

Sato, T., 1981. Methane recovery from coal beds: surface and physical properties of western United States coals; M. Sci thesis, The University of New Mexico, 78 pp., unpublished.

Sing, K.S.W., 1989. The use of physisorption for the characterization of microporous carbons. Carbon, 27: 5-11.

Stoeckli, H.F., 1990. Microporous carbons and their characterization: the present state of the art. Carbon, 28: 1-6.

Stoeckli, F., Huguenin, D., Greppi, A., Jakubov, T., Priblyov, A., Kalashnikov, S., Fomkin, A., Pulin, A., Regent, N., Serpinski, V., 1993. On the adsorption of CO2 by active carbons. Chimia, 47: 213-214.

Stoeckli, H.F., Kraehenbuehl, Ballerini, L., and De Bernardini, S., 1989. Recent developments in the Dubinin equation. Carbon, 27: 125-128.

Toda, Y., Hatami, M., Toyoda, S., Yoshida, Y. and Honda, H., 1971. Micropore structure of coal. Fuel, 50: 187-200.

Unsworth, J.F., Fowler, C.S., Jones, L.F., 1989. Moisture in coal 2. Maceral effects on pore structure. Fuel, 68: 18-26.

Weibull, W., 1951. A statistical distribution of wide applicability. Journal of Applied Mechanics, 18: 293-297.

1980 Annual Book of ASTM Standards. Part 26 Gaseous Fuels, Coal and Coke, section D388 77.

CHAPTER 4

VARIATION IN MESOPORE VOLUME AND SIZE DISTRIBUTION WITH COMPOSITION IN A HIGH-VOLATILE COAL OF THE WESTERN CANADIAN SEDIMENTARY BASIN: IMPLICATIONS FOR COALBED METHANE TRANSMISSIBILITY

4.1 ABSTRACT

The influence of composition upon mesopore volumes and surface areas of high-volatile bituminous coals is investigated in the current study. BET surface areas range from 1.1 to 5.3 m^2/g on a raw coal basis and generally increase with an increase in total inertinite content and decrease with an increase in total and structured vitrinite content. Mineral content appears to have little control upon the surface areas. Cumulative mesopore volumes obtained from the adsorption branch of nitrogen isotherms also increase with inertinite content. Isotherm hysteresis loops indicate a slit shape for the mesopores. Gas yields obtained from desorption canister testing generally increase with mesopore volumes obtained from subset samples. Mesopore volumes, which are dependent upon rank and composition, should be considered in methane diffusion modeling through coal seams.

4.2 INTRODUCTION AND RESEARCH OBJECTIVES

Coalbed gas within a coal reservoir is primarily retained as gas adsorbed within the matrix porosity of the coal. Matrix porosity in coals consists of micro-, meso- and macroporosity which represent pore diameters of less than 2 nm, between 2 and 50 nm, and greater than 50 nm, respectively (Orr, 1977). The distribution of pore sizes in coal is primarily a function of two properties: rank and composition. The control of rank upon pore size distribution and surface area of mainly vitrinite-rich coals has been investigated in detail by Gan et al. (1972). The effect of coal composition upon the pore structure of coals, particularly mesoporosity, has only received cursory investigation.

Coal composition has been shown to be an important control upon the macro- and microstructures of coal, and hence, may have an important control upon gas transmissibility (Close, 1993; Gamson et al., 1993). A popular model (Ertekin et al., 1991; Gamson et al., 1993) of how methane gas travels from the micropore network to the cleat system and ultimately to the borehole is as follows: gas is desorbed from the micropore network due to a decrease in pressure associated with the drilling of the hole into the seam; diffusion of methane gas, governed by Fick's law, through the coal matrix to the macrofracture system (cleat); and flow, governed by Darcy's law, through the cleat system to the borehole. The process may be more complex than this, however (Gamson et al., 1993). Gamson et al. have concluded that microstructures in coal, ranging in size from 0.05 - 20 μm and consisting of fractures and cavities, have an important control upon methane gas transmissibility of the coal seam. Although the microstructures as defined by Gamson et al. fall in the upper mesopore - macropore range of pore sizes, smaller mesopores (if present) would surely also affect the diffusion of gas from the micropore network to the microfracture system.

Harris and Yust (1976;1979) utilized transmission electron microscopy to determine the pore structure of the maceral groups vitrinite, inertinite and liptinite and found the inertinite maceral group to be mainly meso- and macroporous, whereas the vitrinite group was found to be mainly microporous. In a recent gas sorption study by Faiz et al. (1993), it was postulated that an increase in mineral matter content causes a decrease in the meso- and macropore volume of coal and hence a decrease in the total volume of adsorbed gas. The effect of the organic composition of coals upon the pore structure was not addressed. In addition, Langmuir volumes obtained from gravimetric gas sorption of carbon dioxide and methane were found in the Faiz et al. study to show a vague negative correlation with inertinite content, but the relationship was masked by the effect of varying rank among the coals. No detailed gas sorption study has been performed to determine the effect of coal organic composition upon mesoporosity.

The objective of the current study is to determine the effect of coal composition, particularly the maceral fraction, upon mesopore volume and size distribution and associated BET surface area. In addition, pore shapes are inferred from isotherm hysteresis loop shapes (or types). Total mesopore volume and the shape and size distribution of mesopores may prove to be an important control upon coalbed gas transmissibility from the micropore network to the microfracture network, and to a lesser extent, coal gas content. It is therefore important to understand the origin of mesoporosity.

4.3 BACKGROUND

4.3.1 Barret, Joyner, and Halenda (BJH) Theory

Mesopores are generally considered to be filled by the duel mechanisms of multilayer formation, described by the Brunauer, Emmett, and Teller (BET) equation (Brunauer et al., 1938), and capillary condensation, described by the Kelvin equation (Barrett et al., 1951). BJH theory, (Barrett et al., 1951), which was developed to describe mesopore distributions, makes two fundamental assumptions: the pores of the adsorbent are cylindrical in shape; and the pores are filled by multilayer formation and capillary condensation. The cylindrical pore would contain adsorbate in two forms: an adsorbed film on the pore wall; and a core of capillary condensate at the center of the pore (Figure 4-1).

BJH theory does not fit the pore size distribution to a known statistical distribution (i.e. a Gaussian distribution). Further, the adsorbed film is assumed to change thickness during adsorption or desorption in the absence of a capillary condensed core of adsorbate liquid.

The BJH theory (Barrett et al., 1951) is based on the Wheeler equation, which may be written as:

$$V_0 - V = \pi \int (r-t)^2 L(r)\, dr$$

where the integration is carried from rp_n, the radius of the largest pore filled with adsorbate at a given pressure, to infinity; V_0 is the volume of adsorbate adsorbed at saturation vapour pressure; V is the volume adsorbed at equilibrium pressure; L(r) is the length of pores with radii lying between r and r + dr; t is the multilayer thickness,

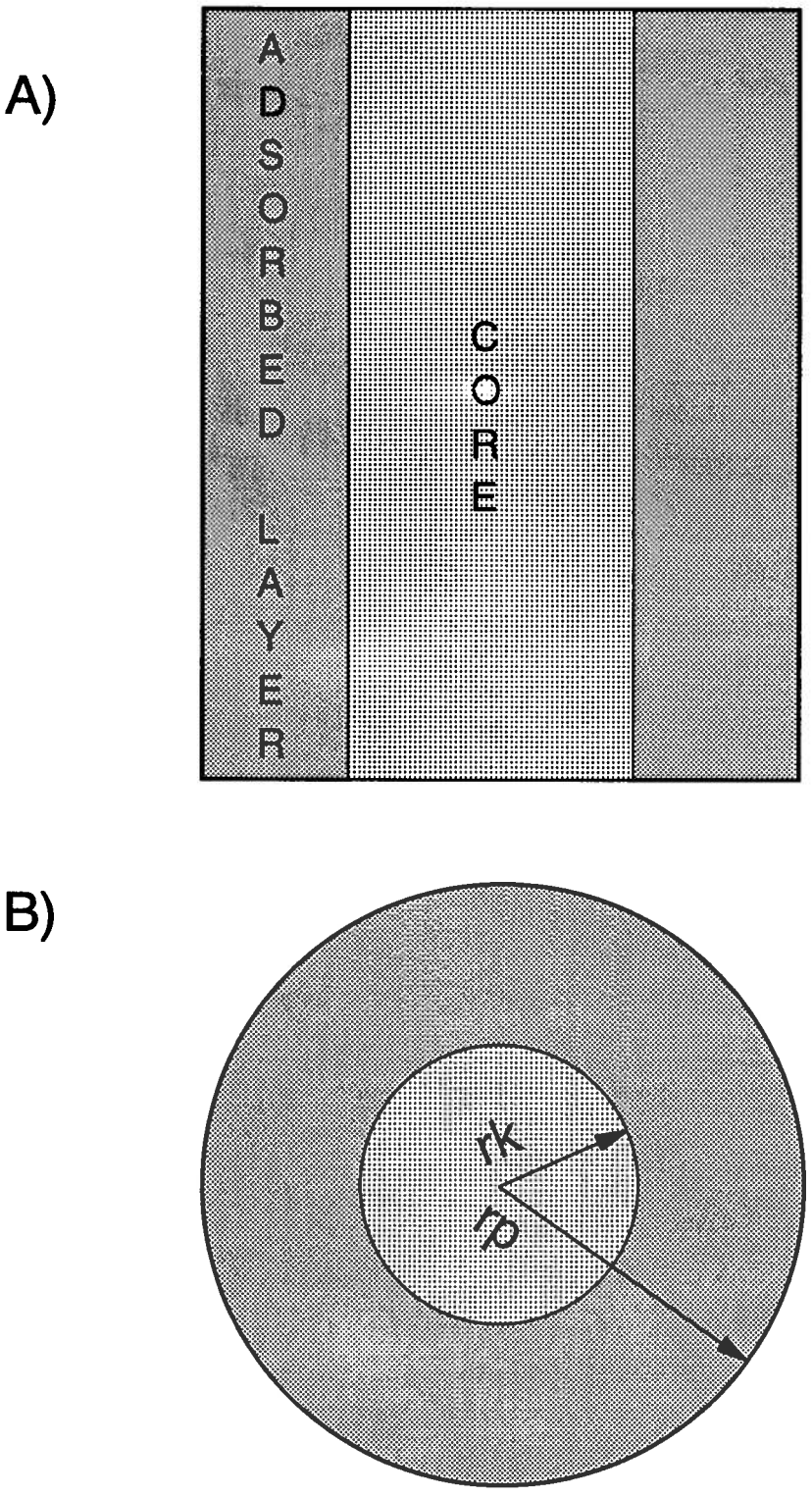

Figure 4-1. Diagram A) shows the location of the adsorbed film and pore core in a cylindrical capillary; B) illustrates the difference between the Kelvin (rk) and pore (rp) radii.

described by the Halsey equation (as used in this thesis), at equilibrium pressure. The form of the Halsey equation used in this thesis is as follows:

$$t = .354 \times [5/\ln(P_0/P)]^{1/3}$$

where t is the thickness of the adsorbed layer; P_0 is the (measured) saturation vapour pressure for nitrogen; and P is the equilibrium vapour pressure. A monolayer thickness of .354 nm is assumed for adsorbed nitrogen in the equation. The step by step description of how BJH theory calculates pore size distributions, volumes and surface areas is discussed by Barrett et al. (1951) and Gregg and Sing (1982).

4.4 METHODS

A sample suite of Western Canadian Sedimentary Basin coal was utilized in this study. The suite, which consists of eight samples, was obtained from drill core of Cretaceous coals from a locality in Alberta. The Alberta coals represent a wide range in lithotype composition.

Petrography (maceral and mineral), proximate, sulphur, random reflectance, and nitrogen adsorption analyses were performed. Petrography, sulphur, and random reflectance procedures used are described in Lamberson and Bustin (1993). Samples were crushed to less than 250 μm screen size for all analyses.

Nitrogen adsorption isotherms were collected using a Micromeritics ASAP 2000® surface area analyzer. Samples were first evacuated at 100°C for at least 16 hours prior to analysis to remove residual volatiles. Each sample (with sample tube) was then transferred to the analysis port on the instrument, back-filled with helium, and re-evacuated. A leak test was then performed. During a leak test, the sample tube is opened up to a pressure transducer, and the rate of increase in pressure, due to loss of volatiles

from the sample, is monitored. If a critical pressure is not reached over a set period of time, analysis is continued. Following the leak test, free space analysis was performed using helium gas.

Nitrogen isotherms at 77 K were then collected. Both adsorption and desorption data was collected with a maximum and minimum relative pressure of about .9995 and .0660, respectively. Only the 2 nm to 50 nm pore diameter range is discussed in this chapter as this range represents the mesopore range. Problems associated with using the Kelvin equation outside this range are discussed in Chapter 2.

Nitrogen gas was the choice of adsorbate for the following reasons (Gregg and Sing, 1982): nitrogen gas is inert; the saturation pressure of the gas is large enough so that a large range of relative pressures may be obtained accurately; the cross-sectional area of the gas is well established and is relatively small; liquid nitrogen is a readily available common refrigerant and the saturation pressure may be monitored throughout analysis.

The following parameters were utilized for nitrogen (at 77 K) in this study: a cross-sectional area of .162 nm^2, a non-ideality gas correction of 6.6×10^{-5}, and a density conversion factor of 1.5468×10^{-3}. Ultra High Purity (99.999 %) nitrogen gas was used as an adsorbate.

4.5 RESULTS

4.5.1 Proximate, rank, and petrographic data

Proximate and sulphur analysis results are summarized in Table 4-1. Sulphur contents range from 0.50 (ACCC-29) to 3.1 (ACCC-1) weight %. Volatile matter content, on a weight %, dry, mineral matter-free (dmmf) basis, varies from 23 % (ACCC-13) to 35 % (ACCC-6). Ash yields (weight %) range from 1.2 % (ACCC-13) to 11 % (ACCC-35).

Table 4-1. Results of proximate and sulphur analyses.

Sample	Ash Yield (w%)	Moisture (AR) (w%)	Volatile Matter (w%, dmf)	Fixed Carbon (w%, dmf)	Total Sulphur (w%)
ACCC-27	4.3	0.1	35.1	64.9	0.6
ACCC-29	1.6	0.2	35.1	64.8	0.5
ACCC-1	6.3	0.4	33.1	66.9	3.0
ACCC-5	4.4	0.3	34.3	65.6	1.5
ACCC-6	2.9	0.1	35.5	64.5	1.3
ACCC-35	10.6	0.5	33.5	66.5	0.5
ACCC-13	1.2	0.4	23.1	76.9	1.0
*ACCC	4.6	0.1	33.8	66.1	0.9

w % = weight percent
AR = As received

dmf = dry, mineral matter free (ASTM)
Equ. Mois. = equilibrium moisture

Random reflectance values for the Alberta suite vary from 0.5 to 0.6, which span the sub-bituminous A/high-volatile bituminous C boundary. The random reflectance values of the Alberta suite may be somewhat suppressed by abundant resinite impregnation within the cell structure of the vitrinite group maceral, telinite. The ASTM rank (ASTM, 1980), based on proximate and sulphur data, assigned to the coals is high-volatile A bituminous, with the exception of ACCC-13, which is medium-volatile bituminous in rank. The ASTM rank classification may give artificially high rank values to inertinite-rich coals (Lamberson and Bustin, 1993) and therefore the rank of the Alberta suite coals is most likely between high-volatile bituminous C and A.

Petrographic composition data is presented in Table 4-2 and shown graphically in Figure 4-2. Maceral percentages were calculated on a volume percent, mineral matter-free (mmf) basis, and were then recalculated to include mineral matter using the Parr formula (Lamberson and Bustin, 1993). The mineral matter-free vitrinite composition (volume %) varies from 37 to 88 %, and the inertinite from 10 to 62 %. On a raw coal basis, vitrinite composition ranges from 36 to 86 %, and inertinite from 10 to 60 %. ACCC-27 has the highest vitrinite and lowest inertinite content, and *ACCC has the lowest vitrinite and highest inertinite content. The coals have a low liptinite content (1-2 %, raw coal), and is thus composed mainly of the two organic components vitrinite and inertinite as well as mineral matter.

Table 4-2. Alberta suite petrography data.

	Maceral	ACCC-27	ACCC-29	ACCC-1	ACCC-5	ACCC-6	ACCC-35	ACCC-13	*ACCC
Volume %, Mineral-Free	Structured Vitrinite	77	73	49	49	34	34	19	13
	Desmocollinite	9	9	14	23	19	17	30	22
	Vitrodetrinite	2	0	6	3	9	5	3	1
	Semifusinite	3	5	19	14	23	25	31	34
	Fusinite	5	3	8	6	11	16	10	3
	Other Inertinite	2	8	2	3	3	2	5	25
	Total Liptinite	2	2	2	2	1	1	2	1
	Total Vitrinite	88	83	69	75	63	55	52	37
	Total Inertinite	10	16	29	23	37	44	46	62
	Struct:Deg Vit	7	8	2	2	1	2	1	1
	Struct:Deg Inert	4	1	13	7	13	18	8	1
Volume %, Raw Coal	Structured Vitrinite	75	73	47	47	33	32	18	13
	Desmocollinite	8	9	13	23	19	16	30	21
	Vitrodetrinite	2	0	6	3	9	4	3	1
	Semifusinite	3	5	18	13	22	24	31	33
	Fusinite	5	3	7	5	11	15	10	3
	Other Inertinite	2	8	2	3	3	2	5	25
	Total Liptinite	2	2	2	2	1	1	2	1
	Total Vitrinite	85	82	66	73	61	52	51	36
	Total Inertinite	10	15	27	22	36	41	46	60
	Ash Yield (vol.%)	2	1	4	3	2	6	1	3

* Structured Vitrinite : Degraded Vitrinite
** Structured Inertinite : Degraded Inertinite

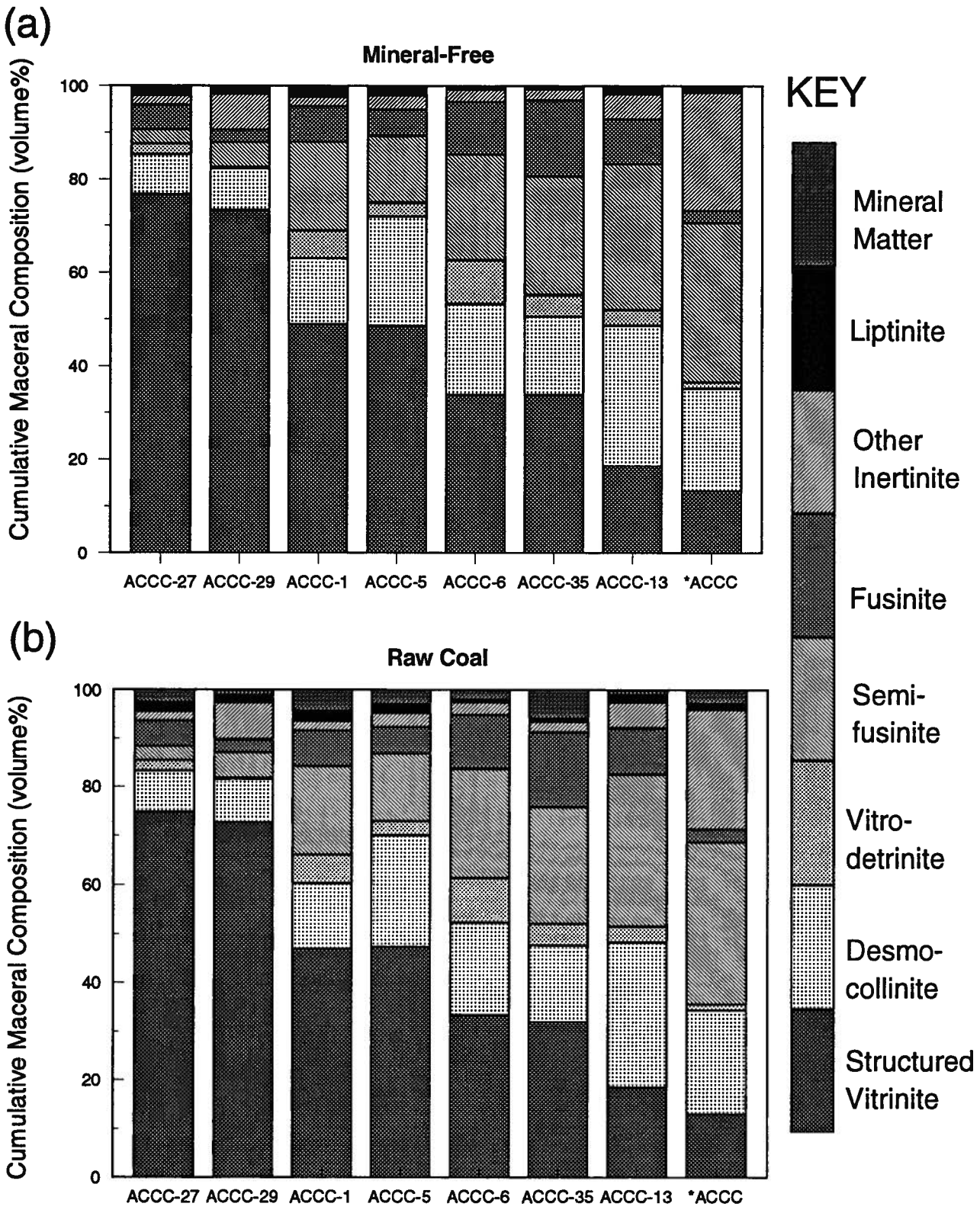

Figure 4-2. Alberta suite petrography data. Samples analysed on a mineral-free (a) and raw-coal (b) basis. Maceral and mineral contents expressed as volume %.

4.5.2 Isotherms and Hysteresis loops

Isotherms, obtained using nitrogen at 77°K, for the Alberta suite, are presented in Figure 4-3. The samples shown are *ACCC and ACCC-27. *ACCC has the highest total inertinite and lowest total vitrinite content (raw coal basis) and ACCC-27 has lowest total inertinite and highest total vitrinite. These two samples thus represent the range in organic composition of the Alberta suite.

The isotherms of the Alberta suite are Type IV, according to the Brunauer, Deming, Deming and Teller (1940) classification. These isotherms are associated with mesoporous solids. A wide hysteresis loop initiates for all samples at relative pressures between 0.4 and 0.5, above the relative pressure at which the first monolayer is believed to be completed (~ 0.3), and closes only at saturation. This hysteresis loop is referred to here as the high-pressure hysteresis loop and is coincident with the onset of capillary condensation in mesopores. In all samples the high-pressure loop, as illustrated in Figure 4-3, is a deBoer Type B hysteresis loop which corresponds to slit-shaped pores. The pore shape is believed to correspond to the mesopore shape in the organic fraction of the coals, as very little clay, which might cause a Type B hystersis, is observed in the samples. As discussed earlier, the Alberta suite coals are generally very low in mineral matter content. Gan et al. (1972) have also postulated that fine mineral particulates entrained in the coal matrix may not be accessible to the nitrogen adsorbate at 77 K and therefore it is unlikely that mineral matter is affecting the hysteresis loop shape.

Some of the sample isotherms display low-pressure hysteresis in which case the hysteresis loop does not close at relative pressures between 0.4 and 0.5 (Figure 4-3). Low-pressure hysteresis described by Gregg and Sing (1982) refers to a lack of closure of the high-pressure loop and is thought to be due to swelling of the coal structure or due to adsorption in materials that contain microporosity. Either of these explanations may be true for the Alberta suite, but since all the samples are microporous, and only some display

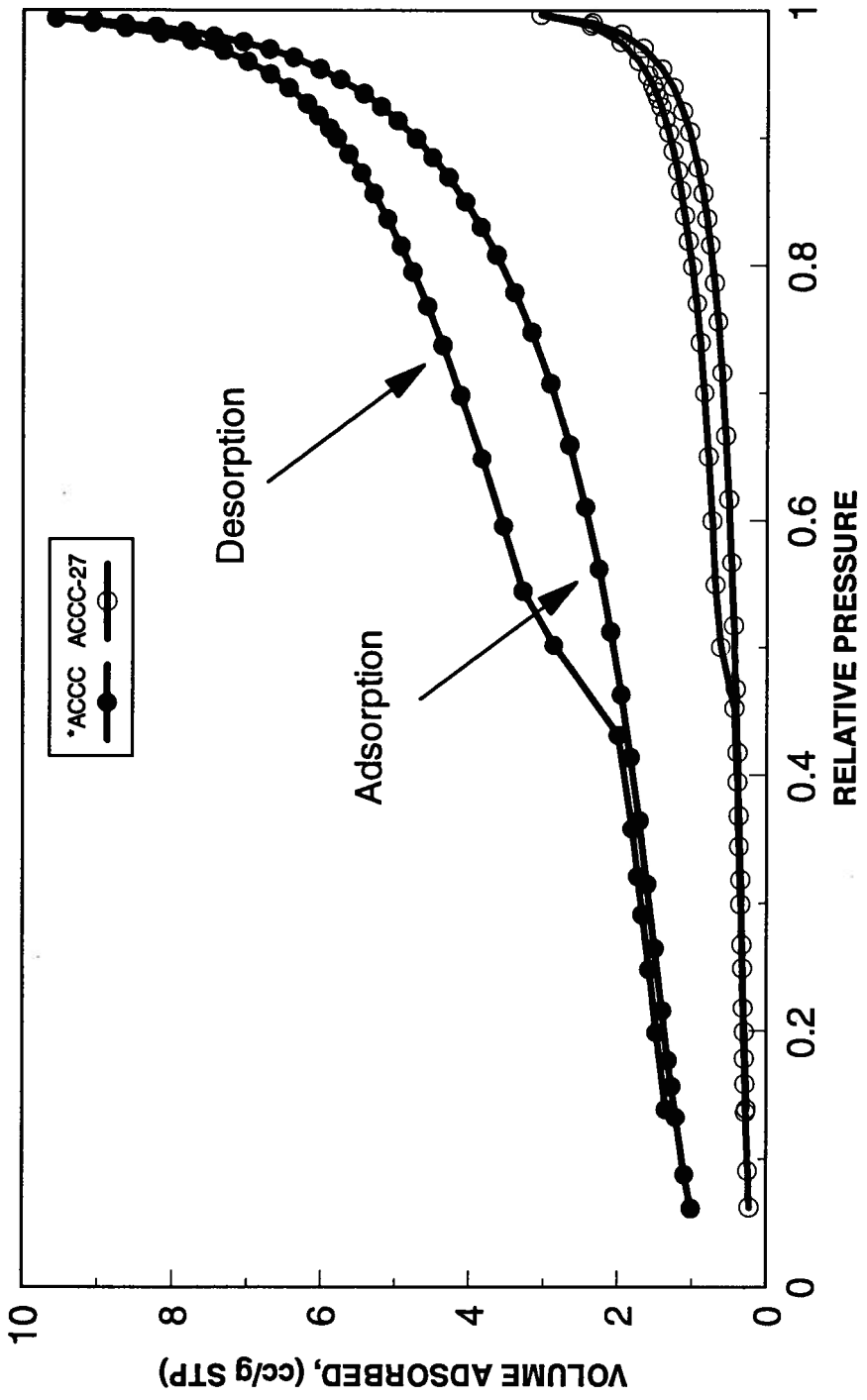

Figure 4-3. Nitrogen isotherms obtained for samples *ACCC and ACCC-27.

low-pressure hysteresis, the first cause appears more likely. This problem requires further investigation.

Gas adsorption increases with total inertinite content. The high-pressure hysteresis loop also becomes wider with total inertinite content (Figure 4-3). The total mesopore volume thus appears to increase with inertinite content. The shape of the high-pressure hysteresis loop is the same for all samples. Because the samples of the Alberta suite vary considerably in organic (maceral) composition and all have similar high-pressure hysteresis loop shapes, it is likely that mesopore shape is not affected by the organic composition of the coals. A slit-shaped mesopore structure is common to all the coals in this suite.

4.5.3 BET and BJH surface areas

BET surface areas, BJH surface areas for pores between 2 and 50 nm diameter, and C values are given for the Alberta suite in Table 4-3. The five-point BET surface areas were at the relative pressures 0.068, 0.091, 0.14, 0.18, and 0.22. The range of relative pressures that the BET equation is applicable is generally assumed to be from 0.05 to 0.35, so all calculation points were taken in this range. BET C values are greater than 20 (average ~ 68) and thus estimation of monolayer capacities from the BET equation for the Alberta suite is assumed to be valid (Chapter 2). The BET equation has been successfully applied to other adsorbent-adsorbate systems yielding Type IV isotherms, because monolayer formation on pore walls in mesopores is thought not to be affected by neighbouring surfaces (Gregg and Sing, 1982, p. 168).

Sample	BET Surface Area (sq. m/g)	BJH Desorption Surface Area (sq. m/g)	*BJH Adsorption Surface Area (sq. m/g)	**BJH Adsorption Surface Area (sq. m/g)	**Cumulative Adsorption Mesopore Volume (cc/g)	BET C Value
ACCC-27	1.11	1.45	1.26	0.99	0.00211	82
ACCC-29	2.47	3.27	2.78	2.49	0.00372	60
ACCC-1	2.52	3.36	3.31	2.63	0.00516	62
ACCC-5	4.80	6.79	6.39	5.12	0.00861	66
ACCC-6	2.22	3.00	2.84	2.22	0.00477	68
ACCC-35	4.11	5.52	4.66	4.07	0.00789	76
ACCC-13	5.26	7.22	6.69	5.45	0.00980	65
*ACCC	5.10	6.91	6.19	5.17	0.00983	65

** 100% pores open at both ends.*
*** 0% pores open at both ends.*

Table 4-3. BET and BJH surface areas and mesopore volumes for the Alberta suite (raw coal basis).

The average value of the BET surface areas of the Alberta suite (~ 3.5 m^2/g, raw coal basis) are much lower than the corresponding average carbon dioxide surface areas determined from the Dubinin-Radushkevich equation from the 298 K isotherm (~ 176 m^2/g, raw coal basis) (Chapter 3). This is not unique as Gan et al. (1972) also found nitrogen BET surface areas of less than 1 m^2/g for coals that exhibited greater than 200 m^2/g of carbon dioxide surface area (at 298 K). The reason for the smaller BET surface areas is that the BET equation is essentially only determining the internal surface area of mesopores (and external surface area), whereas the D-R carbon dioxide surface areas are essentially the surface areas associated with microporosity. Gan et al. (1972) noted that coals with high carbon dioxide surface areas have smaller nitrogen BET surface areas which is also the case here. The cause of this, apart from differences in rank between the coals, may in part be attributed to compositional variation in the samples.

In an attempt to determine the effect of organic composition upon BET surface area of the coals, BET surface areas (5-point) versus total and structured vitrinite content are plotted in Figure 4-4. Plots of BET surface area versus total inertinite content and semifusinite content are also given (Figure 4-5). Results are presented on a raw coal and mineral matter-free basis (Chapter 3). The BET surface areas decrease with structured and total vitrinite content, although some scatter in the data exists. The sample with the highest structured vitrinite content (ACCC-27) has lowest BET surface area (1.1 m^2/g , 5-point, raw coal basis). ACCC-13 has close to the same structured vitrinite content as *ACCC but has a lower mineral-matter content, which may cause the slightly higher BET surface area (5.3 m^2/g, 5-point, raw coal basis) of ACCC-13. There is no apparent correlation between surface area and mineral-matter content in these samples; the organic component of the coals appears to be the main control upon the BET surface area.

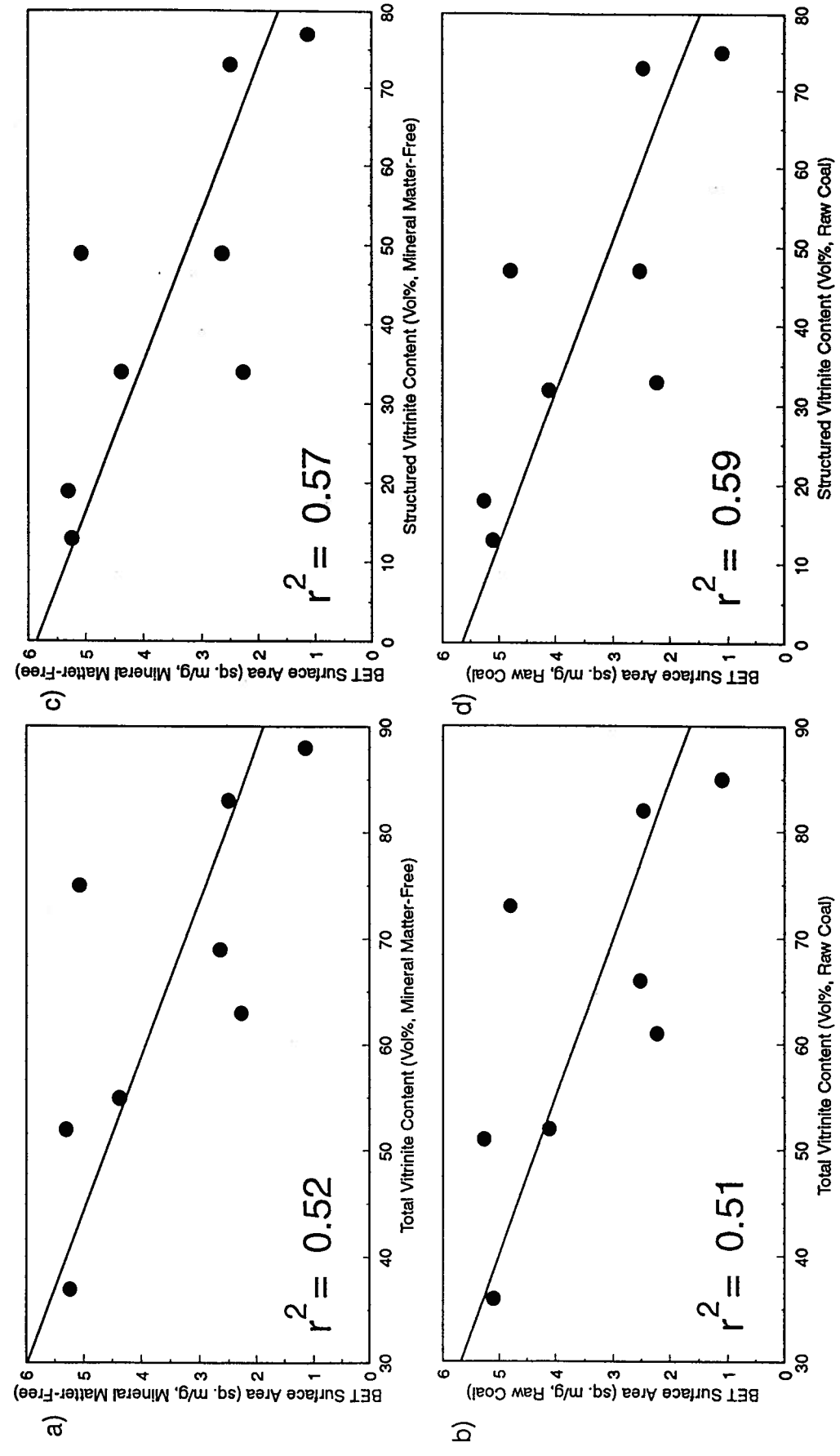

Figure 4-4. Plots of 5-point BET surface areas versus total vitrinite (a, b) and structured vitrinite (c,d). Mineral matter-free (a,c) and raw coal (b,d) values are plotted. Mineral matter-free values calculated using the Parr Formula.

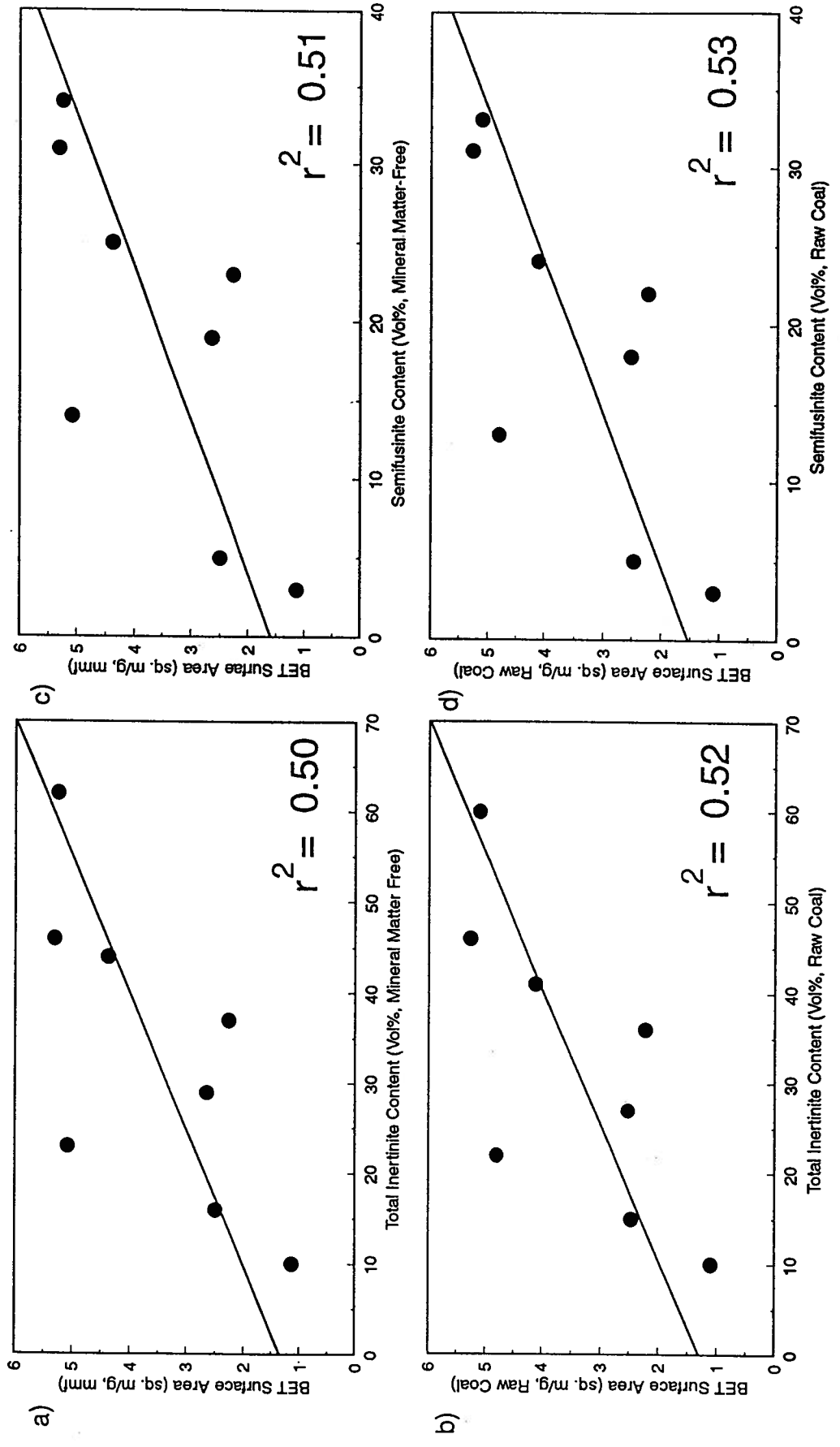

Figure 4-5. Plots of 5-point BET surface areas versus total inertinite (a, b) and semifusinite content (c,d). Mineral matter-free (a,c) and raw coal (b,d) values are plotted. Mineral matter-free values calculated using the Parr Formula.

Gan et al. (1972) showed that a possible way of determining which branch of the isotherm, adsorption or desorption is best for acquiring pore size distributions from the Cranston and Inkley model, which assumes cylindrical pores, is to compare the Cranston and Inkley adsorption and desorption surface areas to the BET surface areas, because BET theory does not assume a geometry for pore shapes. A similar approach is applied here for BJH theory. Adsorption and desorption BJH cumulative mesopore surface areas are plotted against BET surface areas in Figure 4-6. In determining the adsorption BJH surface areas, the percentage of cylindrical pores which are open at both ends were considered; BJH cumulative adsorption surface areas were calculated assuming: 1) that 100% of the pores were open at both ends; and 2) 0% of the pores were open at both ends. Good correlations are achieved between the BET surface areas and the BJH surface areas (desorption and adsorption). The BJH adsorption surface areas, with the assumption that 0% of the pores are open at both ends, appear to agree most closely with the BET surface areas. The adsorption branch should thus be used for pore size distribution analyses, but both the adsorption and desorption branch results will be studied.

The BET surface areas probably measure the surface areas of a larger range of pores than just mesoporosity. In addition, the external surface area of the coal particles is measured by BET. The BET surface areas should theoretically be larger than the cumulative surface area of the mesopores measured by the BJH analysis. Five of the eight Alberta samples have BJH cumulative adsorption mesopore surface areas that are greater than the corresponding BET surface areas. The non-conformity of the mesopore shapes to that of cylinders is likely the cause of this discrepancy. As indicated by the isotherm hysteresis loops, the pores are probably more slit-shaped than cylindrical.

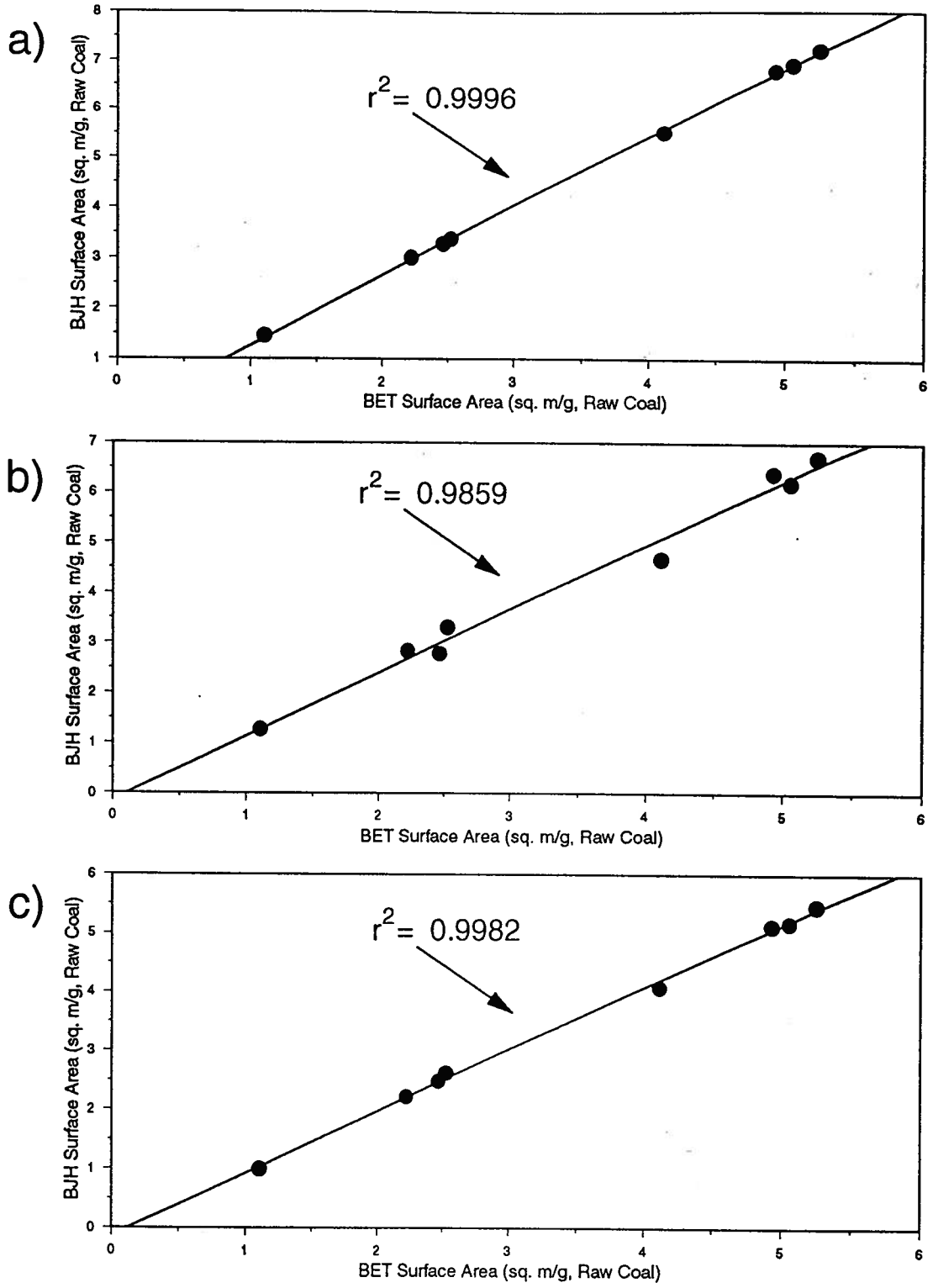

Figure 4-6. Plot of BJH cumulative surface area for pores between 2 and 50 nm diameter versus BET surface area. Plot a) is obtained using the desorption branch of the isotherm; b) is obtained using the adsorption branch with the assumption of 100% pores with both ends open; c) is obtained from the adsorption branch with the assumption of 0% pores with both ends open.

4.5.4 Mesopore size distributions and volume

Plots of mesopore (2 - 50 nm pore diameter) distributions obtained using the BJH method and both adsorption and desorption isotherm branches are given in Figure 4-7. The two samples chosen for these plots are again samples *ACCC and ACCC-27.

Sample *ACCC, the sample with the highest inertinite content and lowest vitrinite content, has the greatest amount of mesoporosity (*ACCC). For the adsorption branch, the mesoporosity declines from 2 nm pore diameters to 50 nm. For the desorption branch, mesoporosity declines in a general way from about 3 nm pore diameter to 50 nm, with a peak at about 3 - 3.5 nm. Caution must be exercised in interpreting this peak, however. As mentioned by Gregg and Sing (1982), the surface tension and molar volume of the adsorbate may vary significantly from that of the bulk liquid. In very fine pores, the Kelvin equation, which is the basis of BJH theory, thus breaks down. The absolute magnitude of the 3 nm peak must therefore be viewed with caution. There is, however, a relative increase in the 3 nm peak with increase in inertinite content (Figure 4-7).

Cumulative pore volume plots, obtained from the adsorption and desorption branches of the isotherm, for samples *ACCC and ACCC-27 samples are given in Figure 4-8. For the adsorption branch, cumulative pore volumes decrease in a steady fashion from 2 nm pore diameters to 50 nm. For the desorption branch, the samples with the highest inertinite content show a steep inflection at around 3.5 nm (corresponding to the peak in figure). This inflection decreases in magnitude for the low inertinite content samples.

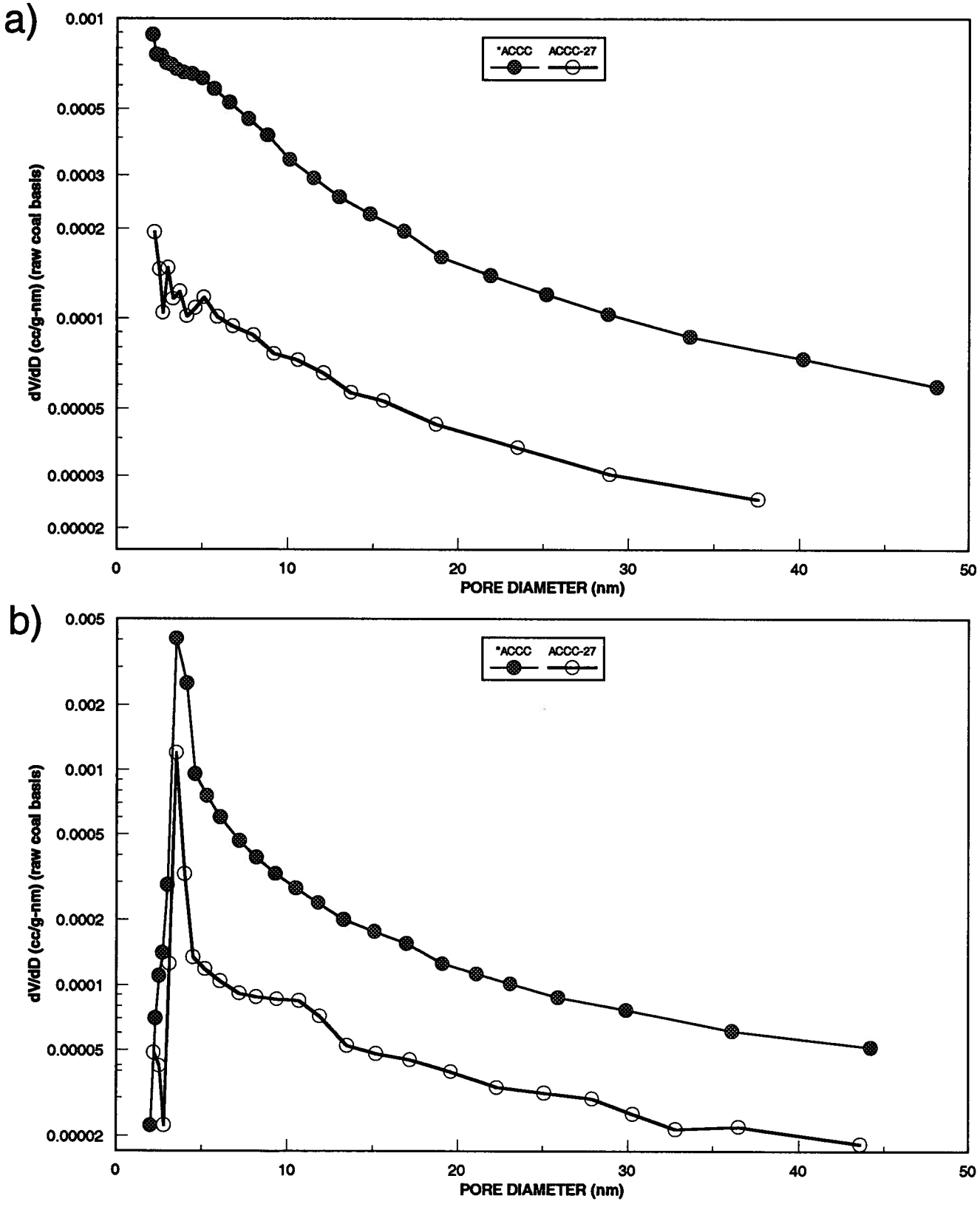

Figure 4-7. Pore volume distribution curves for a) adsorption branch and b) desorption branch of the isotherm. Samples are *ACCC and ACCC-27.

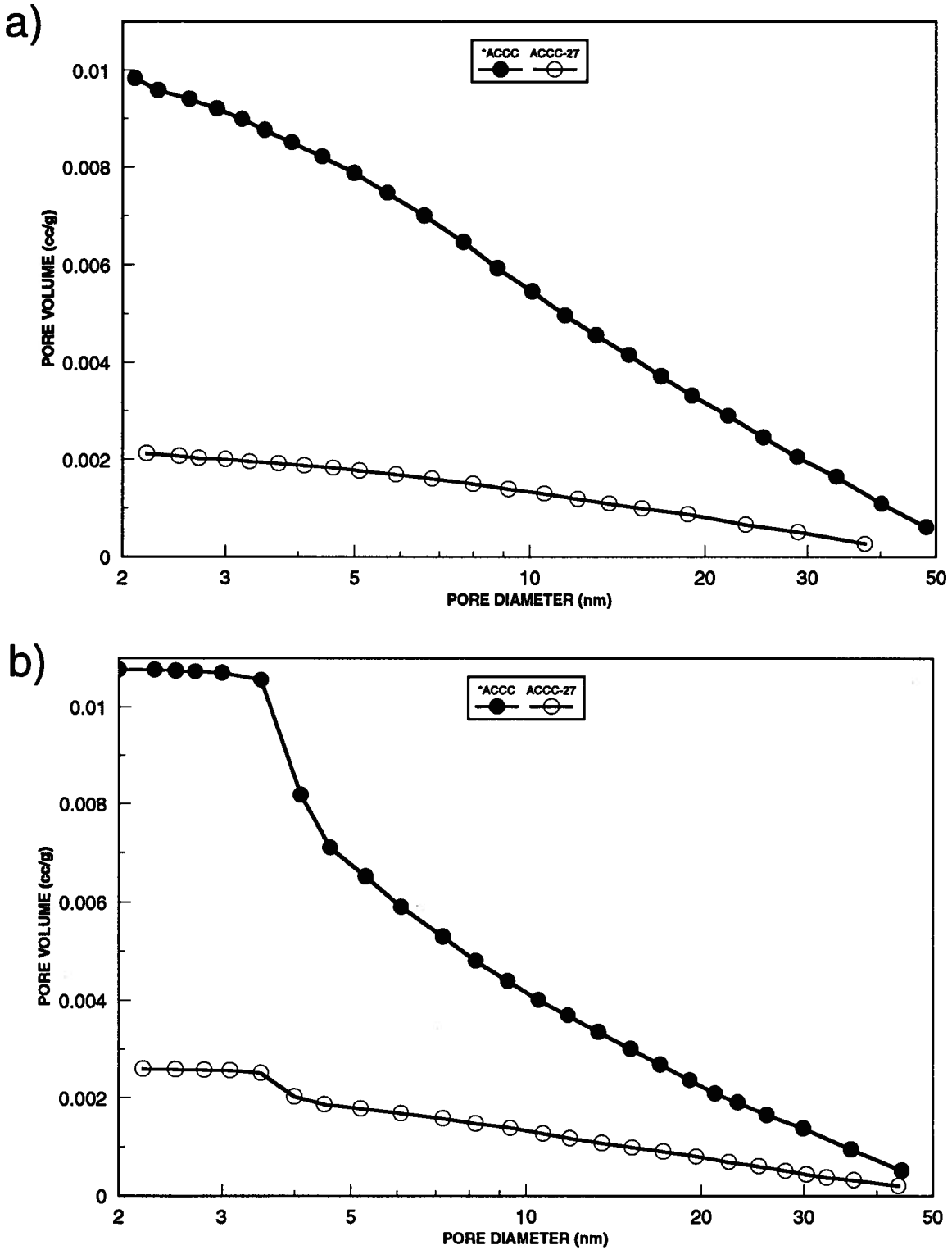

Figure 4-8. Cumulative a) adsorption and b) desorption pore volume plots for samples *ACCC and ACCC-27.

A plot of total mesopore volume, obtained from integrating the pore volumes from 2 to 50 nm, versus vitrinite content is given in Figure 4-9. The adsorption branch of the isotherm was used to obtain total pore volumes, but the desorption branch yields similar results. The cumulative adsorption mesopore volume decreases with an increase in vitrinite content in a linear fashion (Figure 4-9). Slightly better correlations are achieved if the mesopore volumes are plotted against structured vitrinite content . The sample with the highest structured vitrinite content (ACCC-27) has the lowest cumulative adsorption mesopore volume (0.0021 cm^3/g, raw coal basis) and the sample with the lowest structured inertinite content (*ACCC) has the highest cumulative mesopore volume (0.010 cm^3/g, raw coal basis). Plots of mesopore volume versus semifusinite and total inertinite content are also given (Figure 4-10).

The total amount of mesoporosity in coals is therefore governed by composition. Coals enriched in vitrinite, in particular structured vitrinite, lack significant mesoporosity. Coals enriched in inertinite have a greater amount of mesoporosity than vitrinite-rich coals of the same rank. Mineral matter content varies little in this suite of samples (Table 4-2), and therefore the affect of mineral matter content cannot be ascertained.

4.6 DISCUSSION

Composition, particularly the organic fraction of coal, has an important control upon the adsorption of nitrogen gas in coals. In particular, the mesopore volume and BET surface areas using nitrogen gas as an adsorbate are affected by modal abundances of the various maceral groups. A decrease in structured vitrinite and coincident increase in total inertinite leads to an overall increase in mesopore volume and increase in BET surface area. This study confirms the Harris and Yust (1979) TEM study which showed that vitrinite is essentially microporous and inertinite is essentially meso- and macroporous. As shown here, the mesopore shape changes little with composition.

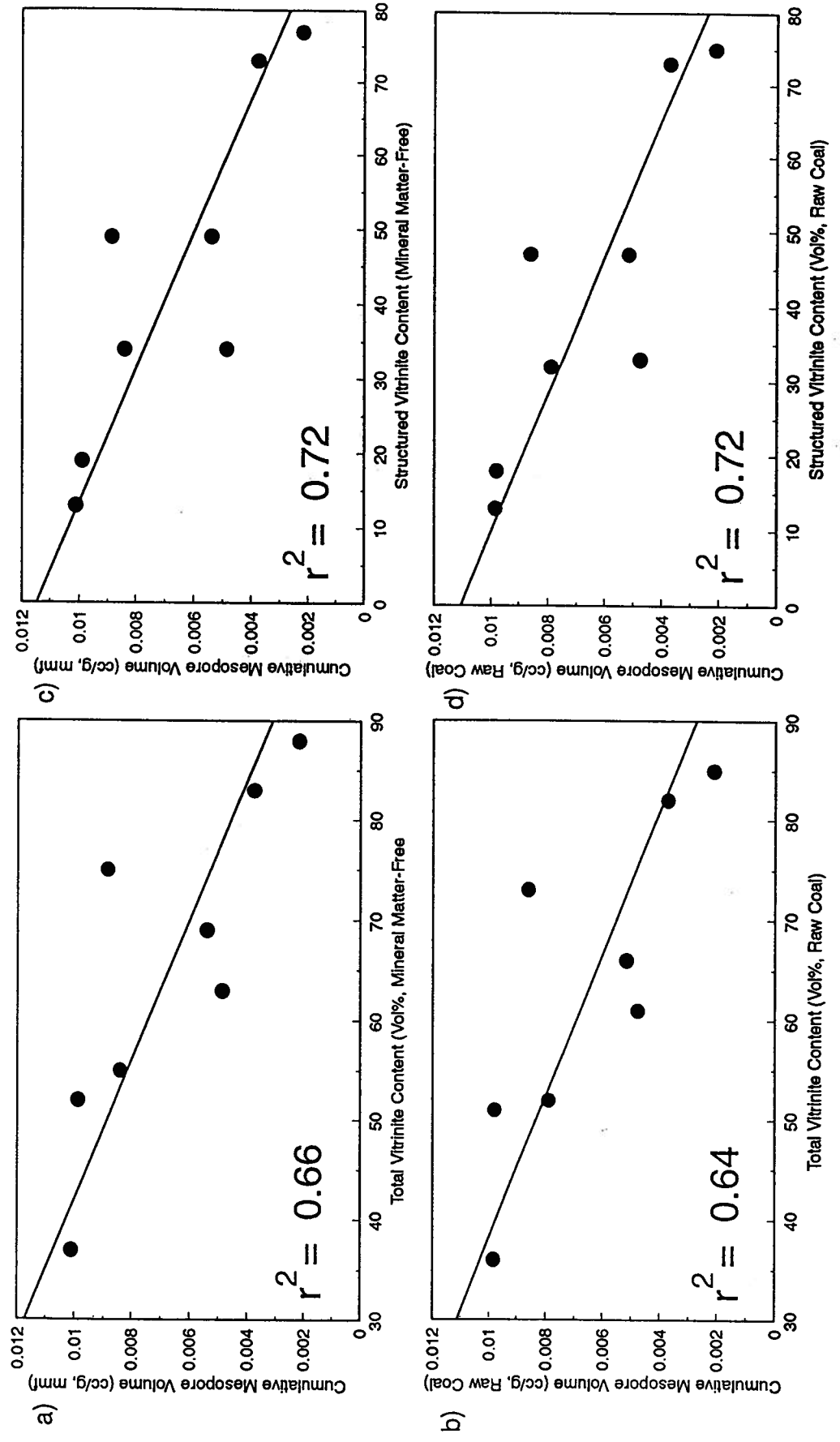

Figure 4-9. Plots of cumulative adsorption mesopore volumes versus total vitrinite (a, b) and structured vitrinite (c,d). Mineral matter-free (a,c) and raw coal (b,d) values are plotted. Mineral matter-free values calculated using the Parr Formula.

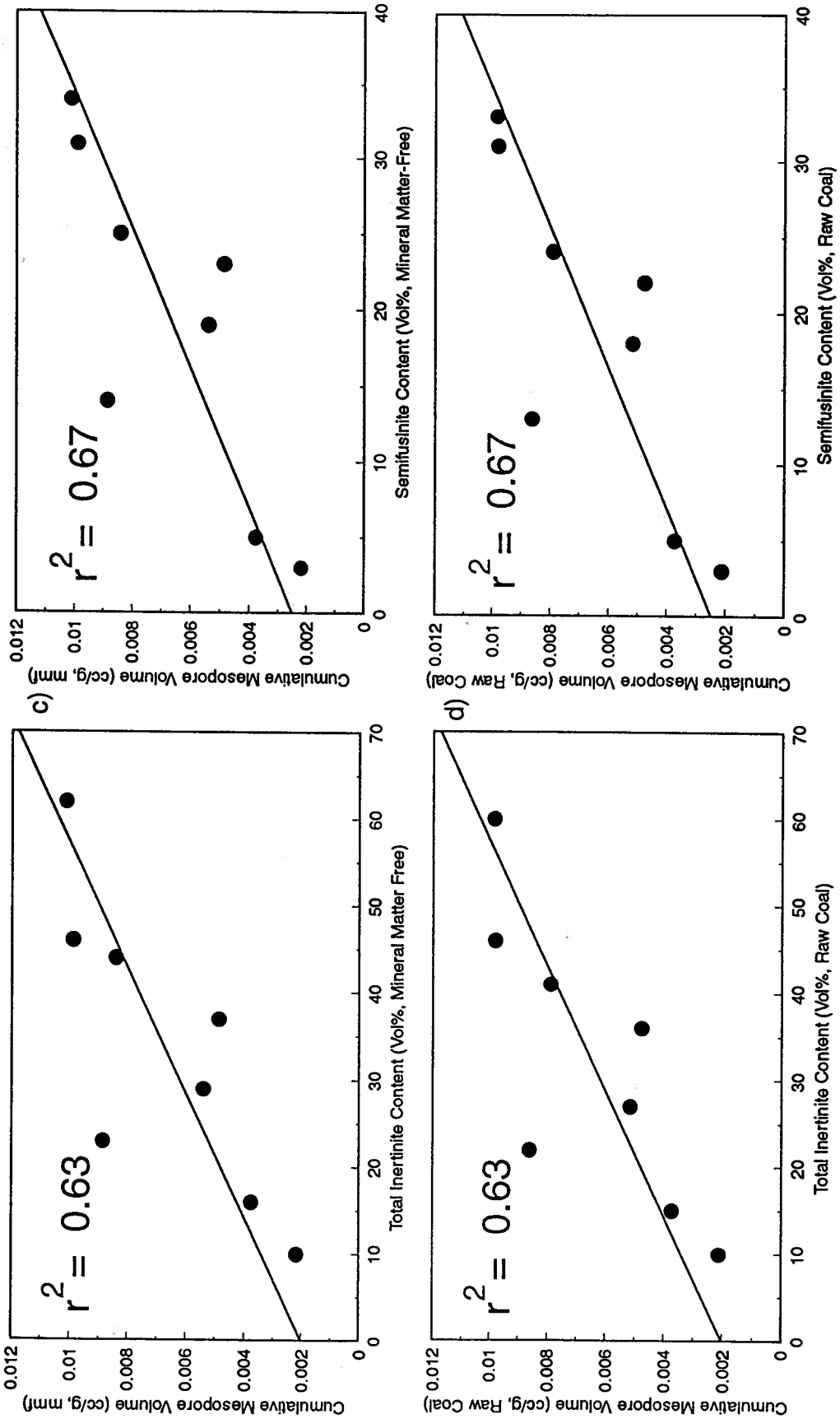

Figure 4-10. Plots of cumulative adsorption mesopore volumes versus total inertinite (a, b) and semifusinite content (c,d). Mineral matter-free (a,c) and raw coal (b,d) values are plotted. Mineral matter-free values calculated using the Parr Formula.

The cause(s) for the difference in pore structure of the two maceral groups, vitrinite and inertinite, is unclear, but must certainly include physical, chemical, and biological affects prior to and during diagenesis. Charring in particular may have an important control upon the ultimate pore structure of the maceral groups. The most common inertinite maceral subgroup in most of the coal samples is semifusinite. The semifusinite content of the Alberta suite decreases with an increase in structured vitrinite (telinite, telocollinite, and pseudovitrinite submacerals) which is possibly related to the fire frequency in wetlands (Lamberson and Bustin, 1993). The burning or charring of semifusinite precursors would lead to an increase in semifusinite and a corresponding decrease in structured vitrinite. It is possible then that the process of burning , which leads to a loss of volatiles, may lead to an increase in mesoporosity. In the previous chapter, it was indicated that this process may lead to an increase in microporosity of the semifusinite macerals. Dubinin and Stoeckli (1980) demonstrated that over activated or strongly activated carbons possess a more heterogeneous pore structure than that of less activated carbons. In particular, supermicropores, pores with diameters between about 1.4 and 3.2 nm, are created through the process of activation. No mention was made about the affect upon mesoporosity, however. The cause of the increase in heterogeneity in microporosity with activation was thought to be due to the burning-out of pore walls between adjacent micropores. It is possible that an analogous process has lead to the increase of mesoporosity in inertinite macerals, in particular semifusinite, over that of vitrinite.

4.6.1 Relationship between mesopore volume and gas yields from desorption tests

A study by Potter (1993) of medium volatile bituminous coals from the Mist Mountain Formation showed that methane gas yields are greatest for high inertinite coals. The high gas yields of the inertinite rich coal, were thought to be, in part, due to increased transmissibility afforded by the presence of open cell lumen in semifusinite and fusinite. Further, Faiz and Cook (1993) found that in situ gas contents, or total desorbed gas from mineral matter-including coal, increased with inertinite content. Conversely, in both studies, gas contents were found to decrease with ash content.

Gas yields (raw coal basis) were obtained from desorption canister testing of the Alberta suite used in the current study and then plotted against cumulative adsorption mesopore volumes (raw coal basis) (Figure 4-11). The Smith and Williams Unipore Model (1984) was used to perform lost gas calculations for the canister data. The gas yields appear to increase very generally with mesopore volume.

4.6.2 Implications for coalbed methane transmissibility

Gamson et al. (1993) classify and discuss the control of microstructures in coals of the Permo-Triassic Bowen Basin of Queensland, Australia upon methane transmissibility. These microstructures, which include fracture, matrix, and phyteral porosity have widths between 0.05 and 20 μm. Gamson et al. also proposed a four-stage model of gas transmission through coal seams: the first stage involves diffusion from the micropore network; the second involves diffusional and/or laminar flow through the microstucture network which may contain entrained mineral matter; the third stage involves strictly

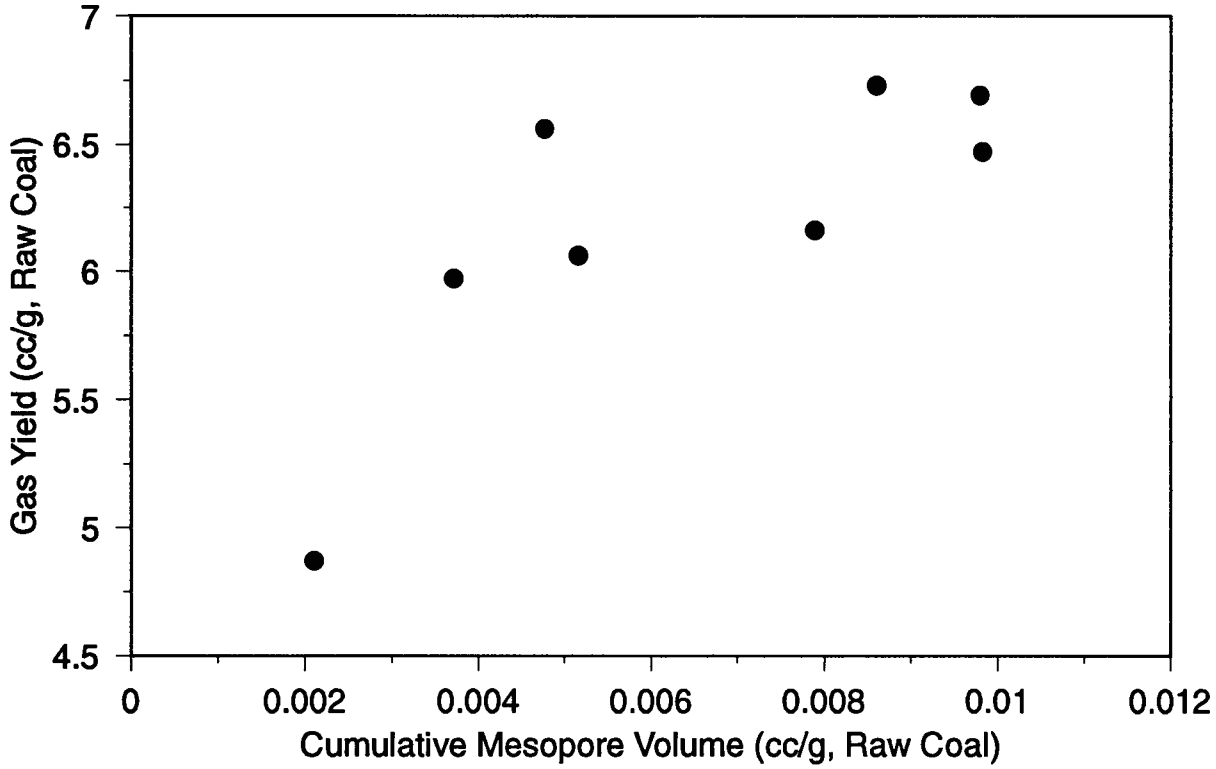

Figure 4-11. Plot of gas yields from desorption canister testing versus mesopore volumes (raw coal basis). See text.

laminar flow through 'open' microstructures; and the fourth stage includes laminar flow through the open cleat system. The microstructure density, orientation and connectivity, shape, size and degree of mineralization among other factors were suggested to be important controls upon diffusional and/or laminar flow through the coal seam on route to the macrofracture or cleat system. Throughout the study, pores intermediate between microporosity (< 2 nm pore diameter) and microstructures (.05 - 20 μm in width) were ignored, and it was suggested that diffusional flow of methane starts and finishes in the micropore network after which flow is governed by the microstructure network. The pores that were not included in the four-stage model include the entire realm of mesoporosity (2 - 50 nm), which, if present, even in minute amounts, must surely have an effect upon the transmission of methane.

The current study has shown that coal composition, particularly the organic fraction, has an important control upon the amount of mesoporosity. In the Gamson study, microstructures were similarly shown to be controlled by composition, whereby a continuous microcleat system was associated with bright bands of coal (vitrinite-rich) and phyteral and matrix porosity was associated with dull bands of coal (less vitrinite-rich, more enriched in inertinite and mineral matter). Ertekin (1991) has shown that the timing and magnitude of the first and second coalbed methane production peak is determined by several reservoir properties such as coal seam thickness, permeability, sorption characteristics and porosity. The increase in mesoporosity with inertinite content of coals, at least for high-volatile bituminous coals, should then be an additional consideration in modeling methane gas transmission through coal seams.

4.7 CONCLUSIONS

Composition, particularly the organic (maceral) constituents, has been determined to be an important control upon the mesopore volume and BET surface areas of an isorank coal. The following observations and conclusions have been made:

1) Nitrogen adsorption isotherms, determined at 77 K, are all Type IV (Brunauer, Demming, Demming and Teller, classification) for the Alberta suite. Prominent high-pressure hysteresis loops are displayed for all samples. The hysteresis loops are Type B (deBoer classification), which are associated with slit-shaped pores. Low-pressure hysteresis, attributed to pore swelling also occurs for some samples.

2) BET surface areas decrease generally with an increase in total and structured vitrinite content and conversely increase with an increase in inertinite content. BJH-derived cumulative surface areas for the mesopore range (2 - 50 nm) are correlative with the BET surface areas but are generally larger. This is believed to be do to the nonconformity of the mesopore shape in these samples to the cylindrical shape assumed in BJH theory. The pores are probably more slit-shaped, as indicated by the obtained isotherms, which explains the discrepancy between the two surface areas.

3) Mesopore volumes decrease in a linear fashion with an increase in total vitrinite content. A better correlation was achieved with structured vitrinite content. The mesopore volumes conversely increase with total inertinite content. Since the inertinite is mainly semifusinite in these samples, increased mesoporosity associated with an increase semifusinite might be the result of burning of vitrinite precursors.

4) Gas yields from desorption canister testing appear to increase generally with mesopore volume.

5) Mesopore volumes, which are dependent upon rank and composition, should be considered in methane diffusion modeling through coal seams.

The importance of microstructures (0.05 - 20 μm) in coals in determining methane transmissibility has been discussed by Gamson et al. (1993). The bulk of these structures fall into the macropore range of pore sizes. Future studies will be aimed at determining and quantifying the effect of coal composition upon macroporosity, presumably using techniques such as mercury porosimetry.

4.7 REFERENCES

Barrett, E.P., Joyner, L.G., and Halenda, P.P., 1951. The determination of pore volume and area distributions in porous substances. I. Computations from nitrogen isotherms. The Journal of the Ammerican Chemical Society, 73: 373-380.

Brunauer, S., Deming, L.S., Deming, W.S., Teller, E., 1940. On a theory of van der waals adsorption of gases. The Journal of the American Chemical Society, 62: 1723.

Brunauer, S., Emmett, P.H., and Teller, E., 1938. Adsorption of gases in multimolecular layers. The Journal of the American Chemical Society, 60: 309-319.

Close, J.C., 1993. Natural fractures in coal. In: B.E. Law and D.D. Rice (Editors), Hydrocarbons from Coal, AAPG Studies in Geology # 38, pp. 119-132.

Dubinin, M.M., and Stoeckli, H.F., 1980. Homogeneous and heterogeneous micropore structures in carbonaceous adsorbents. Journal of Colloidal Interface Science, 75: pp. 34-42.

Ertekin, T., Sung, W., and Bilgesu, H.I., 1991. Structural properties of coal that control coalbed methane production. In: D.C. Peters (Editor), Geology in Coal Resource Utilization. pp. 105-124.

Faiz, M.M., and Cook, A.C., 1993. Influence of coal type, rank and depth on the gas retention capacity of coals in the southern coalfield, N.S.W.

Faiz, M.M., Aziz, N.I., Hutton, A.C., and Jones, B.G., 1992. Porosity and gas sorption capacity of some eastern Australian coals in relation to coal rank and composition. Symposium on Coalbed Methane Research and Development in Australia, 19-21 November, 1992, Townsville 4, 9-20.

Gamson, P.D., Beamish, B.B., and Johnson, D.P., 1993. Coal microstructure and micropermeability and their effects on natural gas recovery. Fuel, 72: 87-99.

Gan, H., Nandi, S.P., and Walker, P.L., Jr., 1972. Nature of the porosity in American coals. Fuel, 51: 272-277.

Gregg, S.J., and Sing, K.S.W., 1982. Adsorption, Surface Area and Porosity, Second Edition. Academic Press, New York. 303 pp.

Harris, L.A., and Yust, C.S., 1976. Transmission electron microscope observations of porosity in coal. Fuel, 55: 233-236.

Harris, L.A., and Yust, C.S., 1979. Ultrafine structure of coal determined by electron microscopy. Preprint paper, American Chemical Society, Division of Fuel Chemicals , 24: 210-217.

Lamberson, M.N., and Bustin, R.M., 1993. Coalbed methane characteristics of the Gates Formation coals, northeastern British Columbia: effect of maceral composition. American Association of Petroleum Geologists, 77: 2062-2076.

Orr, C., 1977. Pore size and volume measurement. In: I.M. Kolthoff, P.J. Elving, and F.H. Stross (Editors), Treatise on Analytical Chemistry Part III, Volume 4. John Wiley and Sons, New York. pp. 359-402.

Potter, J., 1993. Claobed methane potential and the effects of coal composition and fractures in medium-volatile bituminous coals from the Mist Mountain Formation, southwestern Alberta (abstract). Geological Association of Canada/Minerological Association of Canada, Joint Annual Meeting, Program and Abstracts, p. A-84.

1980 Annual Book of ASTM Standards. Part 26 Gaseous Fuels, Coal and Coke, section D388 77.

CHAPTER 5

VARIATION IN PRESSURE-DECAY PROFILE PERMEAMETER-DERIVED PERMEABILITIES WITH LITHOTYPE AND MACERAL COMPOSITION OF COALS

5.1 ABSTRACT

Coal beds are markedly heterogeneous with respect to composition and fabric, which imparts significant vertical and lateral variation in permeability, and thus may be important in making production decisions in the extraction of hydrocarbons from coal. The current study, utilizing a pressure-decay permeameter, quantifies changes in permeability of coal at the lithotype (megascopic) and maceral (microscopic) scale. The order of decreasing permeability with lithotype is: bright > banded > fibrous > banded dull > dull, for the coal samples used. Bright coals are the most permeable because of associated macro- (cleat) fracturing. For a banded dull sample, permeability generally increased with increasing vitrinite content. The lowest permeabilities measured occur in dull coals with a high mineral and inertinite content. Fibrous coal has a higher permeability than dull coal of the same rank due to the abundance of macroporous fusinite in the former. Dull coal permeability decreases with an increase in rank, but these results are obscured by compositional variability between samples. Pressure-decay measurements are more reliable for dull lithotypes as these lithotypes do not fracture as easily during sample preparation. In addition, measured permeabilities are optimistic due to the relaxation of stress upon exposure of coal to atmospheric pressure.

5.2 INTRODUCTION AND RESEARCH OBJECTIVES

Permeability is an important parameter in the prediction of reservoir performance. In conventional reservoirs, the average permeability and permeability heterogeneity control production rate and efficiency, respectively (Georgi et al., 1993).

Coal beds, which are unconventional hydrocarbon reservoirs, are typically heterogeneous with respect to composition. An understanding of the effect of both megascopic (lithotype) and microscopic (maceral) composition upon permeability is thus critical in making completion and production decisions in the extraction of hydrocarbons from coal.

Among the most important factors affecting permeability in coalbeds is the fracture system which, in turn, is largely controlled by composition. At several producing regions of the San Juan Basin, for example, fracture permeability is considered to be the single greatest control upon production (Close et al., 1990).

The current study attempts to quantify the change in permeabilities of coal with lithotype (megascopic) and maceral (microscopic) composition. In addition, the change in permeabilities with coal rank are documented. Permeabilities are measured using a new type of permeameter, referred to as a Pressure-Decay Profile Permeameter^{TM} (PDPK - 300, patent pending, Jones, 1992). The device can measure permeabilities on a bed-by-bed scale, and may thus be used to document permeability variations on the lithotype scale in coal. A detailed account of the permeability variation in the dull components of coal may be important in the accurate prediction of gas producibility in seams rich in dull coal.

5.3 EFFECT OF COAL STRUCTURE ON PERMEABILITY

5.3.1 Cleat systems

Cleats are (natural) fractures in coal which are formed through a variety of different processes including dessication, coalification, lithification, and paleotectonic stress (i.e. Close, 1993). Typically cleat comprises two (usually mutually orthoganal) sets: the continuous face cleat and the less continuous butt cleat which terminates into the face cleat. These two sets are generally perpendicular, or nearly so, to bedding in the coal. In some coals a third cleat set is developed which is also perpendicular to bedding but which is curviplanar and intersects the face and butt cleat (Gamson et al., 1993).

The cleat system is important in controlling gas production in that the cleat system is the principal permeability pathway for water and gas during production (depressurization). The most important properties of the cleat system that affect coal permeability are; cleat spacing and height, aperture width, connectivity, and degree of infilling and closure. Cleat spacing and height are affected by lithotype thickness. Cleats are generally most abundant in bright bands of coal and their height is mainly restricted by the widths of bright bands. Cleat spacing and height appear to decrease with decreasing lithotype thickness (Close, 1993). In addition, rank has an effect upon cleat spacing (Close, 1993)

5.3.2 Microstructures

In addition to the megascopic fractures, coal seams possess microstructures which contribute to the overall permeability of the seam. Microstructures include microfractures and cavities which are micrometre in scale (0.05 - 20 μm in width). Gamson et al. (1993) state that porosity represented by the microstructure system is of three types, including fracture, phyteral, and matrix porosity, and that the porosity lies within the realm of meso- to macroporosity. Figure 5-1 illustrates the microfractures of coal. Because of the continuity of the microstructure system of coals, the microstructures are thought to be an important control upon gas transmissibility.

In the Gamson et al. (1993) study, it was assumed that the microstructure distribution as well as size, shape, and continuity is affected by coal lithotype. The phyteral and matrix porosity is generally associated with duller coals whereas fracture porosity is more typical of brighter lithotypes. The microcleat system in brighter coals often forms a continuous network with the larger cleats.

The transmissibility of methane through a coal seam is dependant upon the megascopic and microscopic fracture and pore systems and their degree of connectivity. The orientation, continuity, and density of these structures, in addition to the coal rank and composition (organic and mineral) are important considerations in the production of coalbed gas.

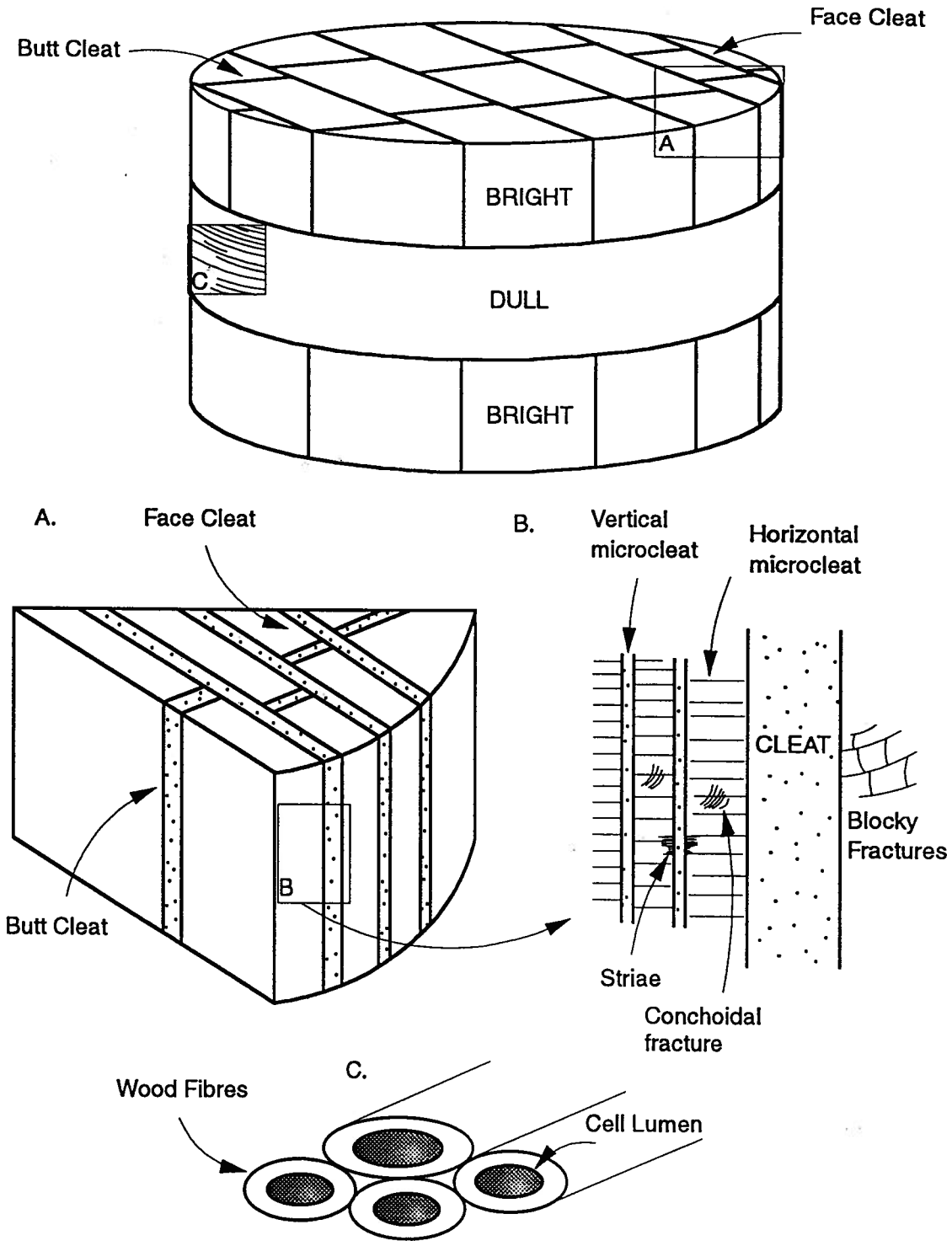

Figure 5-1. Diagram illustrating microstructures in coal. (a) relationship between face and butt cleat; (b) various microstructures in bright coal and their relationship with the larger cleat; (c) cell lumen in dull coal. Modified from Gamson et al., 1993.

5.4 THE PRESSURE-DECAY PROFILE PERMEAMETER

The PDPK - 300 is a steady-state permeameter developed by Core Laboratories which is capable of measuring permeabilities in the range of 0.001 to 20,000 md within 2 to 35 seconds of measurement time (Jones, 1992; Georgi and Jones, 1992). Low permeability samples require longer measurement times (i.e. 30 seconds for .001 md rock). Measurements can be corrected for gas-slippage (Klinkenburg) and inertial flow resistance effects (Georgi and Jones, 1992).

The instrument consists of a manifold and probe (Figure 5-2) which together comprise four volume-calibrated tanks of varying volumes (Georgi and Jones, 1992). Nitrogen gas is bled into one of the chambers and then injected through a probe tip, which is flush against the flat surface of the sample, and into the sample. A practise blowdown is performed prior to the actual measurement in order to determine which manifold volume to use for the sample point. A larger volume is chosen for high permeability samples, and the probe tip volume itself maybe used for very low permeability samples.

During the measurement, once the gas is bled through the probe tip and into the sample, the pressure decay time is monitored. From this, the instantaneous volumetric flow rate is obtained and, through the use of the Forchheimer equation, permeabilities and inertial resistivity coefficients (β) are calculated (Georgi et al., 1993; Jones, 1992). Data precision is about $\pm$ 2%. The rate of change of pressure with time is a reflection of the permeability of the sample; the higher the permeability of the sample, the greater the rate of change of pressure with time.

The probe tip seal may be changed according to the depth of sample that is to be investigated; the smaller the seal, the shallower the depth of penetration. For small core plug measurements, O-rings (~ 5 mm in diameter) maybe used.

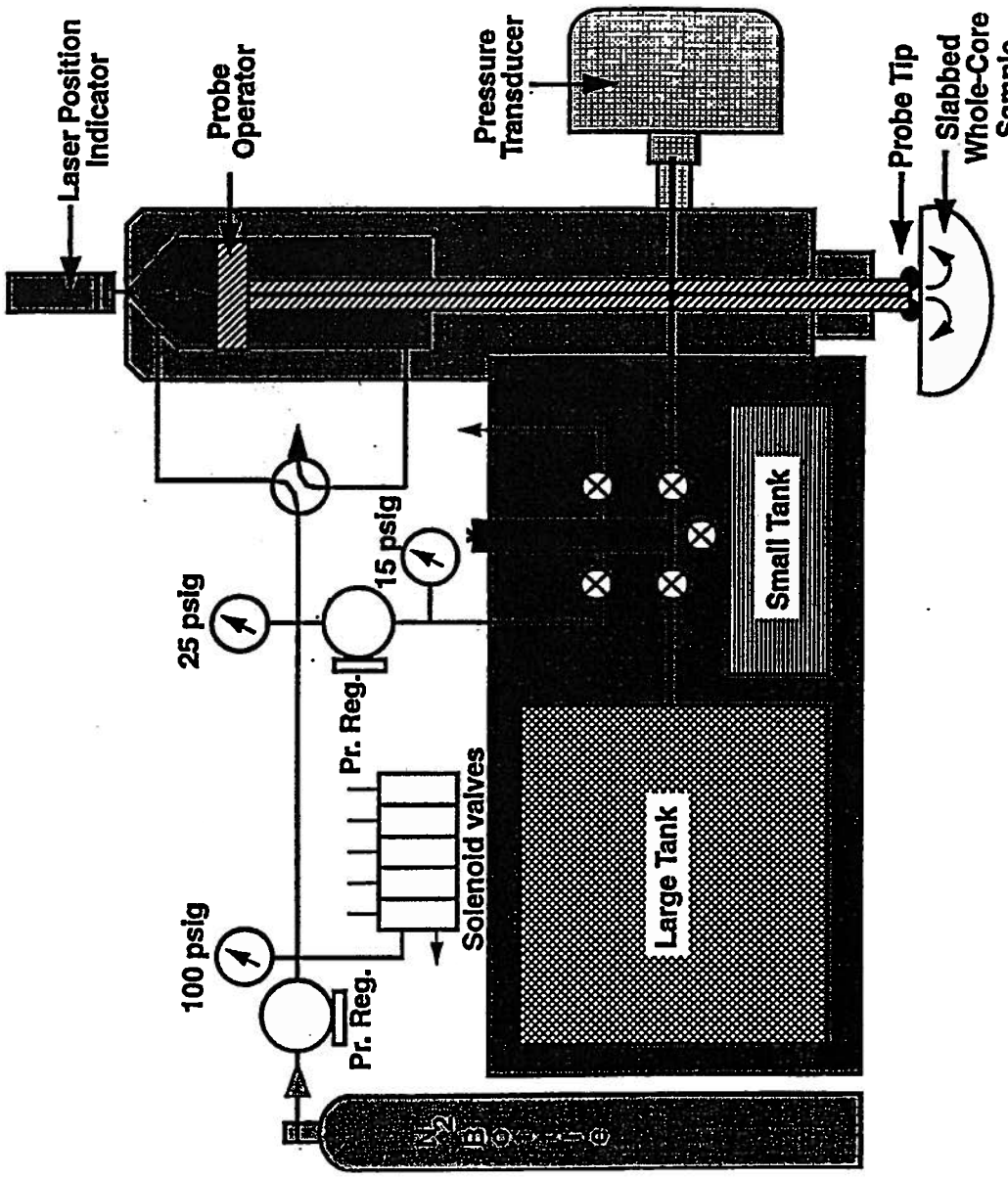

Figure 5-2. Schematic diagram illustrating the Pressure-Decay Profile Permeameter (after Georgi et al., 1993).

The PDPK-300 may be used to obtain closely spaced rapid permeability determinations. Such an instrument is ideally suited to obtain a lithotype permeability profile for coals.

5.5 METHODS

Seven coal samples were used in this study. Four samples were obtained from the Upper Jurassic-Lower Cretaceous Mist Mountain Formation; one (LC-8) from the south Elk Valley coalfields (SEVC) and three from the north Elk Valley coalfields (NEVC) of southeastern British Columbia. Three samples were also obtained from the Lower Cretaceous Gates Formation of northeastern British Columbia.

The coal samples were cut into rectangular blocks with a water-lubricated diamond rocksaw. Care was taken to make sure the cut surfaces were flat and as free from irregularities as possible.

Pressure-decay profile permeabilities were measured at Core Laboratories in Calgary, Alberta. The instrument used was a PDPK-300. Profiles parallel and perpendicular to face cleat (if present) were performed for each sample. Sample points were spaced at least one centimeter apart. Portions of the coal surface that exhibited surface irregularities or artificially (sawcut)-induced fracturing were avoided. For all samples, with the exception of LTC-11, a Gates Formation sample, points were taken on at least two cut surfaces. Profiles were taken on all four cut surfaces of the SEVC (LC-8) sample, the largest sample of the seven used.

Sample points were located with the use of a laser sight. A shot was then fired whereby the probe tip was neumatically projected against the coal surface at a pressure of about 173 kPa (~25 Psi). A practise blowdown was performed to determine which calibrated volume was to be used in the analysis. The reservoir chosen was then filled with nitrogen gas to a pressure of about 69 kPa (10 Psi) and computer-operated valves

opened to bleed gas into the sample. Pressure-decay with time was then recorded to calculate sample permeabilities. Both slip-corrected (liquid-equivalent) and conventional permeabilities were calculated. Measurement times were generally less than 33 seconds and varied depending on the permeability of the sample. An O-ring probe tip with a diameter of 0.5 cm was used in the analyses.

Lithotype descriptions of the samples were performed following standard conventions (Diessel, 1965; Marchioni, 1980; Lamberson and Bustin, 1993). The coal surface within about 0.5 cm of the sample measurement site were observed using a binocular petrographic microscope at 60 X magnification to determine if any irregularities or microfractures existed.

A representative sample of each permeability point was obtained for petrographic analysis. Cubes of about 0.125 cm^3 of coal were cut, with the measured point at the center of the top face, using a gem saw. With an O-ring seal of 0.5 cm diameter on the probe tip, the depth of measurement was about 0.5 cm, thus 0.125 cm^3 is believed to be representative of the volume measured in the permeability analyses. About 90% of the points measured were recovered during the cube-cutting procedure.

The cubes of representative sample were then crushed to less than 250 μm screen size and made into 2.54 cm pellets for standard petrographic analysis. Standard petrographic analysis was then performed for each point (Chapter 3). Because very little sample was utilized for each pellet, some samples had to be discarded due to the loss of coal during the polishing procedure.

Random (vitrinite) reflectances were also performed for each coal sample using standard techniques (Bustin et al., 1985). Mean random reflectances (R_0) for at least two measured permeability points of the hand sample were obtained, with a minimum of 25 reflectance measurements per pellet.

5.6 RESULTS

5.6.1 Lithotype, Megascopic Structure, and Measurement Surface Descriptions

Photos of all coal sample measurement surfaces and points are shown in Figures 5-3 to 5-11. In addition, lithotypes are labeled for samples with permeability profiles. The lithotype classification used in this study is a modification of the Australian classification system (Diessel, 1965; Marchioni, 1980; Lamberson and Bustin, 1993) (Table 5-1).

The SEVCF sample (LC-8) is shown in Figures 5-3 to 5-5. All four cut surfaces are displayed (Figure 5-4 and 5-5) plus the two uncut upper and lower surfaces (Figure 5-3). LC-8 contains a banded dull segment, an upper bright band (~ 1.5 cm thick) and a lower bright band (~ 1cm thick) (Figure 5-4). The upper bright band surface (Figure 5-3), which is parallel to bedding, is sheared (parallel to bedding) and has a prominant face cleat with a regular spacing of about 1 - 2 mm. The lower bright band surface also displays regular face cleating with a 1 - 2 mm spacing. The measurement surfaces of sample LC-8 are both perpendicular (faces 1A-1 and 1A-2) and parallel (faces 1B-1 and 1B-2) to the face cleat of the upper and lower bright bands (Figure 5-4 and 5-5). The banded dull segment of faces A and B has minor pitting associated with very thin bright bands (< 1mm) and some small fractures associated with cutting, which were avoided during measurement. The upper bright band has large pits and fractures which are due to the brittleness of bright coal. The 1B-1 and 1B-2 faces are slightly more pitted than the A faces possibly due to the fact they are parallel to face cleat.

Sample 2, a NEVCF coal is a dull coal (Figure 5-6). This sample has a large amount of artificially-induced fracturing and pitting, and thus there are limited number of points measured on this sample.

Table 5-1. Lithotype classification used in current study. Modified from Lamberson and Bustin (1993).

Stopes-Heerlen (ICCP) Classification	Nomenclature used in this study	Description
vitrain	bright coal (B)	subvitreous to vitreous lustre, conchoidal fracture, less than 10% dull
clairain	banded bright coal (B B)	predominantly bright coal, 10-40% dull
	banded coal (B C)	interbedded dull and bright in approximately equal proportions
	banded dull coal (B D)	predominantly dull coal, 10-40% bright
durain	dull coal (D)	matte lustre, uneven fracture, less than 10% bright coal, hard
fusain	fibrous (F)	satin lustre, friable, sooty to touch

a)

b)

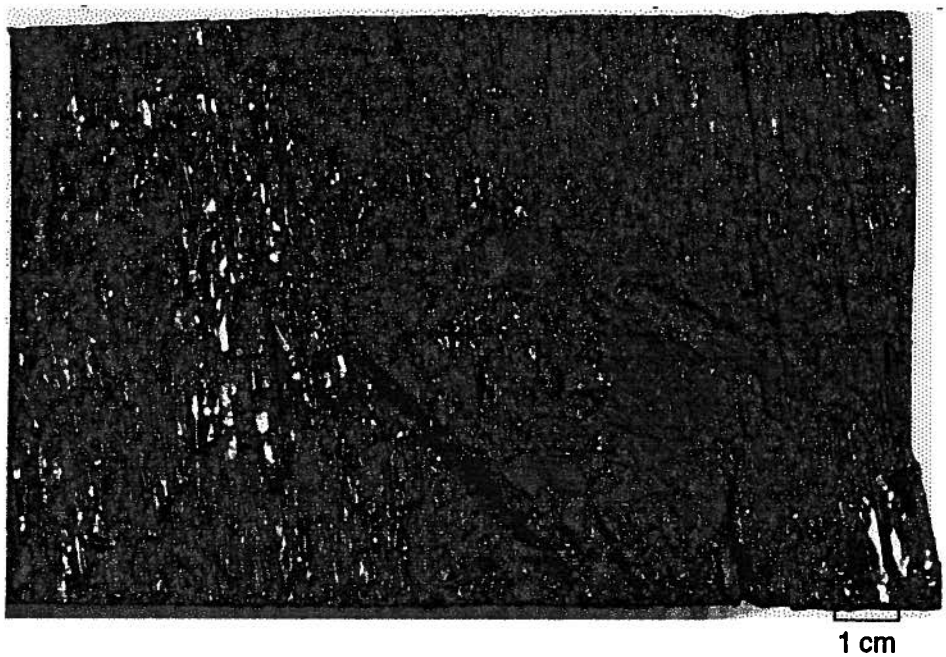

Figure 5-3. Sample 1 showing top (a) and bottom (b) faces.

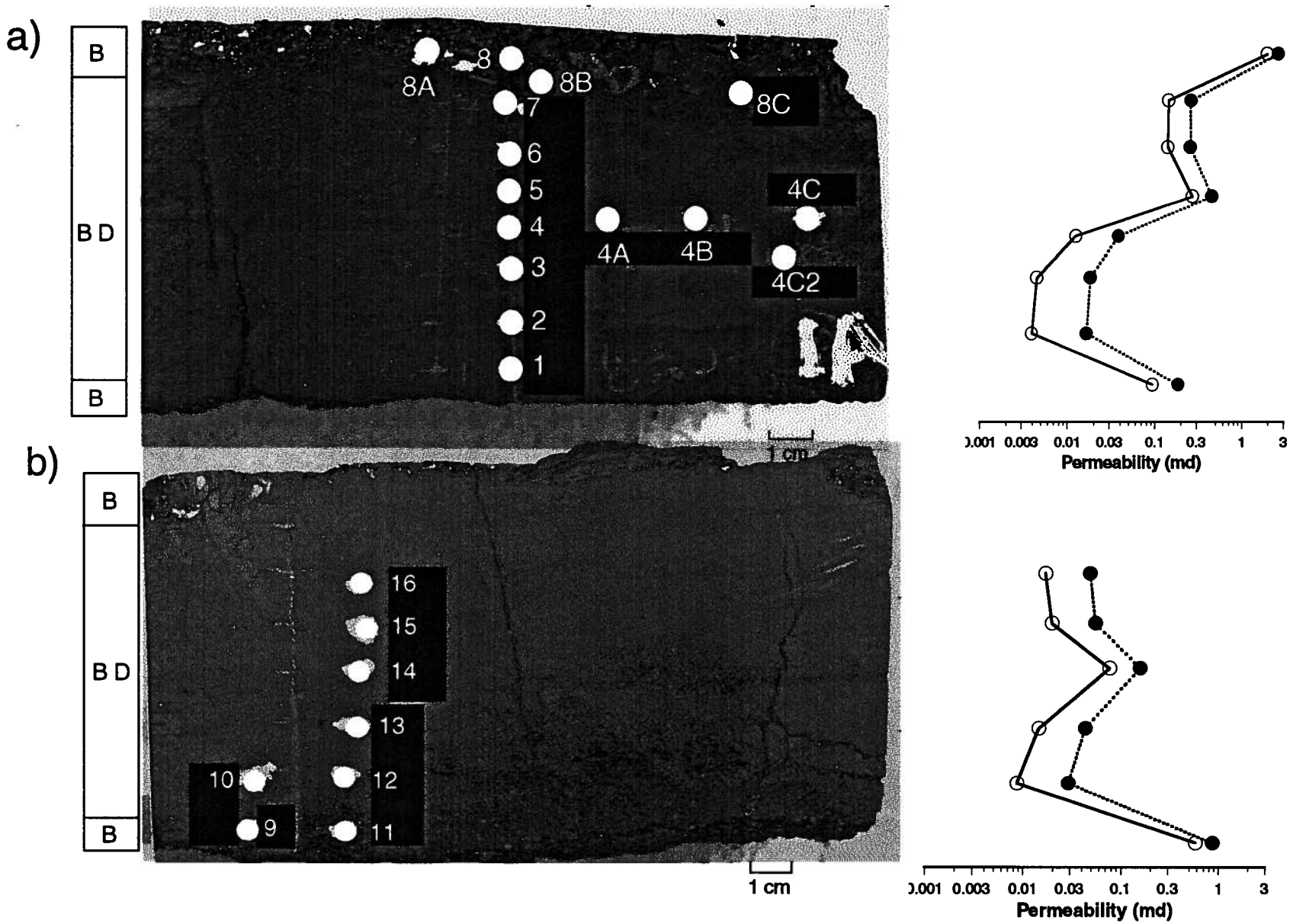

Figure 5-4. Permeability profiles for faces 1A-1 (a) and 1A-2 (b). See text for explanation.

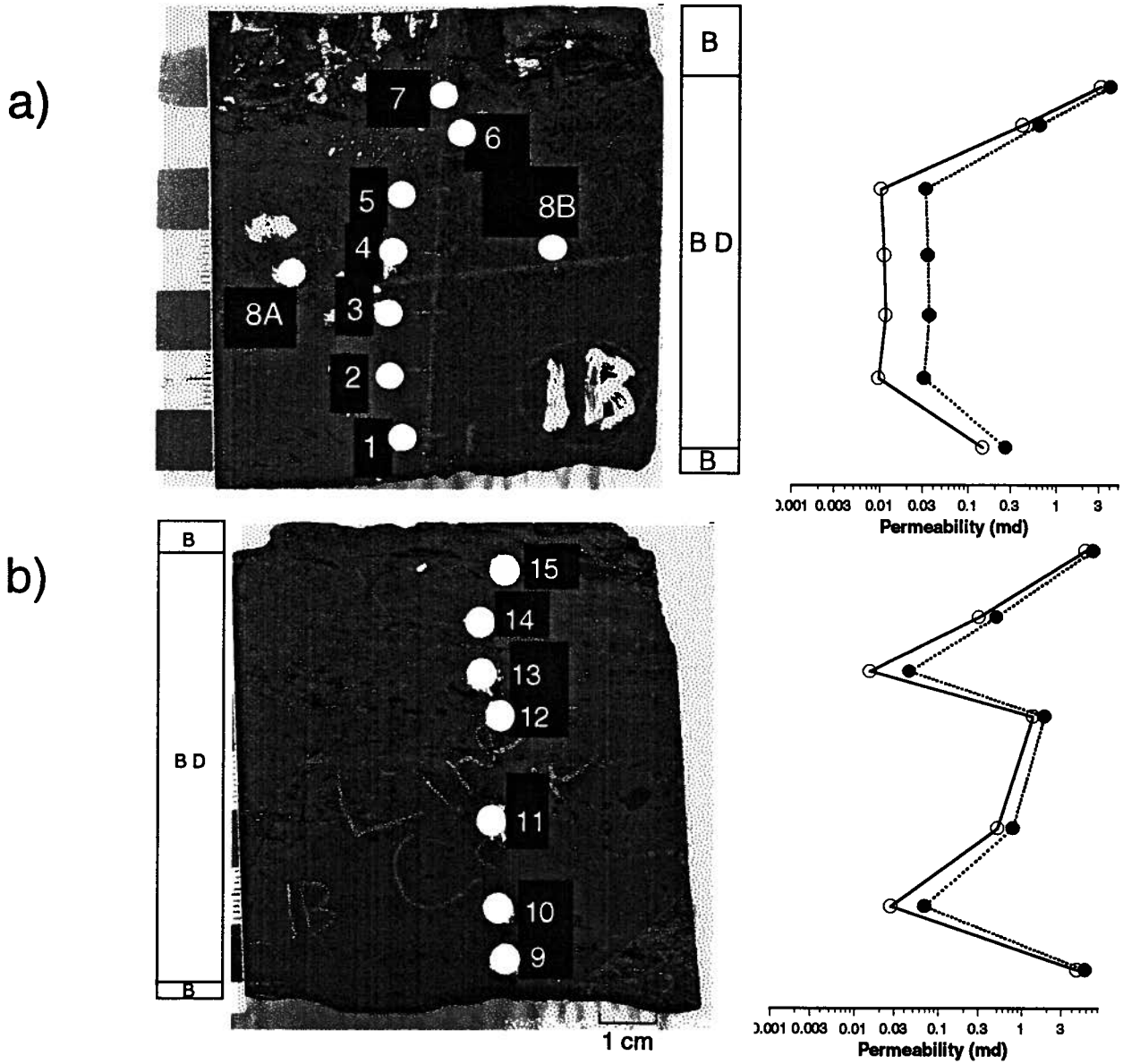

Figure 5-5. Permeability profiles for faces 1B-1 (a) and 1B-2 (b).

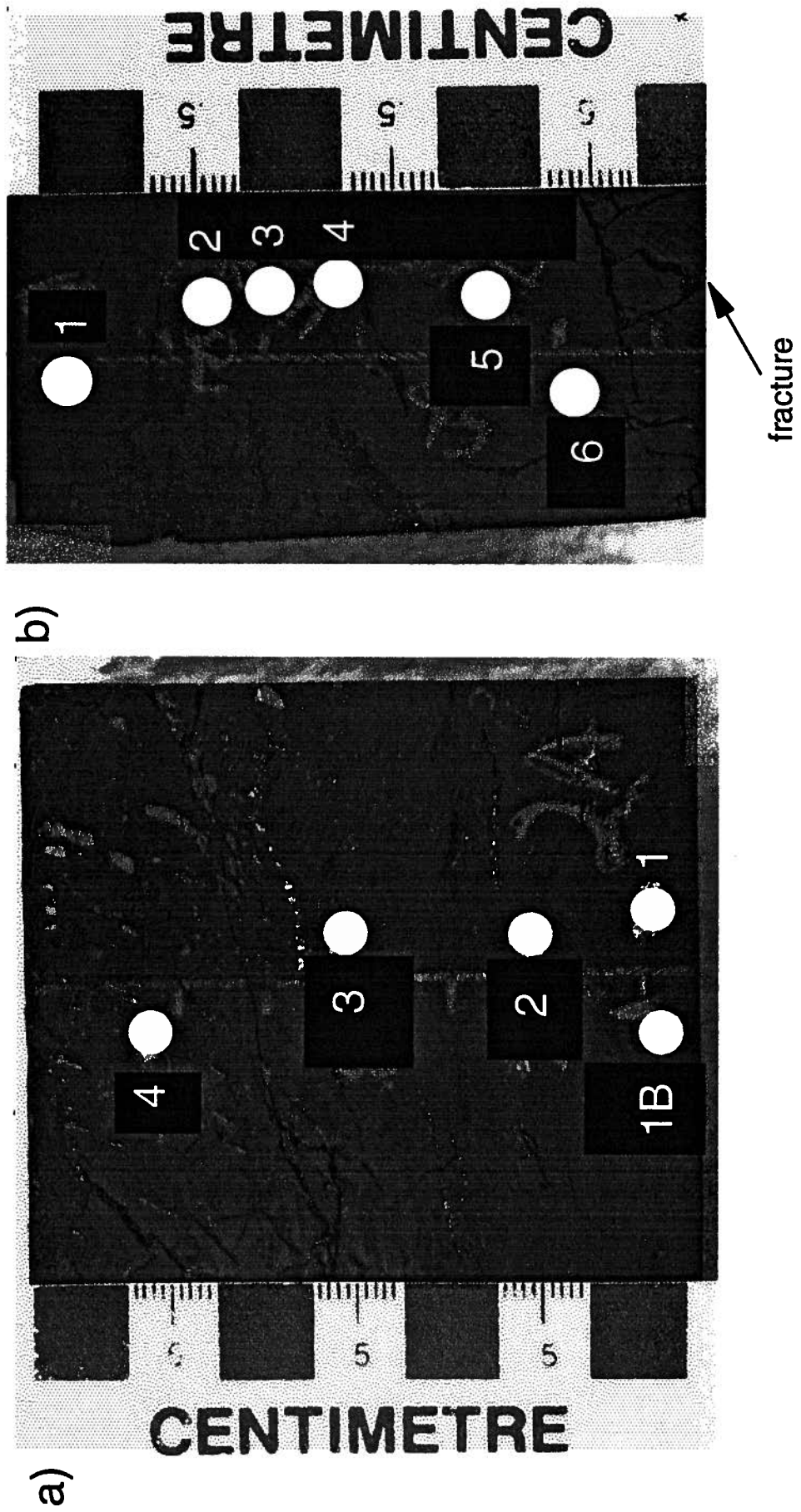

Figure 5-6. Sample 2 showing faces 2A (a) and 2B (b).

Sample 3, from NEVCF, is a banded to banded dull coal (Figure 5-7). The top face of the sample (not shown) displays face cleating with a spacing of ~ 2 mm. Face 3A has a bright band with a thickness of about 5 mm at the bottom of the face. All measurement points are located in the banded dull portion of the coal. Both faces display a large amount of artificially-induced fracturing and pitting.

Sample 4 (LTC-2), from the Gates Formation, is a dull coal with a 2 mm thick bright band at the top of the sample (Figure 5-8). Face cleat is visible on the top and bottom surfaces (not shown) of the sample and has a spacing of ~ 1 mm. All points are located within the dull portion of the coal and each surface is essentially free from pitting and fracturing. Some very fine laminations (fibrous coal or mineral) occur within the dull section.

Sample 5 (Figure 5-9), from NEVCF is similar to sample 3 but is slightly brighter. A 6 mm thick bright band occurs at the bottom of face 5A and a 4 mm thick bright band occurs at the top. Face cleat in the top and bottom bright bands has a spacing of about 1 - 2 mm and is oriented at high angle (not quite orthogonal) to face 5A. Sample 5, like sample 3, has alot of artificially-induced fracturing and pitting in the surfaces.

Sample 6 (LTC-5), from the Gates Formation, is a fibrous coal (silky luster) (Figure 5-10). The sample displays no cleat. Some banding does occur in the sample, which may be attributed to fire cycles.

Sample 7 (LTC-11), also from the Gates Formation, is a banded dull - dull coal with poorly developed face cleating in the thin bright bands (Figure 5-11).

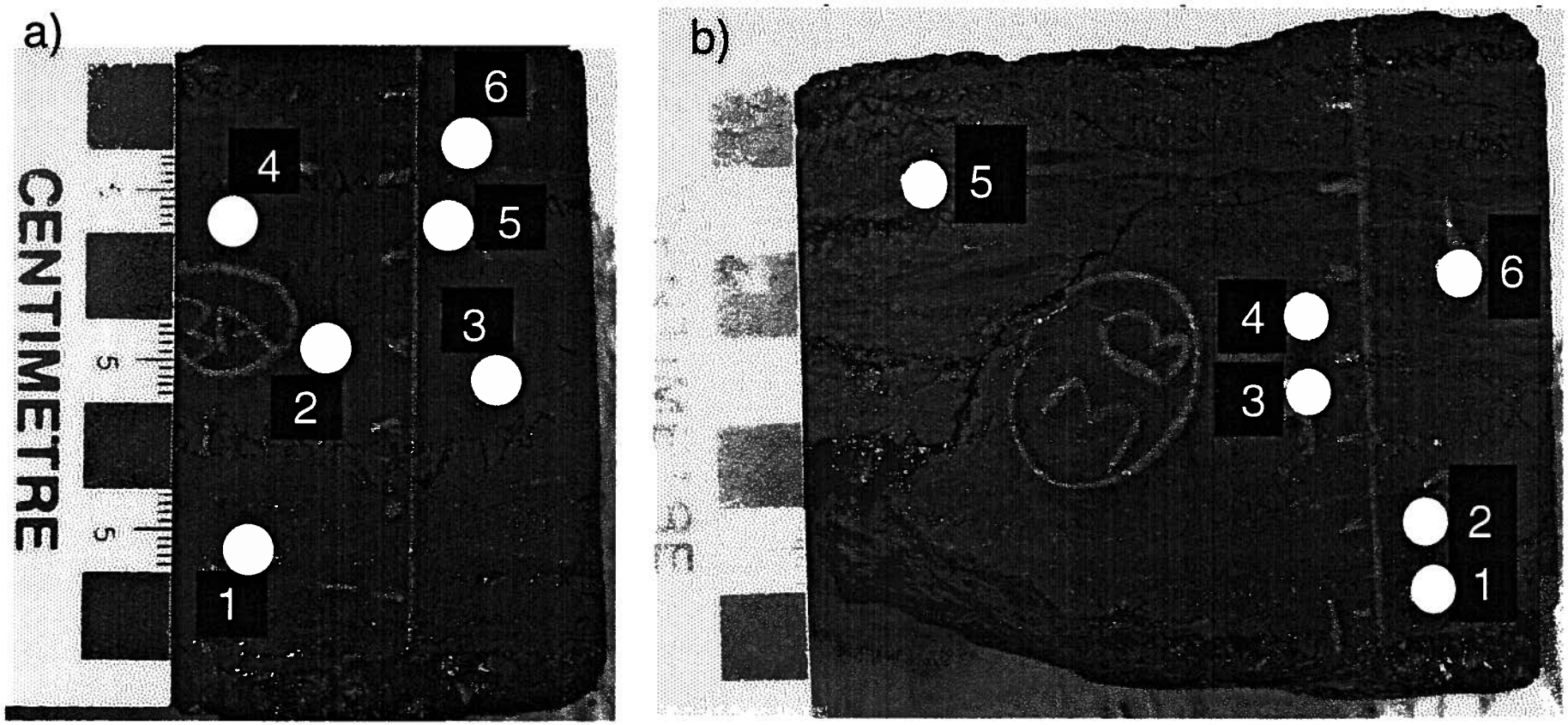

Figure 5-7. Sample 3 showing faces 3A (a) and 3B (b).

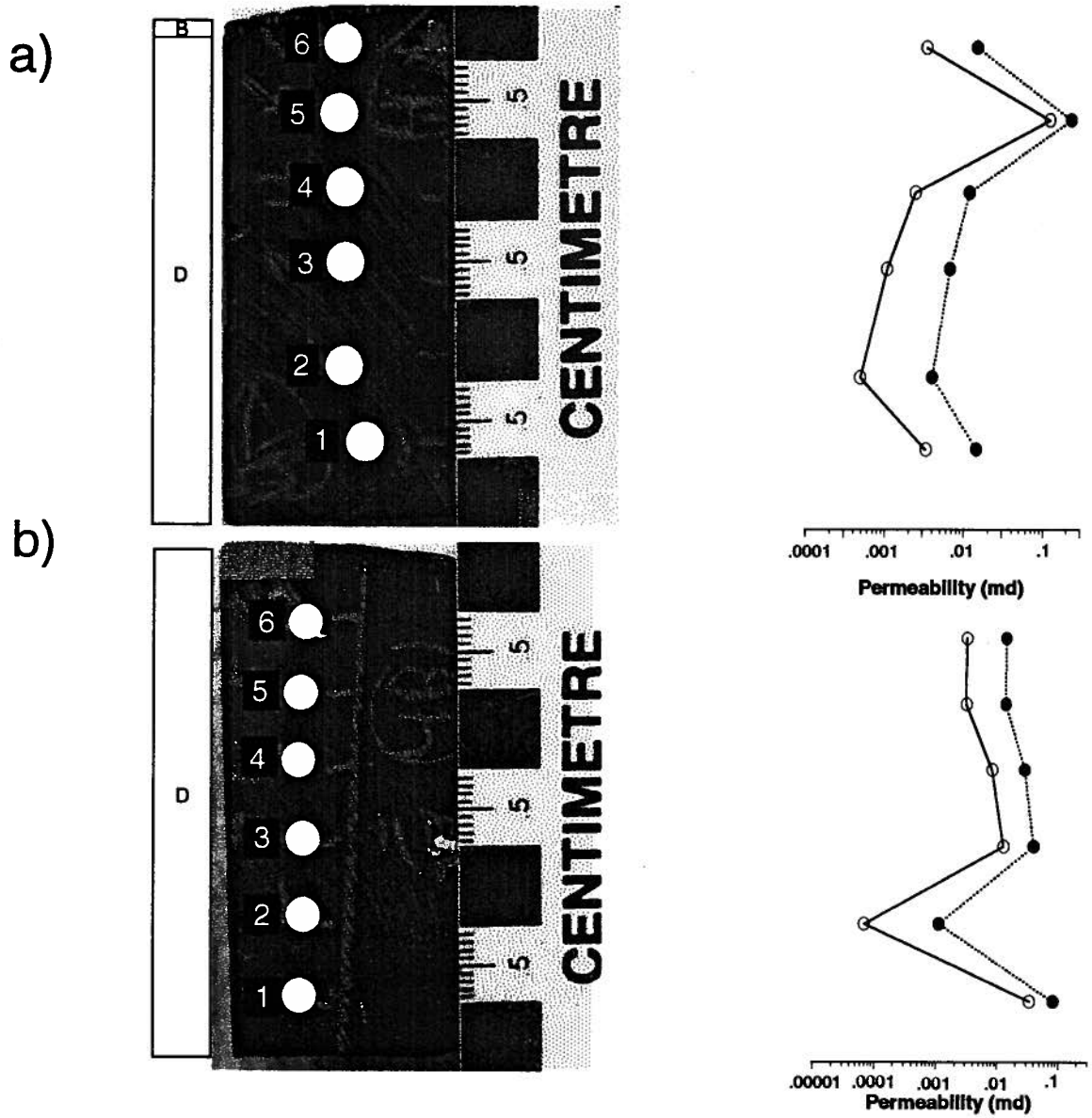

Figure 5-8. Permeability profiles of faces 4A (a) and 4B (b). See text for explanation.

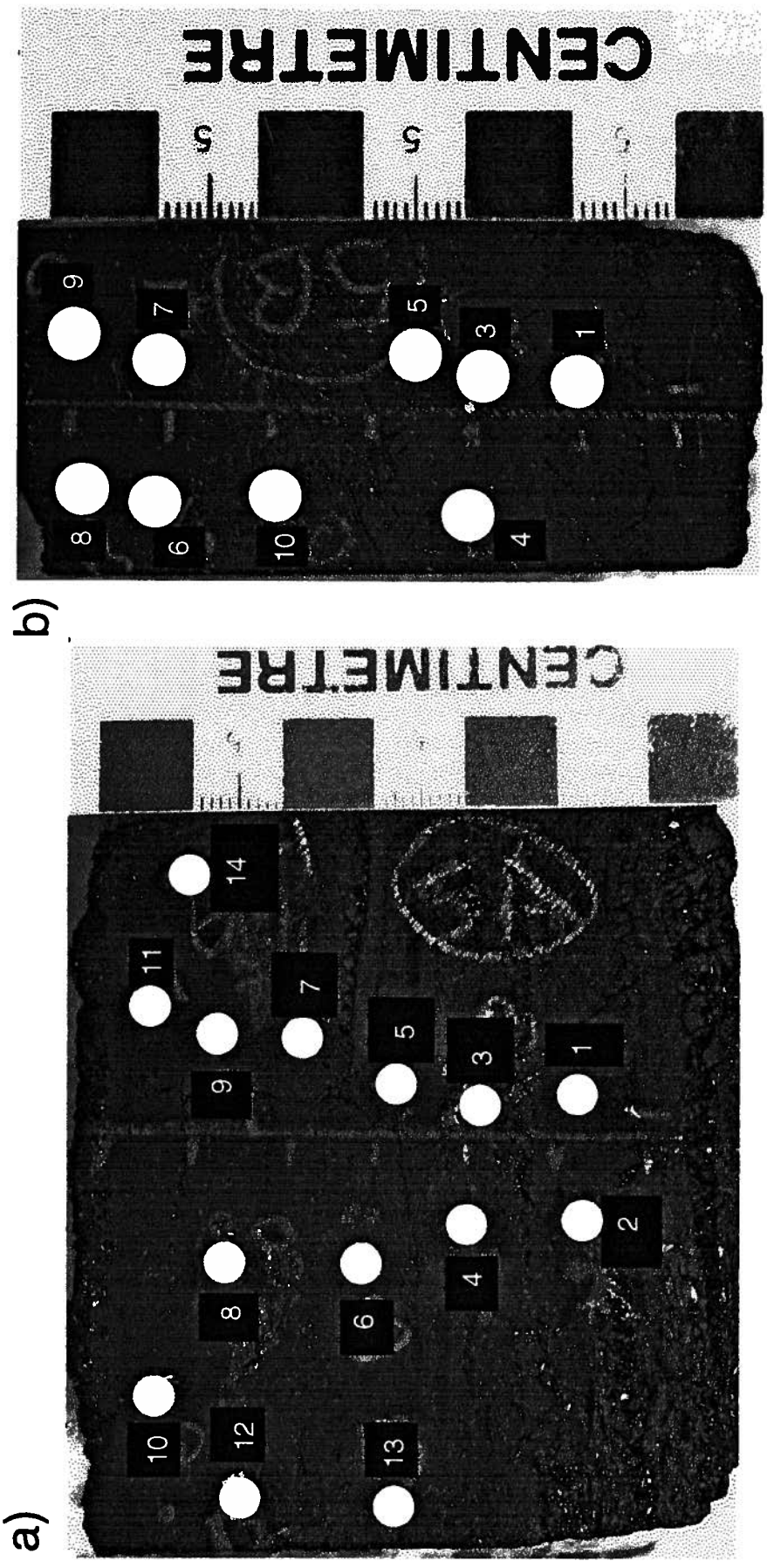

Figure 5-9. Sample 5 showing faces 5A (a) and 5B (b).

Figure 5-10. Sample 6 showing all faces on which points were measured.

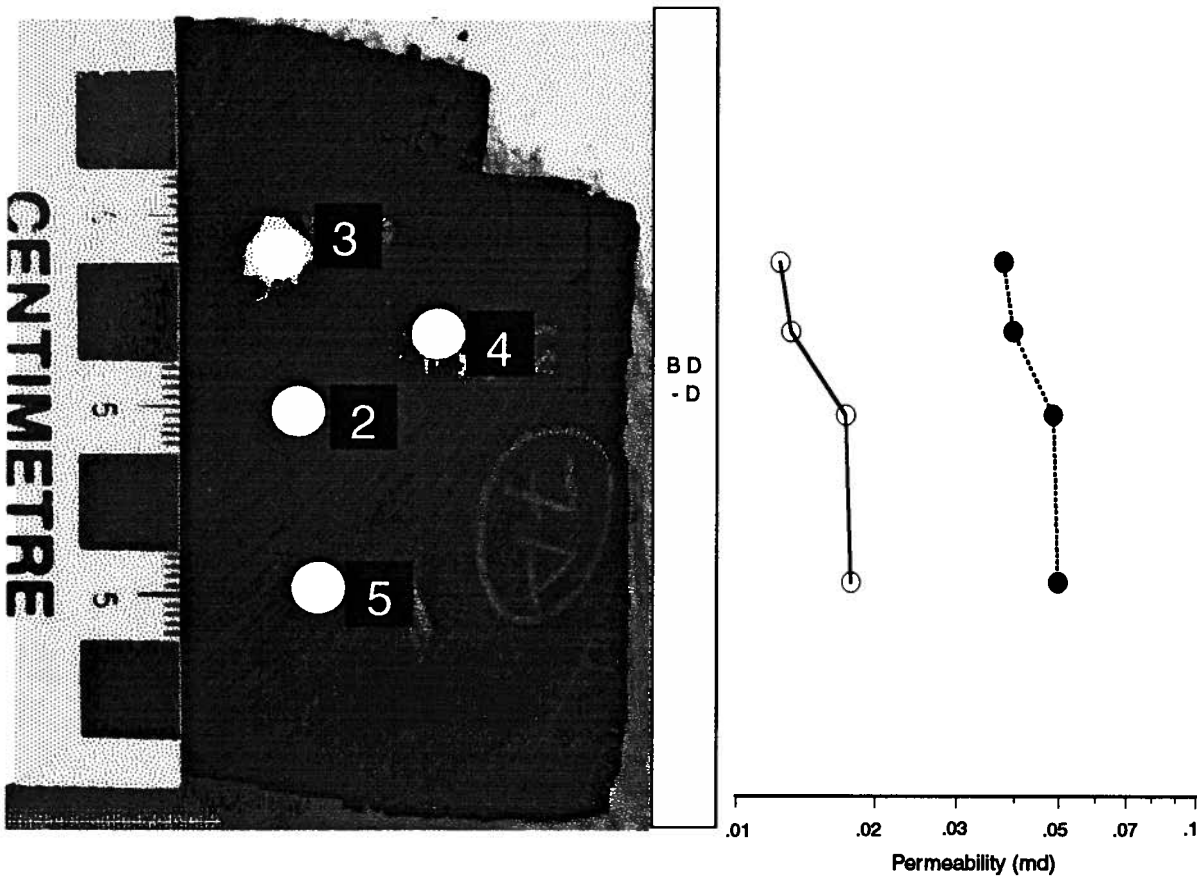

Figure 5-11. Permeability profile of sample 7. See text for explanation.

5.6.2 Permeability Variation with Lithotype Composition

In order to determine the effect of lithotype (megascopic) composition of coal upon measured permeabilities, (vertical) profiles were taken on some of the coal samples at right angles to bedding. The spacing of measured points was generally around 1 cm, but because of surface irregularities such as pitting or artificially-induced microfracturing, spacing varied. Both non-slip corrected permeabilities (Ka) (solid circles in profile) and liquid equivalent permeabilities (Kl) (open circles in profile) are given.

Vertical profiles are plotted adjacent to coal photos in Figures 5-4, 5-5, 5-8, and 5-11 for coal samples 1, 4, and 7. The other samples were not chosen, as it was difficult to obtain vertical profiles due the irregularities on the measurement surfaces.

Profiles of faces 1A-1 and 1A-2 (cut perpendicular to face cleat) are plotted in Figure 5-4. The profile of face 1A-1 shows a slight increase in permeabilities from the bottom to the top of the sample. Permeabilties in the bright bands at the top and bottom are higher than those in the banded dull lithotype. The permeabilities of face 1A-2 show a similar trend as in face 1A-1; the highest permeability is for point 11, located in the lower bright band, and the permeabilities in the banded dull lithotype are considerably lower.

Profiles of faces 1B-1 and 1B-2 (cut parallel to face cleat) are shown in Figure 5-5. The profiles show similar trends as the 1A faces. The highest permeabilities are associated with bright coal. The banded dull band of face 1B-1 is remarkably uniform in permeability, and is considerably tighter than the bright bands. The dull banded band of face 1B-2 a greater variability in permeability than face 1B-1.

Profile permeabilities for sample 4 are shown in Figure 5-8. The permeabilities within the dull band of faces A and B are fairly uniform and are quite low (Kl generally < 0.02 md). The slight variation in permeabilities may be due to compositional variability, but the dull band appears to be quite uniform. Point 2 of face B has a very low permeability (Kl = .00006 md), but there is no visual compositional difference between this point and the rest of the dull band.

A permeability profile of sample 7 is presented in Figure 5-11. The Kl permeability is less than 0.02 md and is quite uniform throughout the profile.

In general, the brighter lithotypes have the greatest permeabilities. The bright bands of sample 1 have the highest average permeability (average = 4.1 md, range = 2 - 7 md) of the samples, and the dull bands of samples 4 and 7 have the lowest average permeabilities (average = .016 md, range = 0..00006 - .12 md). Sample 2 is a dull lithotype and has permeabilities ranging from 0.03 to 1 md (average = .13 md), which is higher than for samples 4 and 7, but this may be attributable to the high amount of pitting and artificial fracturing in this sample. The banded dull band of sample 1 has a range in liquid permeabilities from .01 - 1.5 md (average = .14 md) which is intermediate in permeability to the dull and bright lithotypes. The banded to banded dull coals (3 and 5) have permeabilities ranging from .07 - 4 md (average = .79 md). The range in Kl for the fibrous sample (6) is 0.2 - 1 md (average = .5 md). In the above averages, points that are not thought to be representative of the sample and are anomolously high, due to surface pitting, fracturing, proximity to an edge, or loss of seal, are not used. The following relationship of decreasing permeabilities with lithotype thus occurs for the samples in this study: bright > banded > fibrous > banded dull > dull.

5.6.3 Permeability Variation with Maceral Composition

Petrography was performed upon 0.125 cm^3 volumes of coal for each point in the permeability analysis. The results are presented in the Appendix.

Samples of similar rank are grouped in the following analyses in order to eliminate the effects of rank upon measured profile permeabilities. The sample 1 (LC-8) has the highest rank, with a random vitrinite reflectance of 1.25 % (medium-volatile bituminous), and will be considered seperately. Samples 2, 3 and 5 have random reflectances of 0.90, 0.91, and 0.92 %, respectively, are of similar rank (high-volatile bituminous A) and will be discussed together. Samples 4, 6 and 7 have random reflectances of 1.08, 1.03, and 1.06 %, respectively, are of similar rank (high-volatile bituminous A) and will be considered together.

Sample 1 (LC-8)

A plot of total vitrinite versus liquid-equivalent profile permeability is shown in Figure 5-12. Both mineral-matter free (mmf) and raw (mineral-matter including) vitrinite contents are plotted.

The profile permeabilities appear to increase in a general way with total vitrinite content and the two parameters can be correlated linearly.

No apparent correlation occurs between the permeability and mineral matter content. This may in part be due to the way in which mineral matter content was determined. The mineral matter content was obtained petrographically through visual point count, instead of through ASTM proximate and sulphur analysis and the Parr formula (Chapters 3 and 4), which is believed to be a more reliable method for mineral matter content determination. Not enough material was recovered for each point to

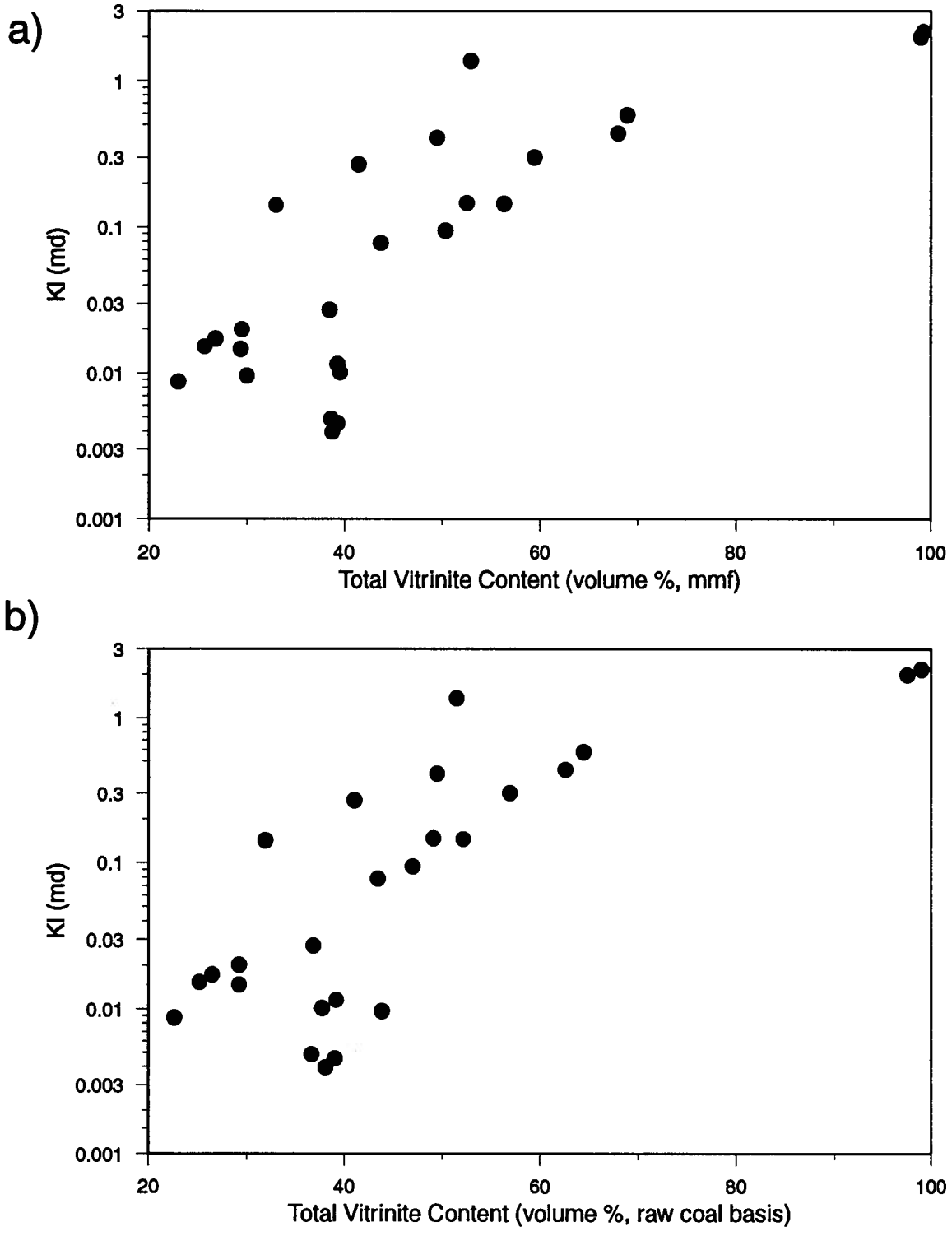

Figure 5-12. Plots of Kl versus total vitrinite content of sample 1 on a; a) mineral matter-free, and ; b) raw coal basis.

facilitate the use of the ASTM method. A bulk sample mineral matter analysis was not thought to be relative because it would not have been representative of the individual volumes measured in the profile permeability analysis. Mineral matter content was quite low in this sample (0 - 7 %) and thus does not appear to be an important controlling factor on the permeability measurements.

Scatter in the plot of Figure 5-12 is attributable to several factors. Firstly, artificially-induced (sawcut) fractures or pitting near or at the point may cause variations in the measured permeabilities for points of similar composition. Secondly, the sample volume cut for petrographic analysis may not be completely representative of the volume measured either compositionally or structurally. Thirdly, some sample points that have a high vitrinite content but low permeabilities may lack macroscopic fracturing which would lead to higher permeabilities. Although great care was taken to avoid any areas of sample with artificial fracturing or choose points where the coal appeared homogeneous in composition, this task proved to be very difficult. The permeability data presented here must be interpreted with care.

Samples 3 and 5 (SEVCF)

Samples 3 and 5 are grouped together because of similar reflectance values (rank). Sample 2, although of similar rank is not used in this analysis because it is highly fractured (artificially-induced).

No significant correlation is obtained between maceral composition and permeability. This is due mainly to the highly fractured nature of samples 3 and 5 (Figures 5-6 and 5-8). The fracturing is caused by the frequent occurrence of brittle bright bands which "fall apart" during the cutting procedure. Even the duller material between bright bands is fractured, and the obtained permeabilities are suspect.

Samples 4, 6 and 7 (Gates Formation)

Samples 4 and 7 are dull and dull to banded dull coals, respectively, and sample 6 is a fibrous coal. Of these samples, sample 4 has the lowest average permeability and sample 6 has the highest.

Samples 4 and 7 are similar in appearance and texture. Sample 4 has an average total vitrinite content (volume percent, mmf) of 21 % and sample 7 an average vitrinite content of 23% (mmf), which is consistent with the latter sample's higher average permeability. The high average mineral matter content for samples 4 and 7 of 7.4 and 5.0 volume %, respectively, may also be a cause of low permeability.

Sample 6 is unique in that it has a very high fusinite content (69 %, mmf). The average permeability of this sample is higher than samples 4 and 7 despite the high average mineral matter content of sample 6 (7.5 volume %).

5.6.4 Effect of Rank upon Profile Permeability

Although it is difficult to determine the effect of rank upon permeability of the chosen coal suite because of compositional variability, a few general statements can be made. Typical banded dull permeabilities of sample 1, the highest rank coal, are between 0.01 - 0.02 md, and are often less than 0.01 md. The dull band permeabilities of samples 2, 3, and 5, which are of lower rank are never less than about 0.03 md. It appears that dull coal permeabilities decrease slightly with rank, but the above result is not conclusive. Pore size distribution studies of coal of varying rank (Gan et al., 1972) have shown that macroporosity generally decreases with increasing coal rank such that medium volatile coals (ie. sample 6) typically contain less macroporosity than a high volatile A bituminous coal (ie. samples 2, 3, and 5). Because macroporosity may be an important contributor to

permeability, it is consistant that sample 1 has lower dull coal permeabilities than samples 2, 3, and 5.

5.7 DISCUSSION

Permeabilities vary with lithotype composition of coals. The order of decreasing permeabilities of the lithotypes is as follows: bright > banded > fibrous > banded dull > dull.

The abundance and orientation of macroscopic fracturing as well as the type, size, shape, density, orientation, distribution, and connectivity of microstructures is dependant upon lithotype. The well-defined macroscopic fracturing (cleating) of bright coal probably contribute to its high permeability. Too few measurements were taken on bright bands to determine the effect cleat orientation, however. Bright coals also have a continuous microcleat network which may contribute to the overall permeability. Duller lithotypes, on the other hand, typically lack macroscopic fracturing and have a greater abundance of phyteral porosity, such as cell lumens in fusinite.

On the microscopic level, an increase in total vitrinite content of sample 1 correlates with an increase in permeability. The thick bright bands have a very high vitrinite content and associated permeabilities. In the banded dull lithotype, variation in vitrinite content is probably due to the presence or absence of thin bright bands in the sampled volume used for petrographic analysis.

Permeabilities are generally less variable for samples 4 and 7 than for sample 1, which is due to the relative compositional homogeneity of the former samples. The lack of macrofracturing associated with these dull lithotypes is a cause of their overall low permeabilities. In both samples 4 and 7, high mineral matter contents are an additional cause of low permeabilities. Sample 6 has a higher permeability than samples 4 and 7, which may be caused by the abundance of fusinite, some of which has open cell lumen.

Bright coals may provide the most permeable pathways for methane transmission. As discussed in Chapter 3, high rank coals rich in vitrinite tend to have a greater amount of microporosity than those rich in inertinite. This leads to a higher capacity for methane gas storage. The microcleat network, along with conchoidal fracturing and striae, may create a continous permeable pathway from the micropore network through to the macrofracture network. Brighter lithotypes thus not only provide a high gas storage capacity for high rank coals, but also have the potential to provide continuous transmission of methane gas to the borehole.

Although profile permeabilties reflect to a certain degree the compositional variation of the samples measured, caution must be taken when interpreting the data if a substantial amount of fracturing induced by sampling, core slabbing, or sample cutting is present. The duller lithotypes are less prone to artificial fracturing and the profile permeameter technique appears to be most useful to the study of such lithotypes. Samples 3 and 5 include highly fractured bright bands and hence the measurements taken on these samples are suspect.

It is also important to note that the samples utilitized in this study were sampled from outcrop and hence do not represent subcrop coal permeabilities. The resulting stress relaxation from surface exposure (McElhiney et al., 1993) and brittleness during cutting procedures probably accounts for higher permeabilities of the coal than would be obtained during well testing.

5.8 CONCLUSIONS

A pressure-decay permeameter is useful in determining variation in measured permeabilities with lithotype and maceral composition of coals of the Western Canadian Sedimentary Basin. The technique is reliable for dull lithotypes, which due not fracture as easily during core slabbing, sample cutting or handling techniques. The following conclusions are obtained from this study:

1) The order of decreasing profile permeabilities with lithotype is as follows: Bright > banded > fibrous > banded dull > dull. The increased permeabilities with increased brightness of the coals is due to the presence of abundant macrofracturing (cleating) in bright coals.

2) A general increase in permeability is associated with an increase in total vitrinite. The highest permeabilities are associated with bright bands with a high vitrinite content.

3) The lowest permeability dull coals lack macroscopic fracturing and have a high mineral and inertinite content. Fibrous coal has a higher permeability than dull coal of the same rank. This is possibly due to the high content of fusinite in fibrous coal, which is highly macroporous.

5) Dull coal permeabilities appear to decrease with an increase in rank. These results are obscured by compositional differences between samples of the same rank.

6) Pressure-decay permeability measurements are more reliable for dull lithotypes.

7) Measured permeabilites are optimistic due to the relaxation of stress upon exposure to the atmosphere which opens up fractures in the sample.

If care is taken in measuring profile permeabilities, the technique may provide a valuable method of predicting methane recoverability from coals of various lithotype compositions and rank.

5.9 REFERENCES

Close, J.C., 1993. Natural fractures in coal. In: B.E. Law and D.D. Rice (Editors), Hydrocarbons from Coal, AAPG Studies in Geology # 38, pp. 119-132.

Close, J.C., Mavor, M.J., and McBane, R.A., 1990. Importance, genesis, and recognition of fracture permeability in Fruitland coalbed methane reservoirs of the northern San Juan Basin, Colorado and New Mexico. Petroleum Society of CIM/Society of Petroleum Engineers International Technical Meeting, Calgary, Alberta, Canada, Paper no. CIM/SPE 90-106.

Diessel, C.F.K., 1965. Correlation of macro- and micropetrography of New South Wales coals. In: J.T. Woodcock, R.T. Madigan and R.G. Thomas (Editors), Proceedings-General, 8th Commonwealth Mineralogy and Metallurgy Congress, Melbourne, 6: 669-677.

Gamson, P.D., Beamish, B.B., and Johnson, D.P., 1993. Coal microstructure and their effects on natural gas recovery. Fuel, 72: 87-99.

Gan, H., Nandi, S.P., and Walker, P.L., Jr., 1972. Nature of porosity in American coals. Fuel, 51: 272-277.

Georgi, D.T., and Jones, S.C., 1992. Application of pressure-decay profile permeametry to reservoir description. Society of Petroleum Engineers, 9212: 1-12.

Jones, S.C., 1992. The profile permeameter: a new, fast, accurate minipermeameter. Society of Petroleum Engineers, 24757: 973-983.

Lamberson, M.N., and Bustin, R.M., 1993. Coalbed methane characteristics of the Gates Formation coals, northeastern British Columbia: effect of maceral composition. American Association of Petroleum Geologists, 77: 2062-2076.

Marchioni, D.L., 1980. Petrography and depositional environment of the Liddell Seam, Upper Hunter Valley, New South Wales. International Journal of Coal Geology, 1: 35-61.

McElhiney, J.E., Paul, G.W., Young, G.B.C., and McCartney, J.A. Reservoir engineering aspects of coalbed methane. In B.E. Law and D.D. Rice (Editors), Hydrocarbons from coal, AAPG Studies in Geology # 38: pp. 361-372.

1980 Annual Book of ASTM Standards. Part 26 Gaseous Fuels, Coal and Coke, sections D3174-73 and D3177-75.

CHAPTER 6

SUMMARY AND CONCLUSIONS

6.1 EFFECT OF COAL COMPOSITION UPON GAS SORPTION CAPACITY AND TRANSMISSIBILITY

Coal is a compositionally complex material containing both organic and inorganic constituents. The proportion of these two constituents can vary widely within a seam. Coal type ultimately controls its utilization potential and hence lateral and vertical variations in coal seams should be accounted for in exploration and development strategies.

Similarly, coal composition variability should be considered in exploration programs for natural gas from coal seams. The current thesis has demonstrated that coal gas capacity is affected by maceral and mineral content. Specifically, gas capacity of bituminous coals increases with vitrinite content. Conversely, gas capacity generally decreases with increasing inertinite and mineral matter content. The sorption capacity of coal is a function of the pore size distribution which is in turn affected by maceral content: vitrinite is more microporous than inertinite whereas inertinite has a greater amount of mesoporosity. The ultimate gas content of coal is hence intimately related to the relative proportion of the maceral groups.

The permeability of coal is greatly affected by lithotype (megascopic) and maceral (microscopic) composition. Brighter coals typically have a higher permeability due to abundance of associated macro- (cleat) fracturing. Permeability also generally increases with vitrinite content, although further work is required to confirm this.

Ignoring rank and other factors affecting gas content, a bright coal with low mineral matter content and abundant macrofracturing should have a high gas content and transmissibility.

6.2 FUTURE WORK

The current study has focused upon the controls of coal composition upon single component gas sorption. Previous studies (Greaves et al., 1993; Harpalani and Pariti, 1993) have already documented the relative sorption capacities of single and multicomponent gases. The effect of maceral composition upon the sorption of mixtures require study.

The effect of coal composition upon gas permeability requires further investigation. The pressure-decay permeametry technique in conjunction with more conventional laboratory techniques should yield further insight into the effects of both maceral and mineral composition upon gas transmission.

6.3 REFERENCES

Greaves, K.H., Owen, L.B., McLennan, J.D., and Olszewski, A., 1993. Multi-component gas adsorption-desorption behaviour of coal. In: Proceedings of the 1993 International Coalbed Methane Symposium, The University of Alabama/Tuscaloosa, May 17-21, 1993: 197-205.

Harpalani, S., and Pariti, U.M., 1993. Study of coal sorption isotherms using a multicomponent gas mixture. In: Proceedings of the 1993 International Coalbed Methane Symposium, The University of Alabama/Tuscaloosa, May 17-21, 1993: 151-156.

APPENDIX

Appendix

Petrography data

Mineral matter-free data - volume %

SAMPLE	POINT #	SV	DESMO	VITDET	SFUS	FUS	OTHERI	TOTLIP	TOTVIT	TOTIN
1	1A-1	44	6	0	4	0	46	0	50	50
	1A-2	27	12	0	21	0	40	0	39	61
	1A-3	38	13	0	8	0	41	0	51	49
	1A-4A	30	9	0	7	0	54	0	39	61
	1A-5	23	19	0	21	0	38	0	42	58
	1A-6	29	4	0	13	0	53	0	33	67
	1A-7	56	1	0	40	1	2	0	56	43
	1A-8	99	0	0	0	0	1	0	99	1
	1A-8A	99	0	0	1	0	0	0	99	1
	1A-9	58	10	0	6	0	26	0	68	32
	1A-11	60	9	0	2	0	29	0	69	31
	1A-12	17	6	0	33	0	44	0	23	77
	1A-13	28	2	0	13	0	58	0	29	71
	1A-14	36	8	0	6	0	51	0	44	56
	1A-15	23	7	0	11	0	60	0	30	70
	1A-16	24	3	0	12	0	61	0	27	73
	1B-1	37	15	0	16	1	30	0	53	47
	1B-2	29	17	0	12	0	43	0	45	55
	1B-3	30	9	0	22	0	38	0	39	61
	1B-5	29	10	0	20	0	40	0	40	60
	1B-6	32	18	0	27	0	24	0	50	50
	1B-10	29	10	0	12	0	49	1	39	61
	1B-12	31	22	0	15	0	33	0	53	47
	1B-13	22	4	0	20	0	55	0	26	74
	1B-14	51	9	0	15	1	25	0	59	41
2	2A-2	23	7	0	17	6	47	1	30	69
	2A-3	15	2	0	31	10	42	1	17	82
	2A-4	23	5	0	23	0	46	3	28	69
	2B-1	29	11	0	14	2	40	4	41	55
	2B-3	22	7	0	12	5	53	1	29	71
	2B-5	26	3	0	36	0	35	1	29	70
3	3B-1	17	10	0	22	2	50	0	26	74
	3B-2	14	6	0	24	2	50	3	20	77
	3B-3	22	7	0	39	0	30	1	30	69
	3B-5	7	2	0	63	0	27	0	9	90
	3B-6	26	8	0	32	0	34	1	34	65
	3A-1	23	14	0	25	0	38	0	36	63
	3A-2	23	2	0	30	0	45	0	25	75
	3A-3	11	11	0	41	0	36	0	22	78
	3A-4	21	3	0	42	0	34	0	24	76

SAMPLE	POINT #	SV	DESMO	VITDET	SFUS	FUS	OTHERI	TOTLIP	TOTVIT	TOTIN
4	4A-1	20	5	0	15	0	61	0	25	75
	4A-2	14	7	0	18	1	62	0	21	79
	4A-3	12	2	0	11	0	74	0	14	85
	4A-4	19	7	0	15	1	57	0	26	73
	4A-5	12	3	0	13	0	73	0	14	86
	4B-1	19	8	0	26	0	48	0	27	73
	4B-2	23	11	0	21	0	44	1	34	65
	4B-3	13	0	0	23	0	64	0	13	87
	4B-5	13	5	0	23	1	58	0	18	82
	4B-6	11	7	0	16	0	65	1	18	81
5	5A-1	16	3	0	71	1	11	0	19	82
	5A-2	24	2	2	60	1	11	1	28	72
	5A-4	22	6	0	35	1	35	1	28	72
	5A-5	12	14	2	61	0	11	0	28	72
	5A-6	25	3	1	47	1	23	1	29	71
	5A-7	28	11	0	34	1	25	1	39	60
	5A-8	26	4	1	45	1	23	0	31	69
	5A-9	32	6	0	32	0	27	3	38	59
	5A-10	27	4	0	28	4	36	2	31	67
	5A-11	35	4	0	35	5	20	1	39	60
	5A-12	20	5	0	10	0	63	2	25	73
	5A-13	27	11	0	40	0	22	0	37	62
	5A-14	16	4	0	39	0	42	0	19	81
	5B-3	23	7	0	19	0	50	2	30	69
	5B-5	22	6	0	24	0	48	0	28	72
	5B-6	20	3	0	38	0	38	1	23	76
	5B-7	27	4	0	52	4	13	0	30	70
	5B-8	27	0	1	55	1	14	2	28	70
	5B-9	25	7	0	22	0	43	2	32	65
	5B-10	27	7	0	50	1	15	1	33	66
6	6-3	10	3	0	12	73	2	0	13	87
	6-6	13	11	2	13	57	5	0	25	75
	6-7	8	5	0	11	59	18	0	13	87
	6-8	5	1	0	2	89	4	0	6	94
7	7A-2	12	4	0	17	0	66	0	16	84
	7A-3	16	4	0	21	0	60	1	19	80
	7A-5	26	6	0	22	0	45	0	32	68

Raw coal data - volume %

POINT #	SV	DESMO	VITDET	SFUS	FUS	OTHERI	TOTLIP	MM	TOTVIT	TOTIN
1A-1	41	6	0	3	0	43	0	7	47	46
1A-2	26	12	0	21	0	39	0	2	38	60
1A-3	36	12	0	8	0	39	0	5	48	47
1A-4A	28	9	0	6	0	52	0	5	37	58
1A-5	22	19	0	20	0	38	0	1	41	58
1A-6	28	4	0	13	0	51	0	3	32	65
1A-7	52	1	0	37	1	2	0	7	52	40
1A-8	98	0	0	0	0	1	0	1	98	1
1A-8A	99	0	0	1	0	0	0	0	99	1
1A-9	53	10	0	5	0	24	0	8	63	29
1A-11	56	9	0	2	0	27	0	7	64	29
1A-12	17	6	0	33	0	43	0	2	23	76
1A-13	28	2	0	13	0	58	0	0	29	70
1A-14	35	8	0	6	0	50	0	1	43	56
1A-15	23	6	0	10	0	59	0	1	29	70
1A--16	23	3	0	11	0	60	0	1	26	72
1B-1	35	14	0	15	1	28	0	7	49	44
1B-2	28	16	0	12	0	42	0	2	44	54
1B-3	30	9	0	22	0	38	0	0	39	60
1B-5	28	10	0	19	0	38	0	5	38	58
1B-6	32	18	0	27	0	24	0	0	50	50
1B-10	27	10	0	11	0	47	1	4	37	58
1B-12	30	21	0	14	0	32	0	3	51	46
1B-13	22	4	0	19	0	54	0	2	25	73
1B-14	48	9	0	14	0	24	0	4	57	39
2A-2	20	6	0	15	5	41	1	12	26	61
2A-3	14	2	0	29	9	39	1	6	16	77
2A-4	22	5	0	22	0	43	3	5	26	65
2B-1	27	10	0	12	1	37	4	8	37	51
2B-3	20	6	0	11	5	49	1	8	26	64
2B-5	25	3	0	35	0	34	0	2	28	69
3B-1	16	9	0	22	2	50	0	1	26	73
3B-2	14	6	0	23	2	48	3	5	19	73
3B-3	22	7	0	39	0	30	1	1	29	69
3B-5	7	2	0	61	0	27	0	3	9	88
3B-6	26	8	0	31	0	33	1	1	34	65
3A-1	23	14	0	25	0	38	0	0	36	63
3A-2	23	2	0	29	0	45	0	0	25	75
3A-3	11	11	0	41	0	36	0	0	22	78
3A-4	21	3	0	42	0	33	0	1	24	75

POINT #	SV	DESMO	VITDET	SFUS	FUS	OTHERI	TOTLIP	MM	TOTVIT	TOTIN
4A-1	19	5	0	14	0	58	0	3	24	73
4A-2	13	7	0	17	0	60	0	2	20	78
4A-3	11	2	0	10	0	69	0	6	13	80
4A-4	18	7	0	14	1	53	0	8	24	68
4A-5	11	2	0	12	0	67	0	9	13	78
4B-1	16	7	0	23	0	42	0	11	24	65
4B-2	20	10	0	18	0	37	1	14	29	56
4B-5	12	5	0	21	1	55	0	5	17	78
4B-6	10	6	0	15	0	58	1	10	16	73
5A-1	15	3	0	70	0	10	0	0	18	81
5A-2	23	2	2	58	1	10	1	4	27	69
5A-4	21	6	0	35	1	34	1	2	27	70
5A-5	12	13	2	58	0	11	0	4	27	69
5A-6	25	3	1	46	1	23	1	2	28	69
5A-7	27	11	0	34	1	25	1	2	38	59
5A-8	25.	4	1	44	1	22	0	3	30	67
5A-9	31	6	0	32	0	27	3	1	38	59
5A-10	27	4	0	28	4	36	2	0	31	67
5A-11	34	4	0	35	5	20	1	1	38	59
5A-12	19	5	0	10	0	62	2	1	24	72
5A-13	26	11	0	40	0	21	0	1	37	62
5A-14	15	3	0	39	0	42	0	1	19	80
5B-3	23	7	0	19	0	49	2	0	30	68
5B-5	22	6	0	24	0	48	0	0	28	72
5B-6	20	3	0	38	0	38	1	0	23	76
5B-7	26	4	0	52	4	13	0	1	30	69
5B-8	27	0	1	54	1	13	2	3	28	68
5B-9	25	7	0	22	0	43	2	1	32	64
5B-10	26	7	0	49	1	15	1	1	33	65
6-3	9	2	0	11	66	2	0	9	12	79
6-6	12	10	2	12	53	5	0	7	23	69
6-7	7	5	0	10	54	17	0	7	12	81
6-8	5	1	0	1	84	4	0	5	6	90
7A-2	12	4	0	17	0	64	0	3	16	81
7A-3	14	3	0	19	0	54	0	9	17	74
7A-5	26	6	0	22	0	44	0	3	31	66

SV - STRUCTURED VITRINITE
DESMO - DESMOCOLLINITE
VITDET - VITRODETRINITE
SFUS - SEMIFUSINITE
OTHERI - OTHER INERTINITE
TOTLIP - TOTAL LIPTINITE
TOTIN - TOTAL INERTINITE
MM - MINERAL MATTER

Permeability data

SAMPLE	POINT #	Ka (md)	Kl (md)	Comments
1	1A-1	0.186	0.094	
	1A-2	0.0166	0.00394	
	1A-3	0.0183	0.00452	
	1A-4A	0.0383	0.0125	
	1A-4B	0.0240	0.00656	
	1A-4C	0.0449	0.0156	
	1A-4C2	0.0157	0.00369	
	1A-5	0.450	0.267	
	1A-6	0.256	0.141	
	1A-7	0.261	0.144	
	1A-8	2.63	1.98	
	1A-8A	2.84	2.16	
	1A-8c	8.88	7.27	
	1A-9	0.677	0.435	
	1A-10	0.0567	0.0211	
	1A-11	0.869	0.579	
	1A-12	0.0292	0.0087	
	1A-13	0.0434	0.0146	
	1A-14	0.159	0.0774	
	1A-15	0.0553	0.0199	
	1A-16	0.0488	0.0171	
	1B-1	0.265	0.146	
	1B-2	0.0314	0.00958	
	1B-3	0.036	0.0115	
	1B-4	0.0345	0.0110	
	1B-5	0.0324	0.0101	
	1B-6	0.638	0.408	
	1B-7	4.06	3.17	
	1B-8A	2.16	1.60	
	1B-8B	0.0664	0.0259	
	1B-9	5.74	4.59	
	1B-10	0.0688	0.0271	
	1B-11	0.781	0.510	
	1B-12	1.87	1.36	
	1B-13	0.0447	0.0152	
	1B-14	0.491	0.300	
	1B-15	7.03	5.67	
2	2A-1	9.45	7.74	NOT USED IN AVERAGE
	2A-1B	0.126	0.0589	
	2A-2	0.0915	0.0394	
	2A-3	0.0791	0.0325	
	2A-4	0.153	0.075	
	2B-1	0.0779	0.0314	
	2B-2	0.183	0.0923	
	2B-3	0.684	0.442	
	2B-4	0.162	0.0802	
	2B-5	0.662	0.421	

SAMPLE	POINT #	Ka (md)	Kl (md)	Comments
3	3B-1	1.19	0.816	
	3B-2	0.171	0.0825	
	3-B3	0.704	0.448	
	3B-4	3.09	2.33	NEAR SAWCUT IRREGULARITY
	3B-5	0.873	0.575	
	3B-6	2.12	1.57	
	3A-1	0.956	0.645	
	3A-2	1.66	1.19	
	3A-3	0.460	0.278	
	3A-4	0.241	0.129	
	3A-5	4.16	3.24	
	3A-6	5.07	4.01	
4	4A-1	0.0146	0.00334	
	4A-2	0.00403	0.000492	
	4A-3	0.00672	0.00107	
	4A-4	0.0118	0.00243	
	4A-5	0.232	0.124	
	4A-6	0.0149	0.00344	
	4B-1	0.0829	0.0345	
	4B-2	0.00112	6.93E-05	
	4B-3	0.0400	0.0128	
	4B-4	0.0284	0.00834	
	4B-5	0.014	0.00312	
	4B-6	0.0143	0.00322	
5	5A-1	1.07	0.737	
	5A-2	0.383	0.255	
	5A-3	15.4	12.9	CLOSE TO FRACTURE, NOT USED
	5A-4	1.23	0.854	
	5A-5	34.2	30.2	CLOSE TO FRACTURE, NOT USED
	5A-6	0.537	0.334	
	5A-7	0.247	0.134	
	5A-8	0.390	0.230	
	5A-9	0.255	0.140	
	5A-10	1.130	0.780	
	5A-11	0.278	0.154	
	5A-12	0.241	0.130	
	5A-13	1.00	0.681	
	5A-14	0.150	0.0727	
	5B-1	94.4	86.5	NO SEAL, NOT USED
	5B-2	43.6	38.9	NO SEAL, NOT USED
	5B-3	1.27	0.887	
	5B-4	3.11	2.38	
	5B-5	2.19	1.62	
	5B-6	0.0788	0.0323	
	5B-7	0.161	0.0792	
	5B-8	0.335	0.192	
	5B-9	0.416	0.248	
	5B-10	0.203	0.105	

SAMPLE	POINT #	Ka (md)	KI (md)	Comments
6	6-2	7.86	6.38	CLOSE TO FRACTURE, NOT USED
	6-3	0.986	0.672	
	6-4	5.62	4.50	CLOSE TO EDGE, NOT USED
	6-5	0.534	0.332	
	6-6	0.371	0.217	
	6-7	1.44	1.02	
	6-8	0.396	0.235	
7	7A-2	0.0485	0.0172	
	7A-3	0.0379	0.0124	
	7A-4	0.0398	0.0131	
	7A-5	0.0497	0.0177	

All surface observations made using 60X binocular microscope and 16X hand lens.